AFRL-RX-WP-TR-2010-4188

COLLABORATIVE RESEARCH AND DEVELOPMENT (CR&D)

Delivery Order 0014: Anti-Fretting Coatings Research Development

Carl H. Hager

Universal Technology Corporation

DECEMBER 2006
Final Report

AIR FORCE RESEARCH LABORATORY
MATERIALS AND MANUFACTURING DIRECTORATE
WRIGHT-PATTERSON AIR FORCE BASE, OH 45433-7750
AIR FORCE MATERIEL COMMAND
UNITED STATES AIR FORCE

NOTICE AND SIGNATURE PAGE

Using Government drawings, specifications, or other data included in this document for any purpose other than Government procurement does not in any way obligate the U.S. Government. The fact that the Government formulated or supplied the drawings, specifications, or other data does not license the holder or any other person or corporation; or convey any rights or permission to manufacture, use, or sell any patented invention that may relate to them.

This report was cleared for public release by the USAF 88th Air Base Wing (88 ABW) Public Affairs Office (PAO) and is available to the general public, including foreign nationals. Copies may be obtained from the Defense Technical Information Center (DTIC) (http://www.dtic.mil).

AFRL-RX-WP-TR-2010-4188 HAS BEEN REVIEWED AND IS APPROVED FOR PUBLICATION IN ACCORDANCE WITH THE ASSIGNED DISTRIBUTION STATEMENT.

*//Signature//	//Signature//
MARK GROFF Program Manager Business Operations Branch Materials & Manufacturing Directorate	KENNETH A. FEESER Branch Chief Business Operations Branch Materials & Manufacturing Directorate

This report is published in the interest of scientific and technical information exchange, and its publication does not constitute the Government's approval or disapproval of its ideas or findings.

*Disseminated copies will show "//Signature//" stamped or typed above the signature blocks.

REPORT DOCUMENTATION PAGE

Form Approved
OMB No. 0704-0188

1. REPORT DATE *(DD-MM-YY)*	2. REPORT TYPE	3. DATES COVERED *(From - To)*
December 2006	Final	19 May 2003 – 30 November 2006

4. TITLE AND SUBTITLE
COLLABORATIVE RESEARCH AND DEVELOPMENT (CR&D)
Delivery Order 0014: Anti-Fretting Coatings Research Development

5a. CONTRACT NUMBER
F33615-03-D-5801-0014

5b. GRANT NUMBER

5c. PROGRAM ELEMENT NUMBER
62102F

6. AUTHOR(S)
Carl H. Hager

5d. PROJECT NUMBER
4349

5e. TASK NUMBER
L0

5f. WORK UNIT NUMBER
4349L0VT

7. PERFORMING ORGANIZATION NAME(S) AND ADDRESS(ES)
Universal Technology Corporation
1270 North Fairfield Road
Dayton, OH 45432-2600

8. PERFORMING ORGANIZATION REPORT NUMBER
S-531-014

9. SPONSORING/MONITORING AGENCY NAME(S) AND ADDRESS(ES)
Air Force Research Laboratory
Materials and Manufacturing Directorate
Wright-Patterson Air Force Base, OH 45433-7750
Air Force Materiel Command
United States Air Force

10. SPONSORING/MONITORING AGENCY ACRONYM(S)
AFRL/RXOB

11. SPONSORING/MONITORING AGENCY REPORT NUMBER(S)
AFRL-RX-WP-TR-2010-4188

12. DISTRIBUTION/AVAILABILITY STATEMENT
Approved for public release; distribution unlimited.

13. SUPPLEMENTARY NOTES
PAO Case Number: 88ABW 2010-1226; Clearance Date: 17 Mar 2009. Report contains color.

14. ABSTRACT
This research in support of the Air Force Research Laboratory, Materials and Manufacturing Directorate was conducted at Wright-Patterson AFB, Ohio from 19 May 2003 through 30 November 2006. This task examined fretting wear that is an accumulation of damage that occurs at component interfaces that are subjected to high contact stresses coupled with low amplitude oscillation. In the titanium dovetail joints of turbine engines, fretting wear can be severe. Surface treatments, such as plasma sprayed coatings and solid lubricants, have been implemented to mitigate the fretting wear problem. However, the current coating systems are reliant primarily on the applied lubricant. Once the lubricant is worn away the soft plasma sprayed coating is exposed and can damage the mated Ti6Al4V surface. Therefore the blades using the current coating systems need to be replaced before the lubricants are worn completely away, which results in high maintenance costs from schedule based periodic blade replacement.

15. SUBJECT TERMS
fretting, wear regimes, thermal spray coatings, Ti6Al4V

16. SECURITY CLASSIFICATION OF:			17. LIMITATION OF ABSTRACT:	18. NUMBER OF PAGES	19a. NAME OF RESPONSIBLE PERSON (Monitor)
a. REPORT	b. ABSTRACT	c. THIS PAGE			Mark Groff
Unclassified	Unclassified	Unclassified	SAR	76	19b. TELEPHONE NUMBER *(Include Area Code)* N/A

Standard Form 298 (Rev. 8-98)
Prescribed by ANSI Std. Z39-18

TABLE OF CONTENTS

Section **Page**

LIST OF FIGURES

LIST OF TABLES

1. Introduction

Fretting wear is an accumulation of damage that occurs at component interfaces that are subjected to high contact stresses coupled with low amplitude oscillation. Prevalent in Ti-alloy contacts, fretting wear can be especially problematic to the turbine engine industry. One of the most common occurrences of fretting in a turbine engine is in the compressor section at the blade/disk interface. The blade/disk interface, also known as the dovetail joint, is often fabricated from Ti6Al4V (Titanium, 6% Aluminum, 4% Vanadium) because of its high strength to weight ratio and corrosion resistance. Tribologically, mating Ti6Al4V surfaces are especially susceptible to fretting, because titanium alloys have a propensity to gall and can produce hard oxide debris that score the interface [1]. With further study, Sauger et al showed that the debris generated in Ti6Al4V contacts comes from a tribologically transformed structure (TTS) that forms at the fretting interface [2]. In this study the authors also showed that the TTS layer formed in Ti6Al4V interfaces is more than 3 times harder than the bulk material itself. Overtime, this hardened layer cannot accommodate the imposed fretting displacements and hard titanium particles are released from the wear surfaces. Once detached, these particles can get trapped in the fretting wear interface and cause 3rd body wear. In addition, the particles breakup and oxidize as shown in the work by Blanchard et al [3].

In addition to fretting wear at the interface, the combination of the rotating disk and the airflow through the engine imposes centrifugal forces and radial oscillations on the blades causing bulk cyclic stresses and component fatigue. The combination of the bulk cyclic stresses and fretting surface interactions is often called fretting fatigue. In fatigue, most of the component fatigue life is accommodated by the crack initiation phase. However, component fatigue life is reduced exponentially once critical cracks have been formed. The imposition of fretting wear at interfaces subjected to bulk cyclic loading can acceleration crack initiation. This is best described by Zhou et al in their fretting wear experiments with aluminum alloys [4]. In this study the authors conducted pure fretting wear tests using a spherical rider loaded normally onto a flat plate. Tests were conducted under various stroke lengths and loads for different numbers of cycles. At the completion of each test, the samples were cross-sectioned and the fretting wear tracks were investigated for cracks. Zhou et al found that during the fretting wear tests, without bulk loading of any kind, cracks were formed in the fretting contact. It was also found that critical cracks can be formed very quickly when the fretting tests were operated in the mixed fretting regime. In addition to this study, the impact of fretting wear on the reduction of fatigue life has been addressed in many publications, and are neatly summarized by Waterhouse in his fretting fatigue review paper in 1992 [5].

One common mitigation strategy, or solution, to the fretting wear/fatigue problem is to apply plasma sprayed CuNiIn (Copper-Nickel-Indium) coatings and solid lubricants to the dovetails of the Ti6Al4V compressor blades [6]. In this coating system the roughness of the soft plasma sprayed CuNiIn coating is used as a retainer for the application of the bonded solid lubricant. The implementation of this strategy has increased component life; however, recent studies have shown that unlubricated CuNiIn coatings can cause severe damage to mating Ti-alloy counterparts. In fact in 1994 Privet III et al [6] stated that the unlubricated CuNiIn coatings caused a slight reduction in high cycle fatigue life as compared to the uncoated Ti 6242 (Titanium, 6% Aluminum, 2% Tin, 4% Zirconium, 2% Molybdenum, 0.1% Silicon) mated baseline tests. In 2000 Freimanis et al conducted a fretting wear analysis of blades and their

mated disks after engine operation [7]. In this study it was found that the solid lubricant had worn away and the CuNiIn coated dovetails had caused significant damage to the uncoated disk. This clearly shows that the CuNiIn coatings can have a detrimental impact on the fretting fatigue life of dovetailed components once the applied lubricants wear out.

Although the implementation of coatings and lubricants has increased component life; high maintenance costs and safety have created the need for better longer lasting coatings. In order to develop these coatings, it is important to characterize Ti6Al4V surface interactions self-mated, mated with current coatings, and mated with new coatings. This was accomplished by way of 4 research studies:

1. A fundamental study on the transition from mixed to gross slip fretting wear using Ti6Al4V mating surfaces subjected to testing at room temperature and 450°C (842°F).
2. An in-depth study was conducted on the gross slip fretting wear of three Aluminum-Bronze (Al-bronze) coatings of different copper to aluminum (Cu/Al) ratios at room temperature, 163°C, and 450°C.
3. A detailed wear mode analysis was conducted on the gross slip fretting wear of Ti6Al4V mated surfaces as well as Ti6Al4V worn against plasma sprayed copper-nickel-indium (CuNiIn), aluminum-bronze (Al-Br), molybdenum (Mo), and nickel (Ni).
4. A study was conducted to test a new mitigation strategy using thin, hard, and inert PVD coatings (TiAlN and CrCN) to protect the Ti6Al4V worn against the CuNiIn and Ni thermal sprayed coatings.

2. Effect of High Temperature on the Characterization of Fretting Wear Regimes at Ti6Al4V Interfaces

Fretting wear is commonly associated with stick, partial stick, mixed, and gross slip wear [4, 8-15]. When mating surfaces are subjected to low contact loads and relatively long displacements, gross slip will occur yielding high wear. As the contact load increases and/or the stroke length decreases, “mixed” fretting will occur. The mixed fretting regime is complex and involves surface adhesion that results in a mixture of stick and slip throughout the wear track. This minimizes wear and increases galling and material transfer. If the contacts are rounded and the load and/or stroke is sufficiently small, then “partial stick” may occur. The idea of partial stick was first described by Mindlin [8] in 1949. The contact pressure distribution caused by the rounded contact allows the center region to stick while a wear annulus forms around the outside edge, as shown in Figure 2.1. As the contact load is increased, the slip annulus decreases until there is no relative motion and “full stick” occurs.

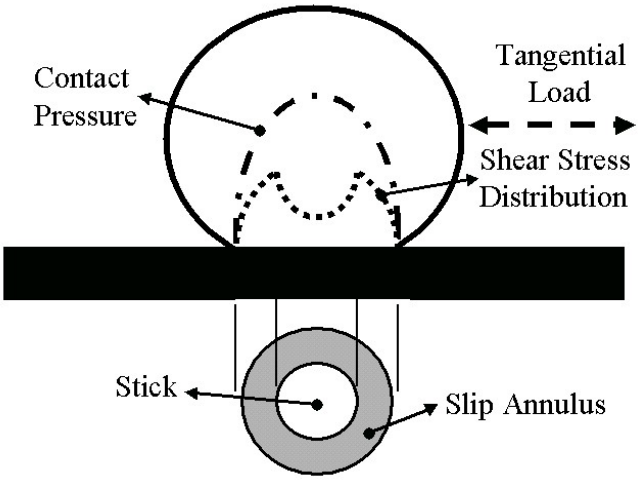

Figure 2.1. Partial stick fretting wear

This was a study on the transition from mixed to gross slip fretting wear using Ti6Al4V mating surfaces subjected to testing at room temperature and 450°C (842°F). The premise for this study is based on the need for new coatings and surface treatments to prolong the life of Ti6Al4V bladed disk assemblies. Creating an understanding of the transition of gross slip to mixed fretting wear at ambient and 450°C will lead to new and improved test methodologies for the evaluation of future coatings, lubricants, and materials.

2.1 Experimental

2.1.1 Specimens

The contact geometry used was an elliptical shaped Ti6Al4V pin pressed against a flat Ti6Al4V disk. The ellipsoid, shown in Figure 2.2, was designed to eliminate stress concentrations that lead to contact edge effects, and to simplify alignment procedures for reproducible contact areas. The plates were flat circular disks with a diameter of 12.7 mm on the test face and 3.2 mm thick. The surface roughness for all specimens was ≈ 0.1 μm Ra.

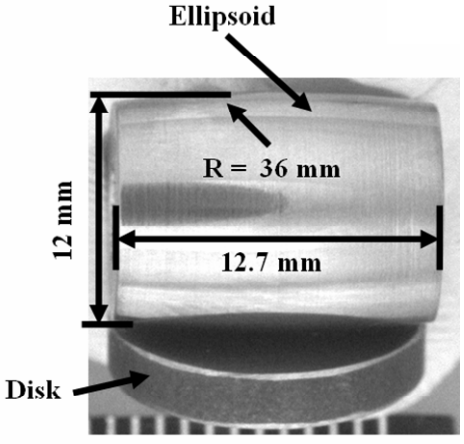

Figure 2.2. Ellipsoid contact geometry and test setup

2.1.2 Tribological Testing

The purpose of this study was to experimentally map the critical loads and stroke lengths associated with the transition from mixed to gross slip fretting wear at room temperature and 450°C. The high temperature tests were conducted at 450°C to simulate the upper limit that titanium alloys may experience in the compressor. Four repeat tests were performed at various stroke lengths ranging from 45μm up to 230μm with an oscillation speed of 30Hz. During each test a normal load of 200N, yielding a maximum Hertzian contact pressure of ≈ 1GPa, was initially applied to impose a mixed fretting condition at the interface. The applied normal load was reduced in increments of 10N every 3 minutes (5400 cycles) until it reached 0N. For the duration of each test the root mean square (RMS) of the friction data and the frictional hysteresis was recorded. The frictional hysteresis was obtained using a laser measuring system and a piezo electric transducer. The fretting wear tribometer, shown in Figure 2.3, uses the piezo electric transducer to measure friction between the mating specimens. A laser measurement device is then used to continuously track the position of the oscillating specimen during the test. The real time friction and displacement traces are then plotted to produce hysteresis loops as shown in Figure 2.4. These plots show the friction force as a function of position while the oscillating specimen moves through one full cycle of the test (positive friction is forward and negative friction is backward). The shape of these plots indicates the fretting mechanism/regime the interface is experiencing [8, 16-21]. Elliptical shaped hysteresis loops, Figure 2.4A, depict mixed fretting behavior and quasi-rectangular shaped hysteresis loops, Figure 2.4B, depict gross slip behavior. The area within the hysteresis loop reflects the energy dissipated by the system. The energy loss per cycle was calculated by using a midpoint rectangular approximation to integrate the area of each loop. Once the varied load tests were completed, a number of tests were conducted with constant load to give further insight into the surface interactions and wear mechanisms that occur. Post test analysis was performed using a scanning electron microscope (SEM) and a 3-D contact profilometer.

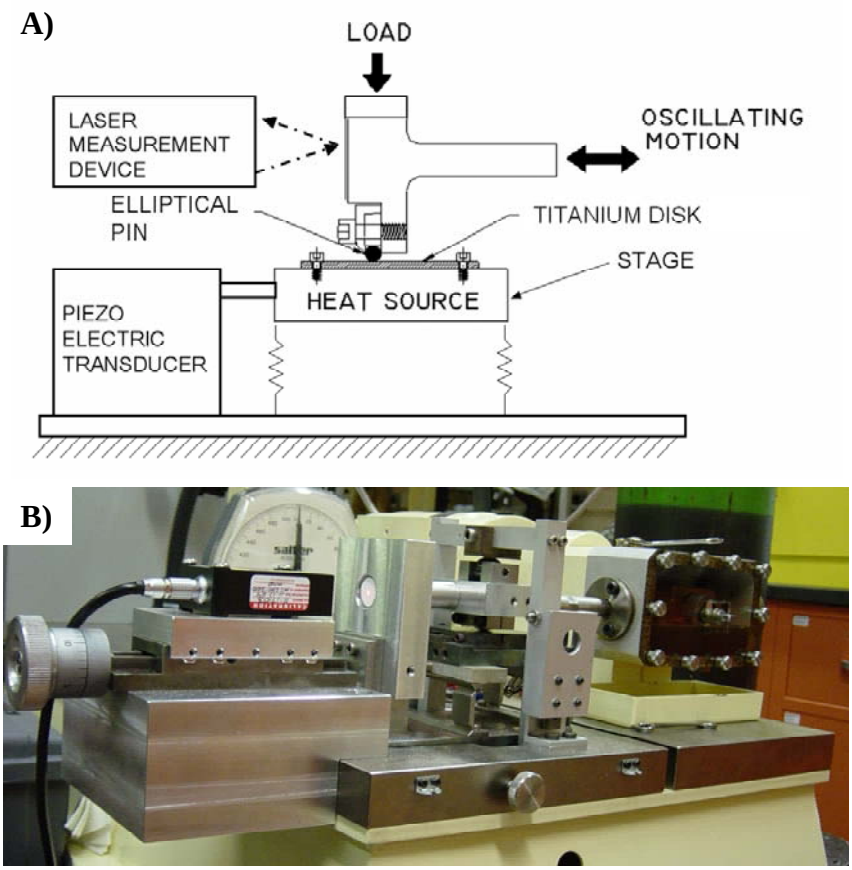

Figure 2.3. A) Fretting wear tribometer schematic and B) Fretting wear tribometer picture

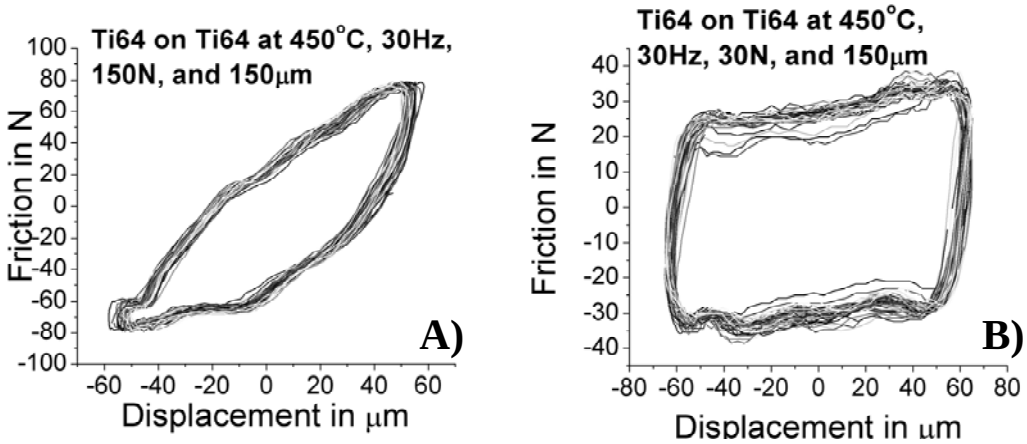

Figure 2.4. Examples of fretting hysteresis loops. A) Shows mixed fretting and B) Shows gross slip. Full stick would be plotted as a straight line.

2.2 Results

2.2.1 Transition Determination

Varied load tests were first conducted at room temperature. These tests had very distinct transitions from mixed fretting to gross slip. An example of the sharp changes in friction force and hysteresis loops is shown in Figure 2.5, which is one particular test conducted at a 150μm stroke length. An in depth investigation of the room temperature phenomena has been reported [16]. This investigation determined that at a critical load and stroke length, adhesive junctions formed between the surfaces fatigue and rupture into pieces forming third body particles that ultimately become rutile titanium oxide. This causes an immediate transition from mixed to gross slip fretting.

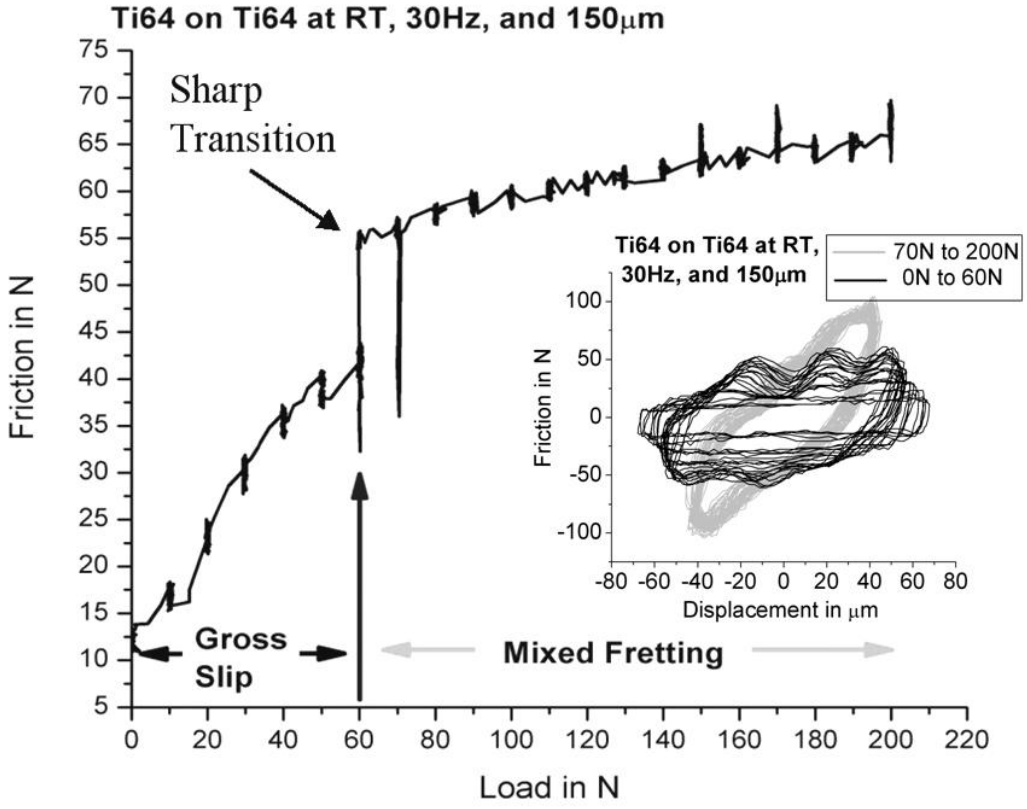

Figure 2.5. Varied load test showing the normal load at which the transition from mixed to gross slip fretting occurred using friction force. The small graph shows the mixed fretting hysteresis loops in gray and the gross slip loops in black.

Once the room temperature varied load tests were completed the tests were then repeated at 450°C. The data from these tests, shown in Figure 2.6, revealed different behavior than the room temperature tests. The sharp transition between regimes, seen in Figure 2.5, was not apparent at 450°C. It was then decided to plot the energy loss per cycle, the area within the hysteresis loops, with respect to the normal load for both the room temperature and 450°C tests. Figure 2.7 and Figure 2.8 show the energy dissipation plots for the respective low and high temperature examples. It was noticed that the plots for both cases show the same trend. In

addition, the sharp transition in all the room temperature tests occurred at a maximum value in the energy loss data. With this in mind a curve was fit to the energy dissipation plots from the high temperature tests. The curve was then differentiated to find the maximum energy loss during the test, and at what load it occurred. The maximum energy loss in the 450°C tests was then investigated to determine if it occurred at the transition load from mixed to gross slip fretting. For the 200μm example shown in Figure 2.8, the transition load was determined to be 80N. The transition load was validated by conducting tests at various loads using the same 200μm stroke length. Each test was conducted at one constant load. Figure 2.9 shows the hysteresis loops that were recorded during each test. At 80N and 90N, the shape of the loops starts to become rectangular signifying gross slip. Wear mode analysis was also conducted after each test at 200μm to further verify the transition load at 80N. The maximum energy loss per cycle was then used as a transition criterion for all of the subsequent tests conducted.

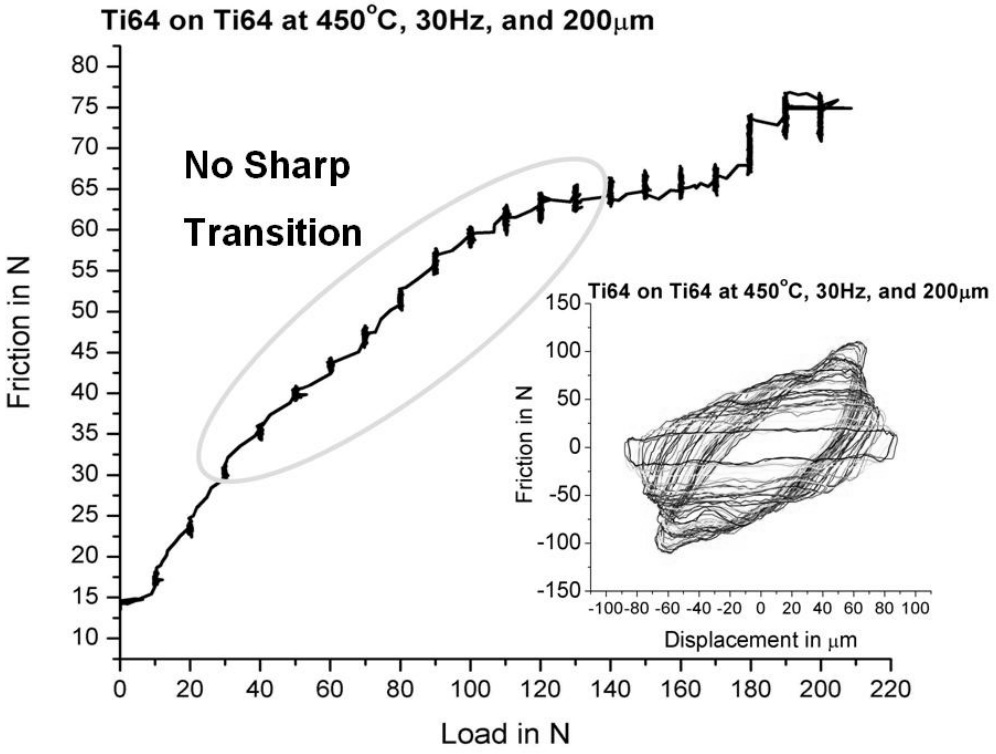

Figure 2.6. Varied load test showing that the transition from mixed to gross slip fretting appears to be gradual at high temperature. The small graph shows the hysteresis loops that were recorded during the test.

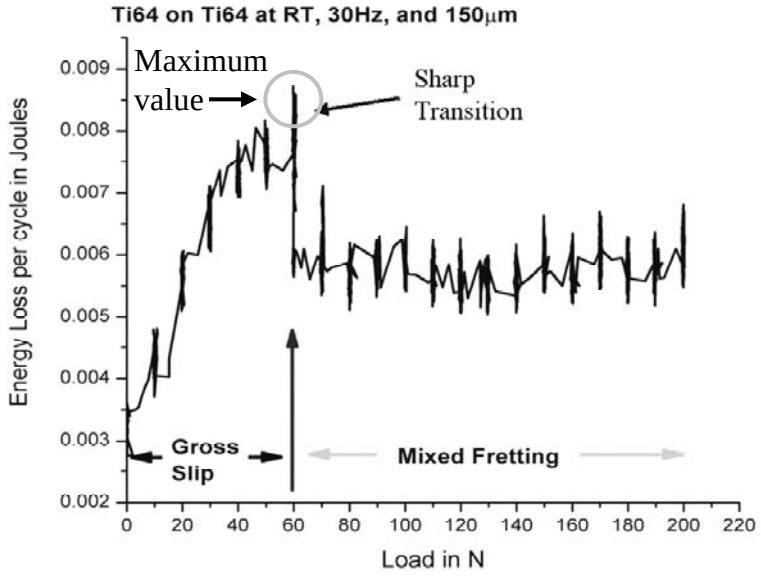

Figure 2.7. Varied load showing the normal load at which the transition from mixed to gross slip fretting occurred using the energy loss per cycle.

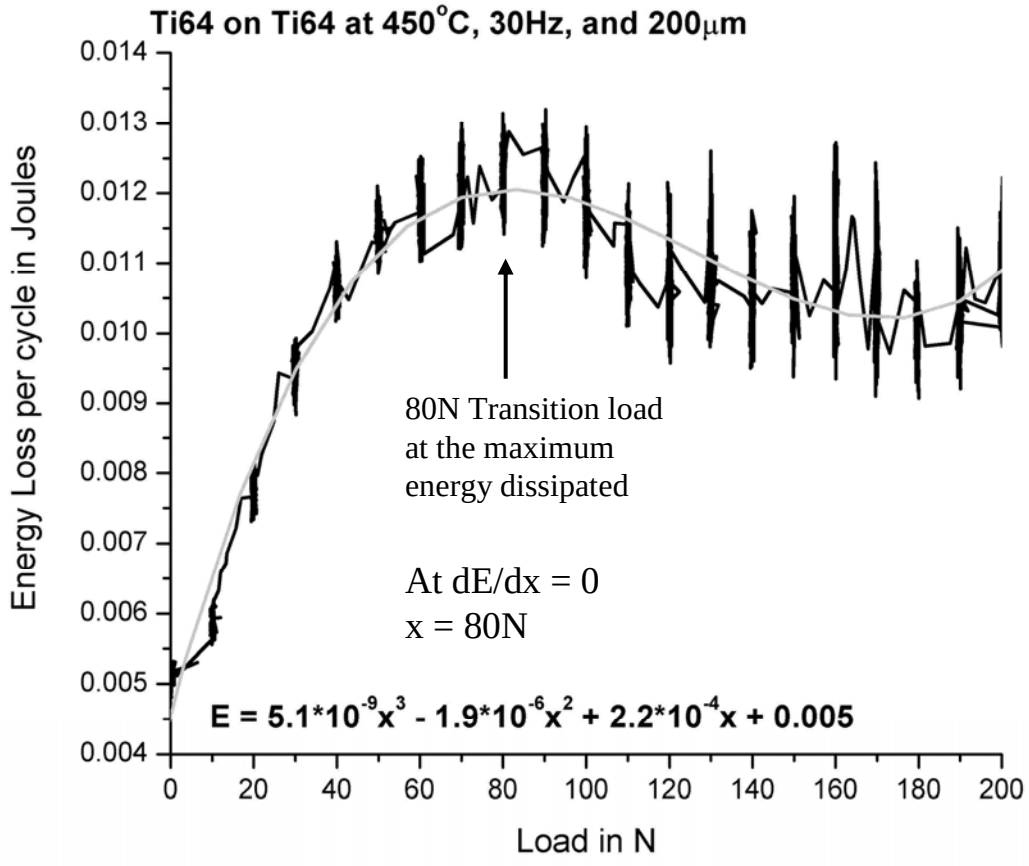

Figure 2.8. Varied load showing the load at which the energy loss per cycle is plotted versus the normal load applied. The equation displayed is a curve that was fit to the data.

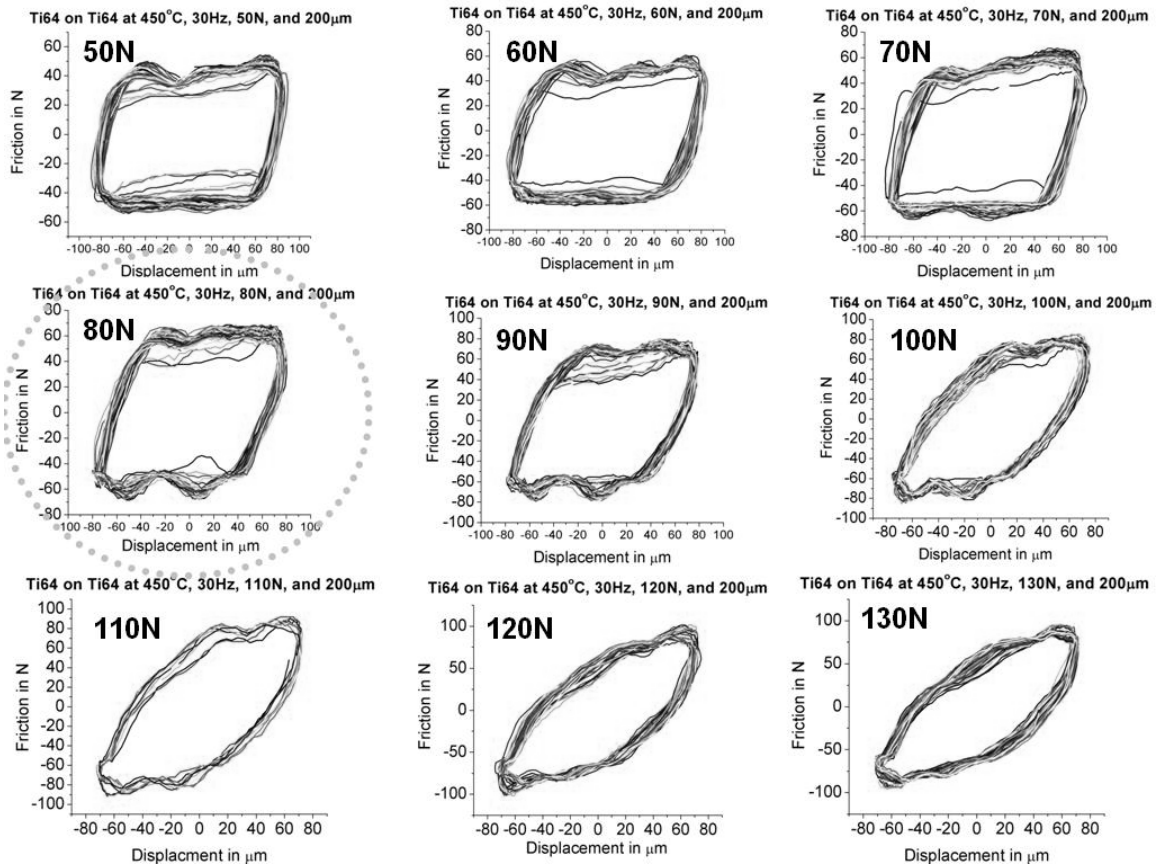

Figure 2.9. The hysteresis loops plotted as friction vs. displacement for each cycle of the test. Each of the nine plots represents a separate test at the given load.

Upon the completion of all the tests, the transition loads at each stroke length were compiled and plotted in Figure 2.10. The 450°C tests appear to be more susceptible to mixed fretting than the room temperature tests at longer stroke lengths. However, at the short stroke lengths the data converges. There is some scatter in the data at 45μm stroke length that can be attributed to the limitations of the machine.

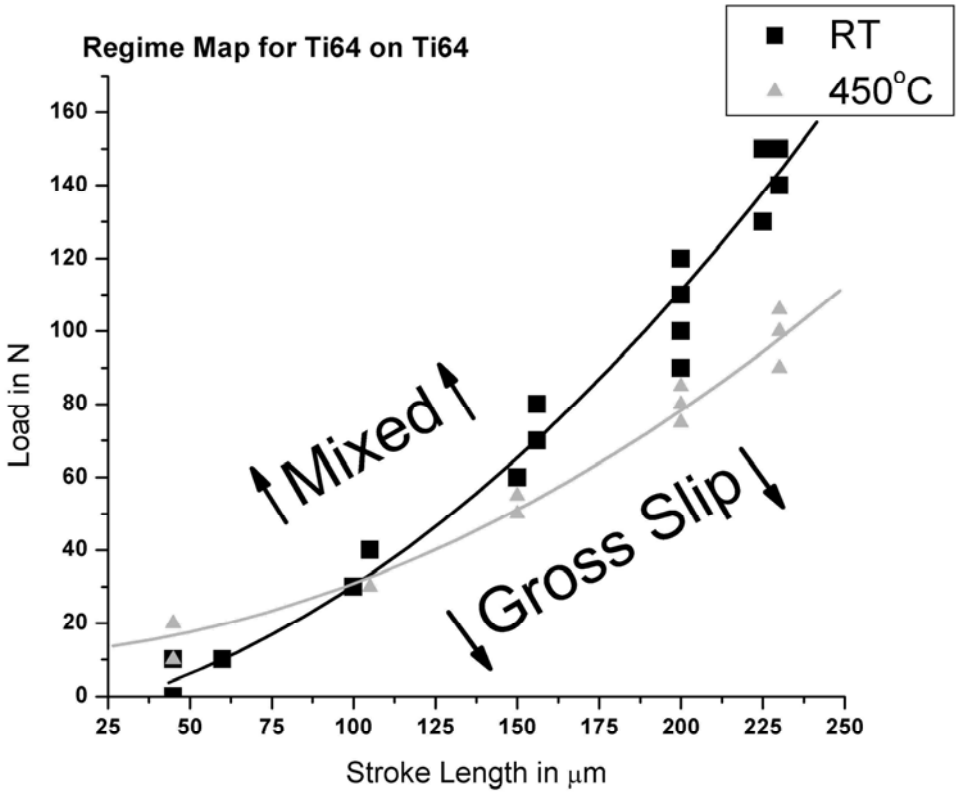

Figure 2.10. The plot shows the load at which the transition from mixed to gross slip fretting occurred for each stroke length. The area above each line corresponds to the conditions that promote mixed fretting wear.

2.2.2 Coefficient of Friction

Friction coefficient can be complex in fretting wear tests. Tests that are conducted in the mixed and partial stick regime yield friction data that cannot be used to determine the dynamic coefficient of friction. The coefficient of friction data for the tests conducted in this study were determined from the gross slip fretting tests only. Therefore, the friction data from all of the varied load tests were separated and the gross slip coefficient of friction was plotted in Figure 2.11 and 2.12. The scattered data from both temperatures show that the coefficient of friction varies inversely with the applied normal load. This trend can also be seen in the data from the tests conducted at constant load, as represented by the dark stars and triangles in Figure 2.11 and 2.12.

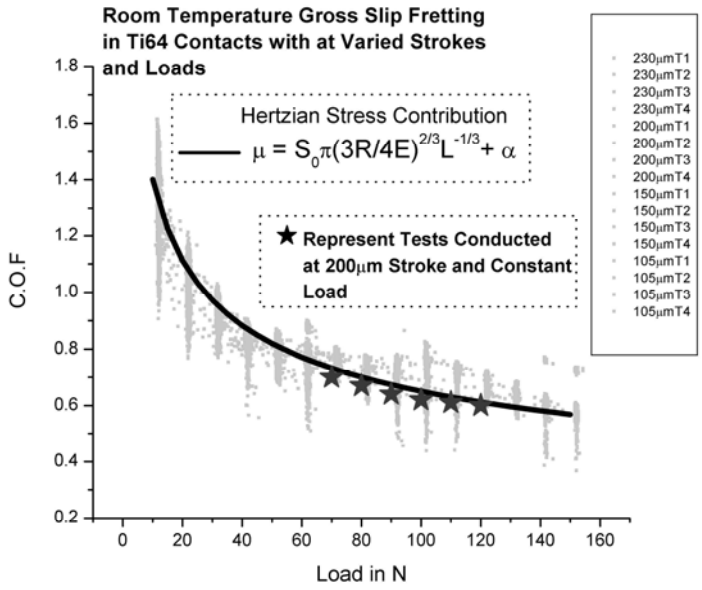

Figure 2.11. The plot shows the change in coefficient of friction with respect to load. The dark line is a plot of the Hertzian contact model and the dark stars are single tests conducted at each specific load.

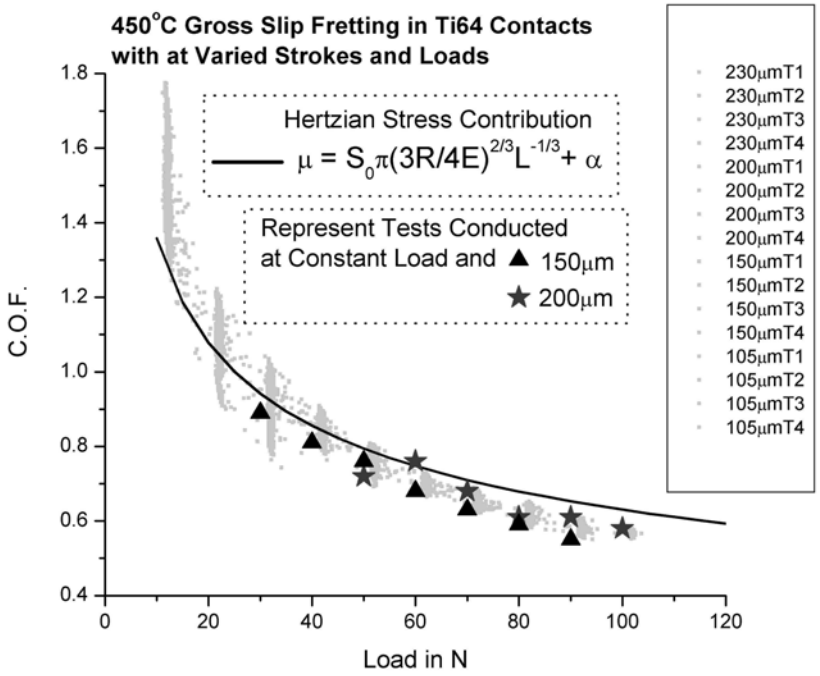

Figure 2.12. The plot shows the change in coefficient of friction with respect to load. The dark line is a plot of the Hertzian contact model and the dark stars/triangles are single tests conducted at each specific load.

2.2.3 Wear Mode Analysis

A complete wear mode analysis was previously conducted [16] on the room temperature Ti6Al4V specimens and will be summarized. The bulk of this work focused on the wear mechanisms associated with the tests conducted at 450°C.

At room temperature, the gross slip tests showed high wear with lots of debris contained within the contact area, and evidence of abrasion around the edges. Near the center of the wear track, where the contact stress is maximum, some localized galling occurred. In the mixed regime, the wear tracks were rough with evidence of debris around the outside of the contact region. Just inside the edge of contact the material was mounded up or extruded. The center of the contact region experienced some localized friction welding that ruptured periodically during the test and when the surfaces are pulled apart after the completion of the test. In the partial stick regime, the central region was virtually unworn. At the edges of contact the material was mounded up or extruded, similar to the mixed fretting tests. At the extreme edges of the contact there was some evidence of abrasion due to wear debris.

At 450°C and gross slip fretting conditions, the Ti6Al4V interfaces experience high wear, shown in Figure 2.13. Figure 2.14 shows an SEM micrograph of a typical gross slip fretting wear scar on the surface of the Ti64 specimens tested at 450°C. The wear track is surrounded by an accumulation of loose debris, with pockets of debris trapped within the contact region. Figure 2.15 indicates that loose debris at the leading and trailing edges of the contact scrape and score the surface as it is evacuated from the wear track. Figure 2.16 shows that at the center of the contact, where the stress is highest, pockets of loose debris are crushed and ground up into fine particles that polish localized regions of the contact surface.

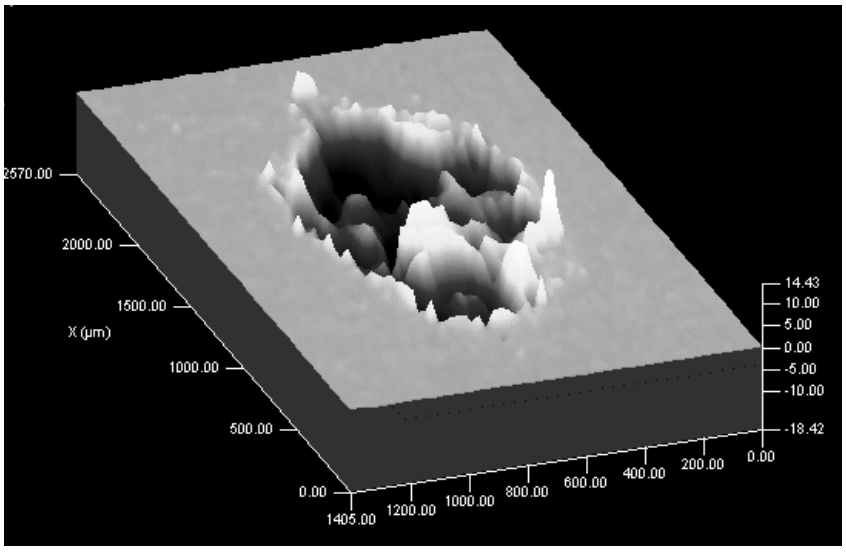

Figure 2.13. The plot shows a 3D contact scan of the fretting damage on the surface of the flat disk after a test was conducted at 450°C with a 200μm stroke length and 50N normal load for 7500 cycles. All dimensions shown are in μm.

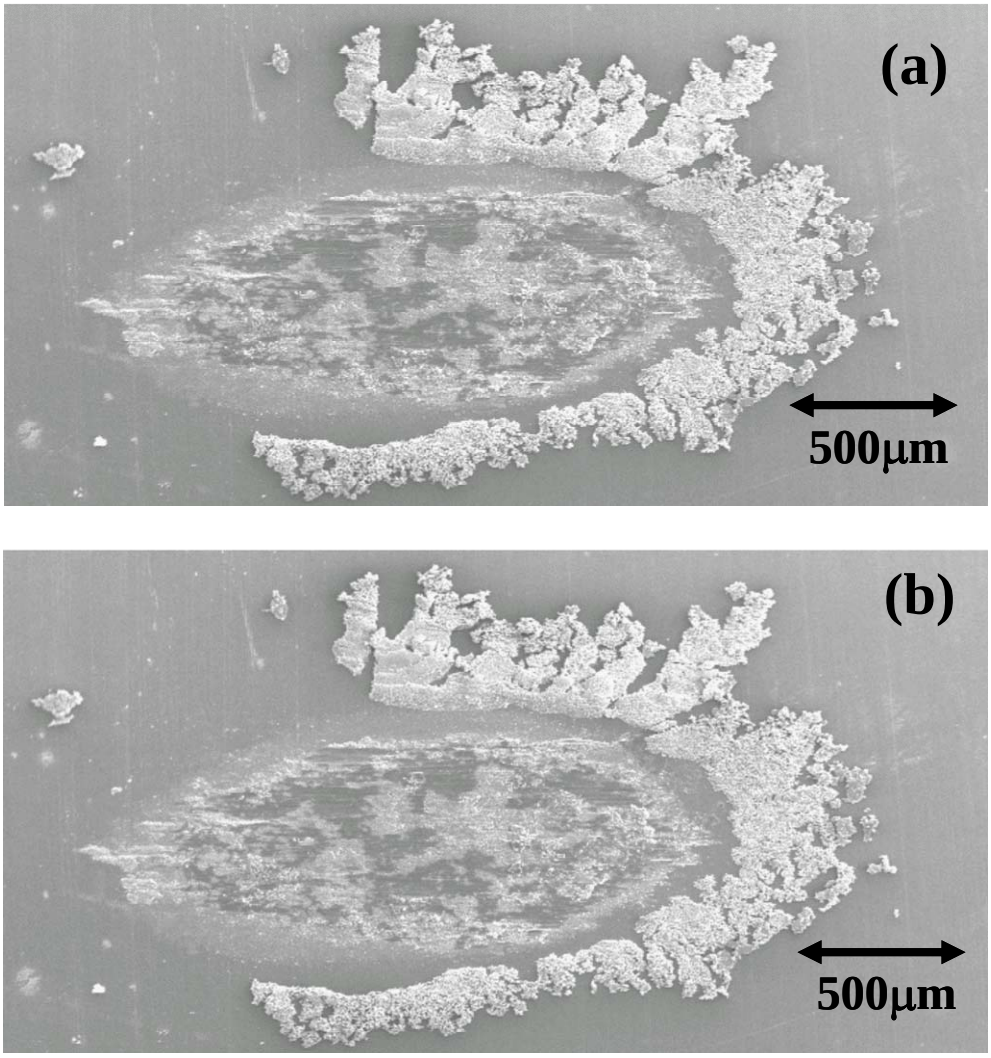

Figure 2.14. The plot shows an SEM micrograph of gross slip fretting damage on the surface of the (a) flat disk and (b) elliptical pin after a test was conducted at 450°C with a 200μm stroke length and 50N normal load for 7500 cycles.

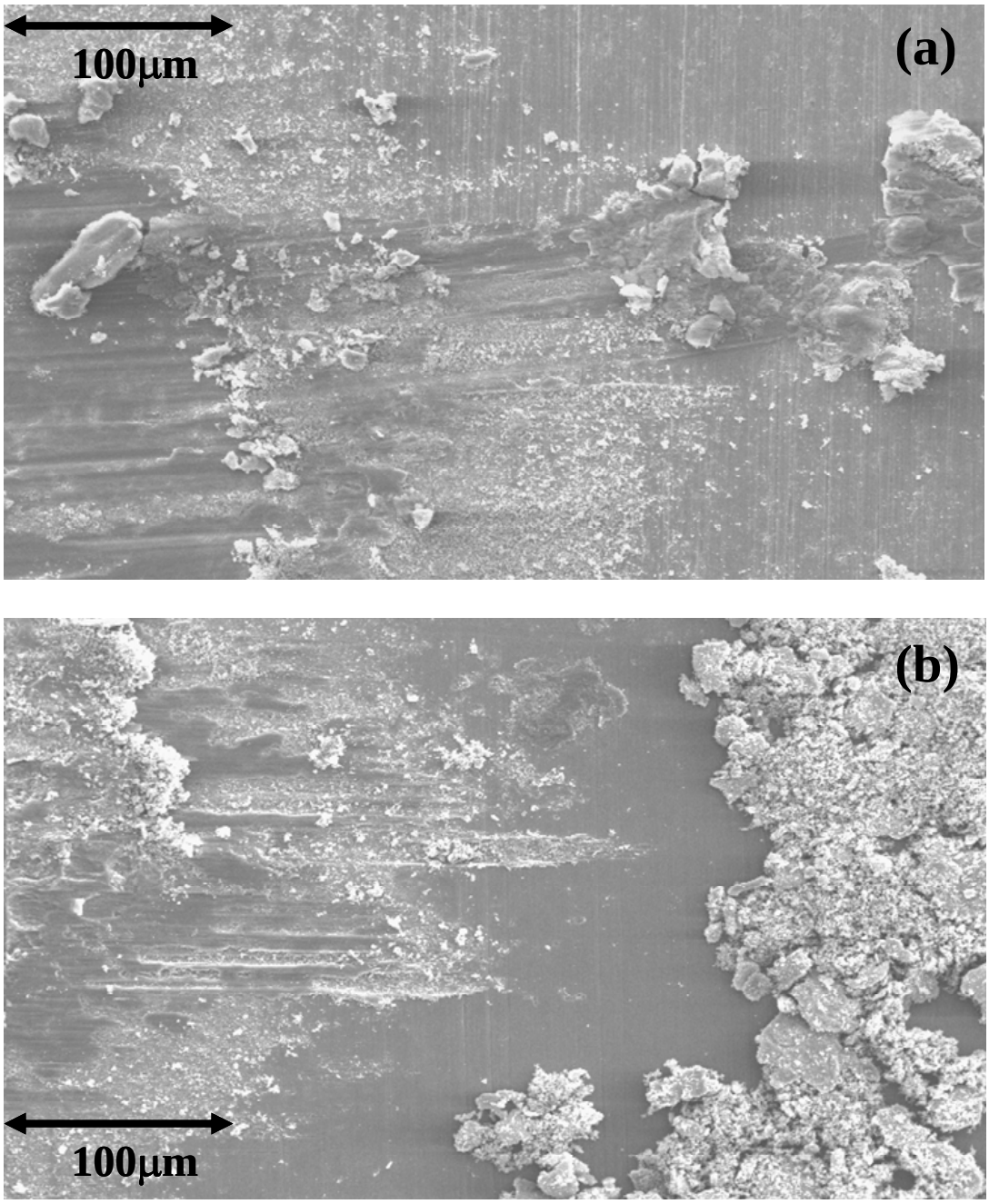

Figure 2.15. The plot shows an SEM micrograph of the edge of the wear track on the (a) flat disk and (b) elliptical pin after a test was conducted at 450°C with a 200μm stroke length and 50N normal load for 7500 cycles.

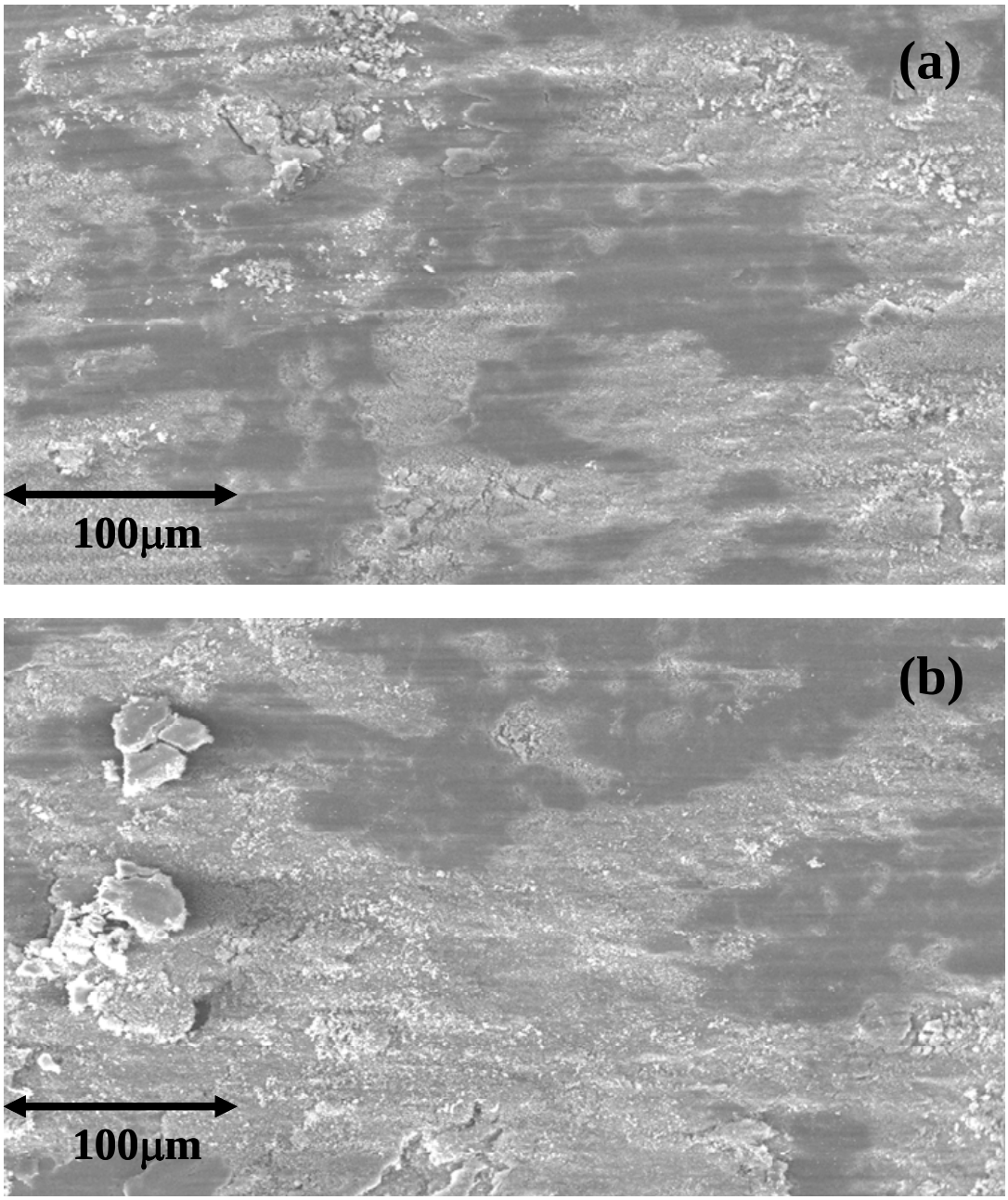

Figure 2.16. The plot shows an SEM micrograph of the center of the wear track on the (a) flat disk and (b) elliptical pin after a test was conducted at 450°C with a 200μm stroke length and 50N normal load for 7500 cycles.

Upon the transition into the mixed fretting wear regime, the wear mode changes. Figure 2.17 shows a micrograph of a typical mixed fretting wear scar on Ti6Al4V tested at 450°C. Less debris formation is noted. Instead of the pockets of crushed debris that are seen in gross slip, the center of the contact shows the formation of large transfer particles and a large crater where material has been extracted from the disk surface and adhered to the pin, shown in Figure 2.18. Figure 2.19 is the 3D profile of the flat disk wear track. The profile clearly shows the crater at

the center of the wear track, where material has been removed, and the mounds of material that transferred to the disk from the mating Ti6Al4V surface. At the leading and trailing edges of the wear track, the mating surfaces appear smooth with evidence of plastic flow in the direction of fretting, shown in Figure 2.20.

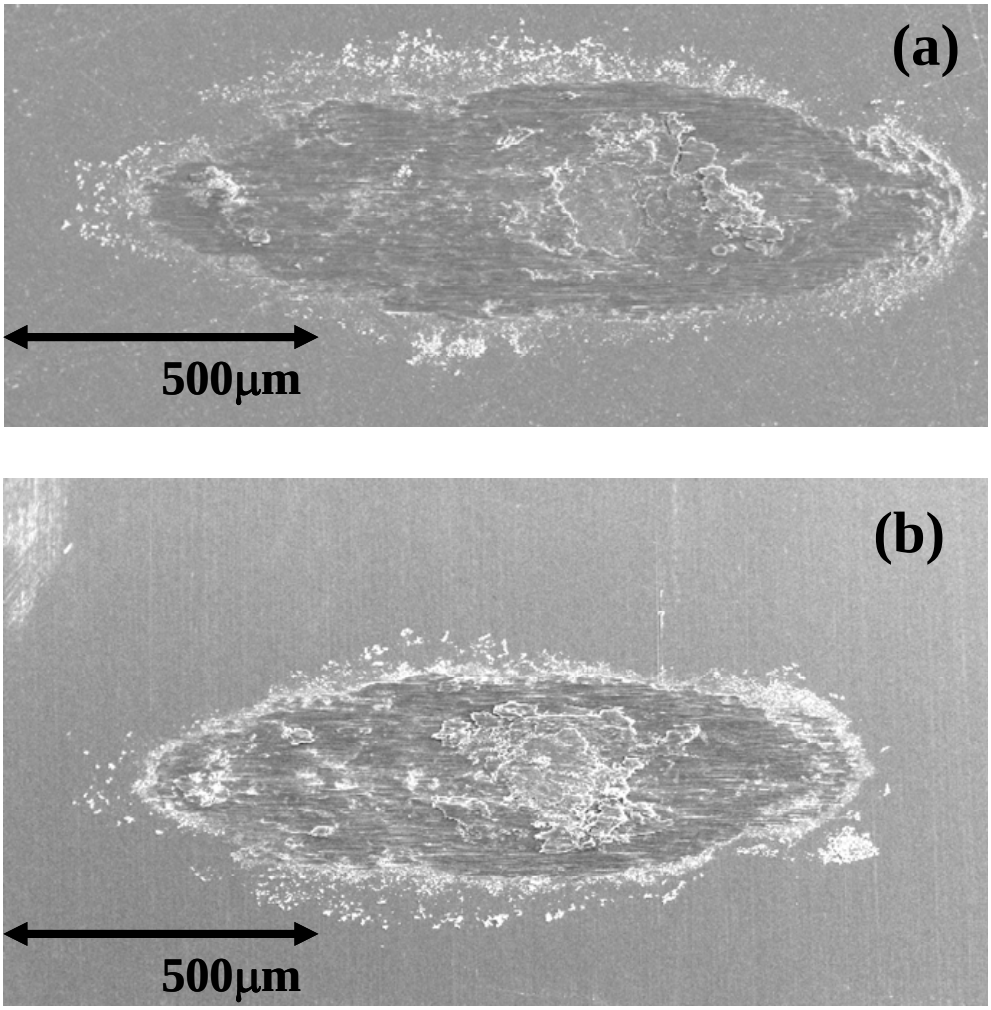

Figure 2.17. The plot shows an SEM micrograph of mixed fretting damage on the surface of the (a) flat disk and (b) elliptical pin after a test was conducted at 450°C with a 200μm stroke length and 150N normal load for 7500 cycles.

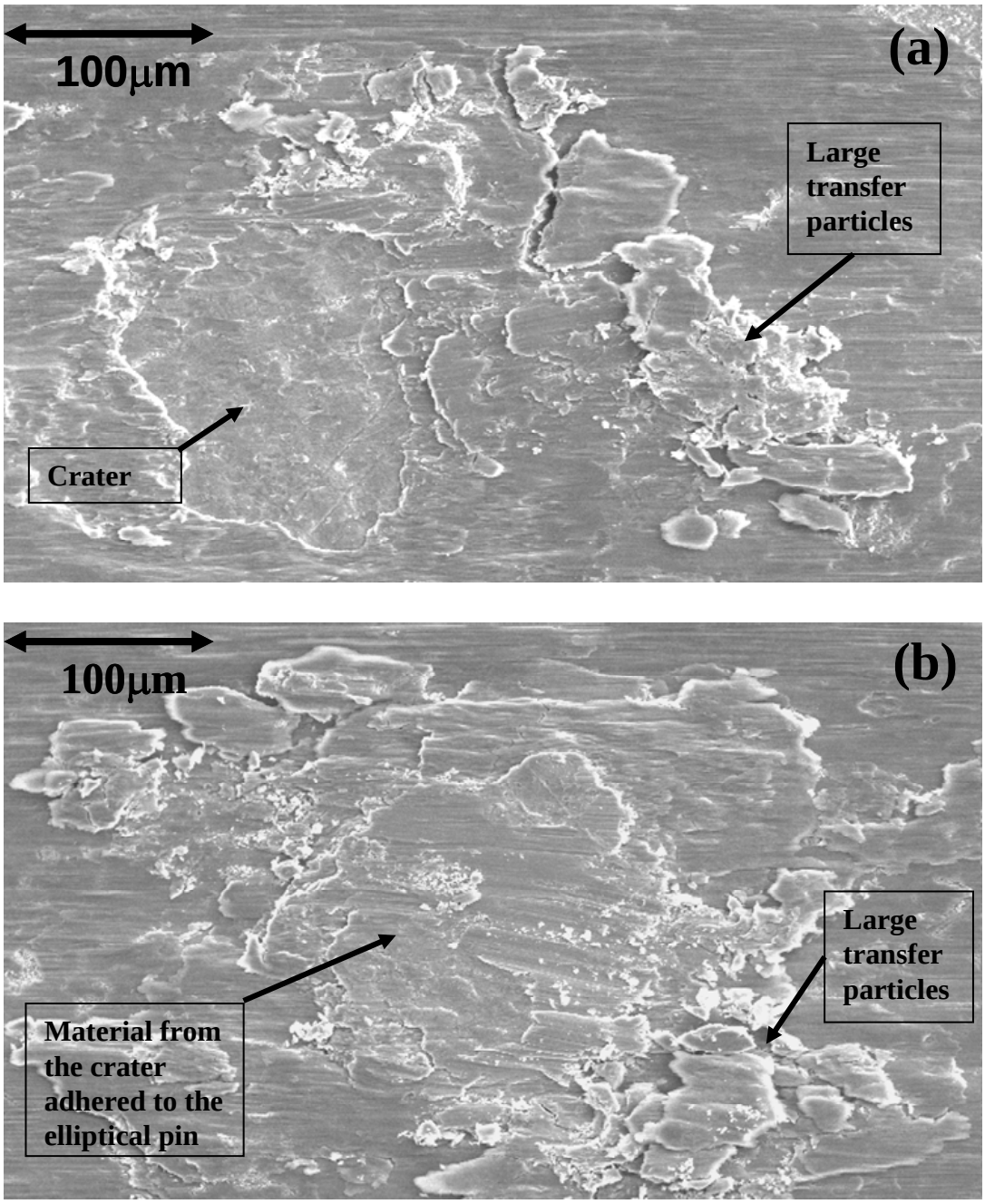

Figure 2.18. The plot shows an SEM micrograph of the center of the wear track on the (a) flat disk and (b) elliptical pin after a test was conducted at 450°C with a 200μm stroke length and 150N normal load for 7500 cycles.

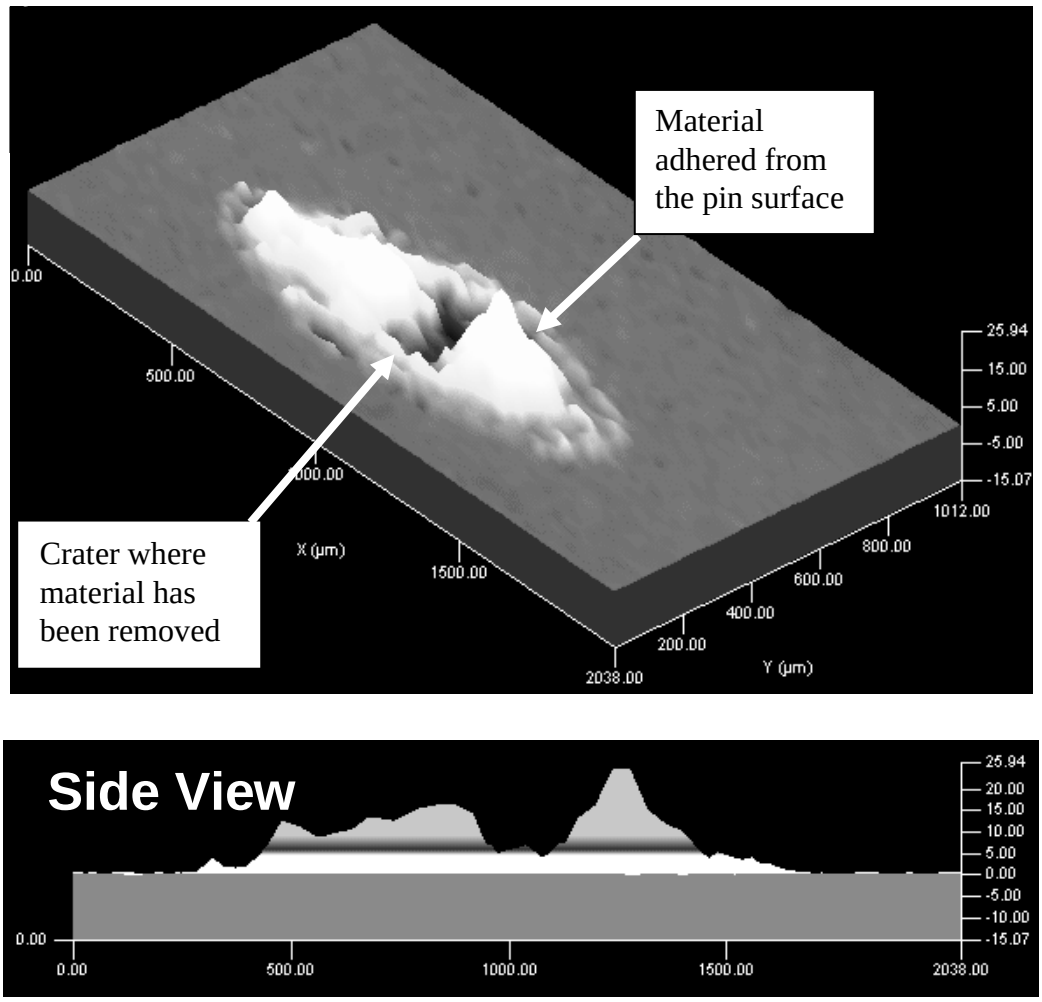

Figure 2.19. The plot shows a 3D contact scan with a side view of the fretting damage on the surface of the flat disk after a test was conducted at 450°C with a 200µm stroke length and 150N normal load for 7500 cycles. All dimensions shown are in µm.

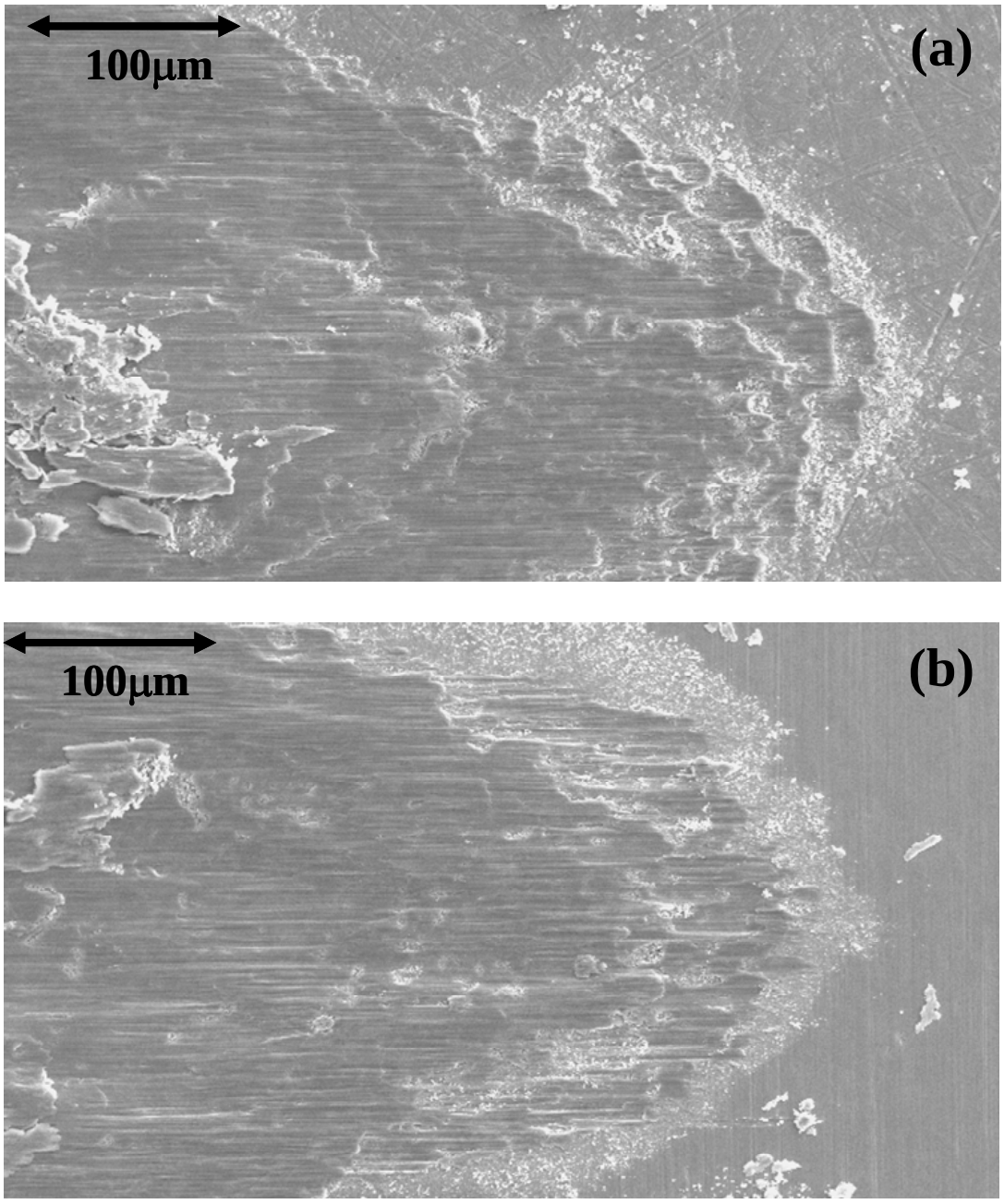

Figure 2.20. The plot shows an SEM micrograph of the edge of the wear track on the (a) flat disk and (b) elliptical pin after a test was conducted at 450°C with a 200μm stroke length and 150N normal load for 7500 cycles.

At the highest normal loads, the wear mode transitioned from mixed fretting wear to partial stick. Partial stick fretting occurs when the tangential forces cannot overcome the contact stresses in the center of the contact. This inhibits gross surface damage in the center of the contact and promotes gross slip and/or mixed fretting wear at the edges of the contact. Figure 2.21 shows a micrograph of a typical partial stick fretting wear scar on the surface of the

Ti6Al4V specimens tested at 450°C. The 3D contact profile, illustrated in Figure 2.22, shows that galling occurs at the edges of the stick region and promotes material transfer between the surfaces. In this particular case, the material has adhered to one of the leading edges of the stick region. Depicted in Figure 2.23, the galled region on the leading edge of contact shows that material has been removed and transferred from one surface to the other. Evidence of gross slip wear just beyond the galled region was also observed.

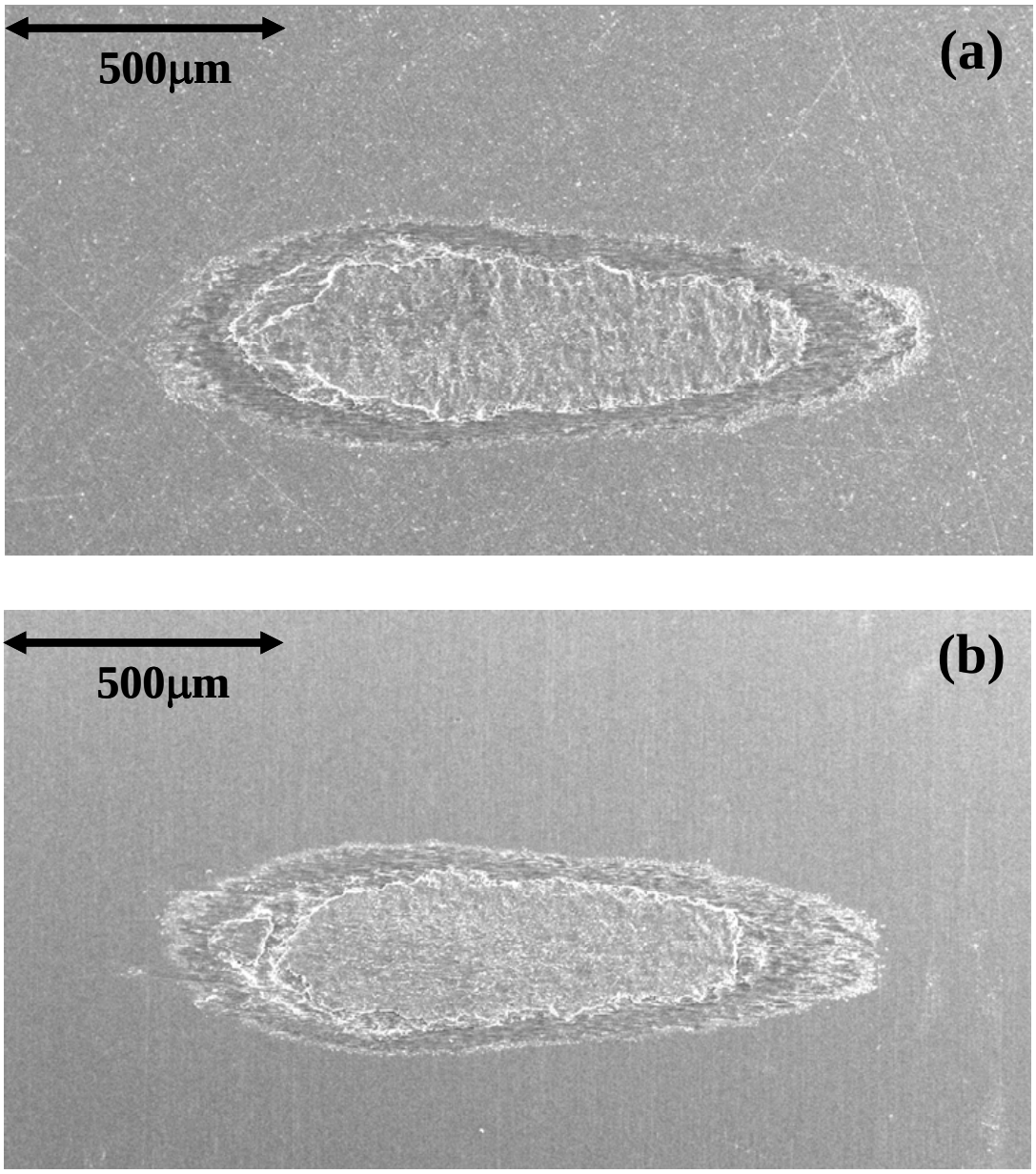

Figure 2.21. The plot shows an SEM micrograph of partial stick fretting damage on the surface of the (a) flat disk and (b) elliptical pin after a test was conducted at 450°C with a 200μm stroke length and 180N normal load for 7500 cycles.

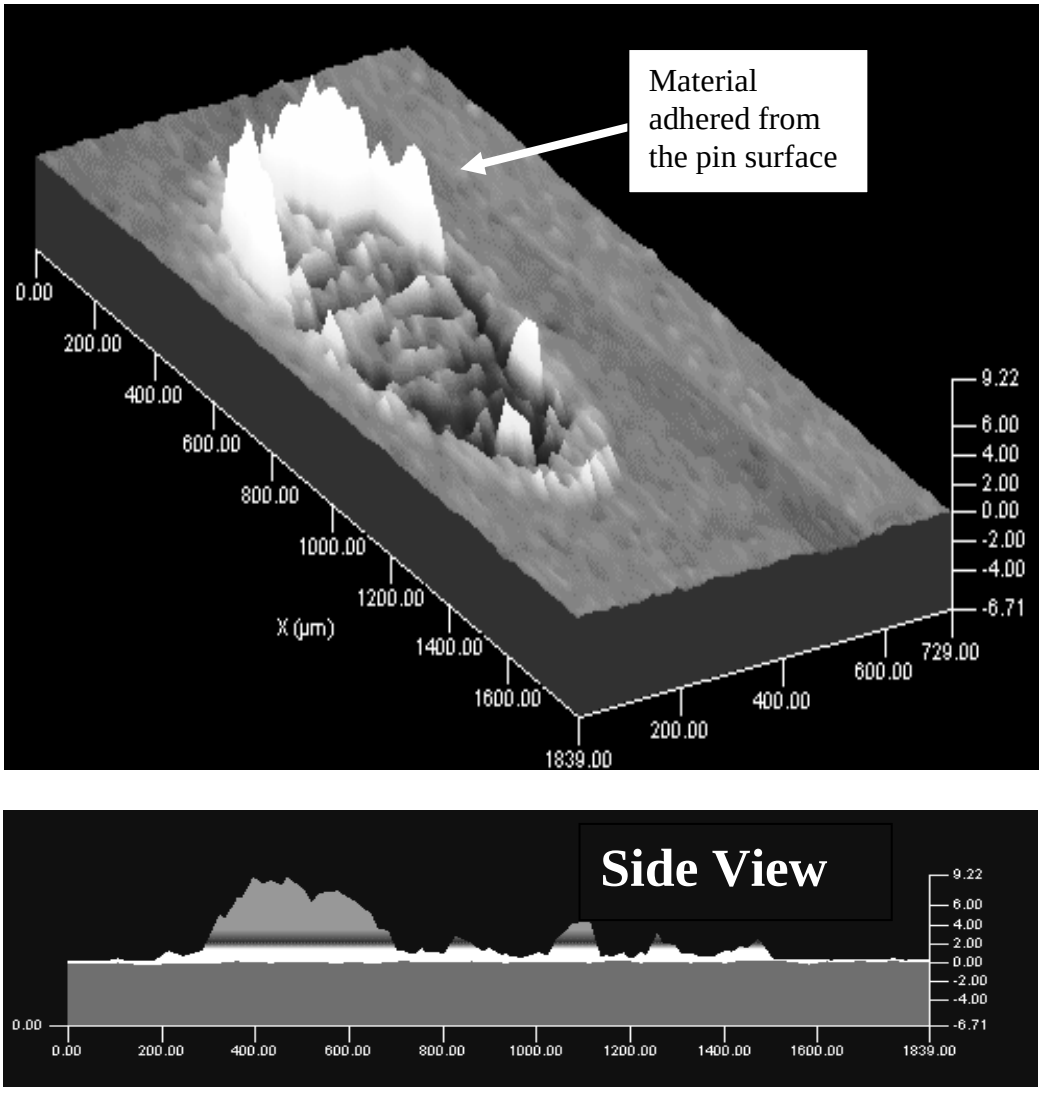

Figure 2.22. The plot shows a 3D contact scan with a side view of the partial stick fretting damage on the surface of the flat disk after a test was conducted at 450°C with a 200µm stroke length and 180N normal load for 7500 cycles. All dimensions shown are in µm.

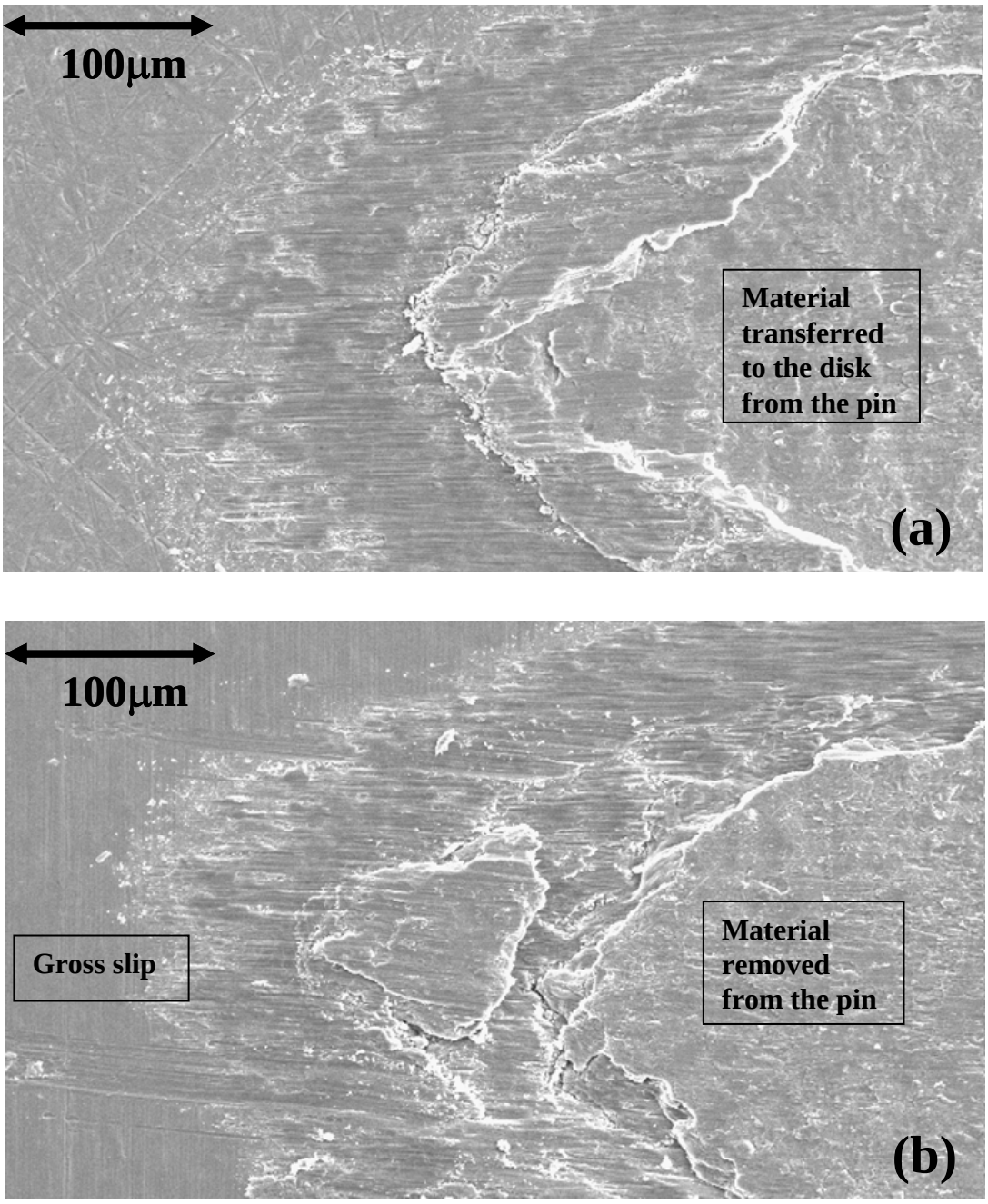

Figure 2.23. The plot shows an SEM micrograph of the edge of the wear track on the (a) flat disk and (b) elliptical pin after a test was conducted at 450°C with a 200μm stroke length and 180N normal load for 7500 cycles.

2.3 Discussion

The varied load tests conducted were designed to determine the amount of load required to impose mixed fretting between mating Ti6Al4V surfaces at various stroke lengths. In the room temperature tests, the transition from mixed to gross slip fretting is abrupt and dramatic. The transition can even be seen in friction data as a sharp drop. This can be explained using the

work by Sauger [2] and Zhou [22] et al on the formation of a tribologically transformed structure (TTS) induced by fretting wear of titanium contacts. TTS is formed by a critical accumulation of plastic deformation, or strain hardening, between mating titanium surfaces and can have as much as twice the hardness of the bulk titanium. Based on the work by Sauger and Zhou, it is believed that strain hardening occurs at the Ti6Al4V interface during the mixed fretting portion of the room temperature varied load tests. Once formed, the hardened TTS layer is very brittle and fractures instantly during the transition from mixed to gross slip fretting [16]. This causes the surfaces to be separated by a layer of metal and metal oxide debris, which can reduce friction [23] and impede surface adhesion.

At elevated temperatures, the transition from mixed to gross slip fretting is gradual and can be determined by the critical load at which the maximum energy loss per cycle occurred. At room temperature, strain hardening (TTS) at the interface is believed to be the primary cause of the acute transition from mixed to gross slip fretting. This sharp transition was not seen at 450°C because more slip systems may be active making it more difficult to build up a network of dislocations that will develop into strain hardening. Therefore, the surfaces do not experience the brittle fracture observed at room temperature.

In addition to the impedance of strain hardening, the hot titanium specimens undergo accelerated surface oxidation and substantial softening. Initially it was believed that the accelerated surface oxidation would favor gross slip wear because of the potential lubricity of the TiO_2 formed at the interface [23]. However, testing showed that the elevated temperature tests favor mixed fretting and increase the propensity for the contacts to gall. This suggests that the softening of the surface becomes the most influential factor governing the transition from mixed to gross slip fretting at high temperatures in Ti6Al4V contacts. At 450°C the Ti6Al4V specimens experience approximately a 50% reduction in tensile strength, a 40% reduction in compressive and shear strength, and a 20% reduction in elastic modulus [24]. The reduction in tensile strength, shear strength and elastic modulus, caused by the heating of the specimens, allows the surface to deform readily without strain hardening. This allows the interface to accommodate longer stroke lengths and/or lower loads while fretting occurs within the mixed regime.

During the varied load tests, it was observed that the dynamic coefficient of friction (COF) varied inversely with applied normal load at room temperature and 450°C, Figure 2.11 and 2.12. This is a phenomenon that was studied extensively by Bowers et al [25-26] in the late 1960's and early 1970's for polymers and thin solid films and then again by Singer et al [27] in the early 1990's for MoS_2 coatings. A Hertzian contact model was used to explain why the friction decreases with increasing load, and to predict what the friction would be at a given load. The model is derived from an equation that relates the coefficient of friction to the material and mechanical properties of the contact. The basic form of the equation is:

$$\mu = S/P$$

Where S is the shear strength of the interface and P is the contact pressure. The shear strength can then be approximated as:

$$S = S_o + \alpha P$$

Which then gives the expression:

$$\mu = (S_o/P) + \alpha$$

In this equation S_o and α represent constants derived from the material properties controlling friction. P is the Hertzian contact pressure for smooth balls and flat substrates loaded below the elastic limit, yielding the following equation in final form:

$$\mu = S_o\pi(3R/4E)^{2/3}L^{-1/3} + \alpha$$

Where E is the elastic modulus of the couples, R is the effective contact radius, and L is the normal load.

Using this equation and modifying it to fit the elliptical contact, a curve was fit to all of the room temperature and high temperature gross slip coefficient of friction measurements, Figure 2.11 and 2.12. For the room temperature tests, the curve displays a good correlation with the Hertzian contact model. At high temperature, the model does not fit quite as well. The data is a function of $L^{-1/2}$ instead of the $L^{-1/3}$. This may be due to the accelerated surface oxidation and the substantial interface softening that occurs at high temperature.

2.4 Conclusions

Using the combination of RMS friction, hysteresis loops, energy loss, surface profilometry, and scanning electron microscopy, the stroke length and loading conditions that induce mixed fretting wear for Ti6Al4V mating surfaces were characterized at room temperature and 450°C. This work revealed that:

- The transition from mixed to gross slip fretting occurs at higher loads in the room temperature fretting tests. This means that elevating the temperature promotes mixed fretting wear.
- The transition from mixed to gross slip fretting wear is an abrupt transition at room temperature. This may be caused by the strain hardening of the surface, which leads to brittle fracture of the surface and create large amounts of debris at the interface. At high temperatures, the softened surface is unable to strain harden resulting in a gradual transition from mixed to gross slip fretting.
- The energy loss per cycle was needed to determine the transition from mixed to gross slip fretting at 450°C. Because the transition was gradual, the maximum energy loss per cycle was used to determine the critical load at which the interface changed from mixed to gross slip fretting.
- The variance in the coefficient of friction with respect to the applied normal load shows a good correlation with the Hertzian contact model at room temperature. At high temperature, the Hertzian model fits the trend, but does not correlate as well as it does at room temperature. This may be due to the accelerated surface oxidation and the substantial interface softening that occurs at high temperature.

3. Gross Slip Fretting Wear Analysis of Aluminum Bronze Coatings for Ti6Al4V Aerospace Components

In this study an in-depth evaluation was conducted on the gross slip fretting wear of three Aluminum-Bronze (Al-bronze) coatings, two plasma sprayed coatings of different copper to aluminum (Cu/Al) ratios and one cathodic arc coating. Bench level gross slip fretting experiments and post test analysis were used to determine the wear mechanisms and damage associated with unlubricated Al-bronze coatings worn against uncoated Ti6Al4V surfaces at room temperature, 163°C, and 450°C. The purpose of this study was to provide an understanding of how plasma sprayed and cathodic arc Al-Br coatings perform when coupled with Ti6Al4V, and subjected to gross slip fretting wear at temperatures ranging from ambient up to 450°C. In addition, the two different plasma sprayed coatings and one cathodic arc were used in the investigation to demonstrate the effect that aluminum and oxygen content in the coatings have on their fretting wear performance.

3.1 Experimental

3.1.1 Specimens

The specimens used for this investigation were Ti6Al4V, and the test geometry was an ellipsoid on a flat plate. The ellipsoid, shown in Figure 2.2, was designed to eliminate stress concentrations that lead to contact edge effects, and to simplify alignment procedures for reproducible contact areas. The plates were flat circular disks with a diameter of 12.7 mm on the test face and 3.2 mm thick. Average surface roughness (Ra) was 0.1μm on both the disk and ellipsoid. Prior to testing some of Ti6Al4V disks were commercially grit blasted and then plasma sprayed with Al-bronze coatings 1 and 2, which have different Cu/Al ratios. The remaining Ti6Al4V disks were also coated with Al-bronze; however, these disks were coated using cathodic arc PVD (physical vapor deposition). Cathodic arc is a vacuum PVD technique that typically yields high adhesion, high density, and minimal oxygen in the coatings. The coating compositions (as measured with EDS prior to testing), surface roughness, hardness, modulus, and thickness measurements are listed in Table 3.1. The Ti6Al4V properties of the ellipsoids and disks used are listed in Table 3.2. Metallography showed that both plasma sprayed coatings were dense, but the cathodic arc coatings had a clearly visible interlayer from the two coating cycles required to obtain the 100μm coating thickness.

Table 3.1. Coating properties

	Deposition	Cu/Al in At%	Roughness Ra (μm)	Nano Hardness (GPa)	Modulus (GPa)	Thickness (μm)
1	Plasma	≈ 6	≈ 12	≈ 1.8	≈ 89.6	≈ 300
2	Plasma	≈ 4	≈ 6.7	≈ 2.9	≈ 107.7	≈ 100
3	Cathodic Arc	≈ 6	≈ 4.2	≈ 2.2	≈ 83.7	≈ 100

Table 3.2. Ti6Al4V properties.

Materials	Composition Weight %	Roughness Ra (μm)	Nano Hardness (GPa)	Modulus (GPa)
Ti6Al4V	90% Ti 6% Al 4% V	≈ 0.1	≈ 4.1	≈ 143

3.1.2 Tribological Testing

Three test temperatures were chosen for the bench level gross slip fretting wear tests conducted in this study, in order to sufficiently mimic real world conditions. Room temperature tests were conducted to simulate cold startup of an engine. 163°C was chosen as a moderate temperature to simulate a steady state temperature in the outer stages of a turbine engine compressor and fan. 450°C was chosen to simulate an extreme upper limit that titanium alloys may occasionally encounter in hot sections of the compressor. Three to four repeat tests were conducted on each coating at every temperature. The tests were conducted using a 200μm stroke length, 30Hz oscillation speed, and a 50N normal load for 100,000 cycles. 50N normal load yields a maximum Hertzian contact stress of approximately 650MPa. For the duration of each test the root mean square (RMS) of the friction data and the frictional hysteresis was recorded. The frictional hysteresis was obtained using a laser measuring system and a piezo electric transducer. The fretting wear tribometer, shown in Figure 2.3, uses the piezo electric transducer to measure friction. The laser measurement device is then used to continuously track the position of the oscillating specimen during the test. The real time friction and displacement traces are plotted to produce insitu hysteresis loops that provide real time monitoring of fretting [9, 15-21]. Elliptical shaped hysteresis loops depict mixed fretting behavior and quasi-rectangular shaped hysteresis loops depict gross slip behavior. This technique was used to ensure that each test operated in the gross slip regime throughout the entire duration of the test. Once the fretting wear tests were completed, post test analysis was performed using scanning electron microscopy (SEM) and 3-D contact profilometery for morphology, along with energy dispersive spectroscopy (EDS) for chemical analysis.

3.2 Results

3.2.1 Coating Wear and Analysis

In the fan and compressor sections of a turbine engine the wear analysis is two fold. As shown in Figure 3.1, the blade/disk interface has a coated surface (blade root) worn against an uncoated surface (disk slot). The damage on the worn coatings was analyzed and is presented in this section.

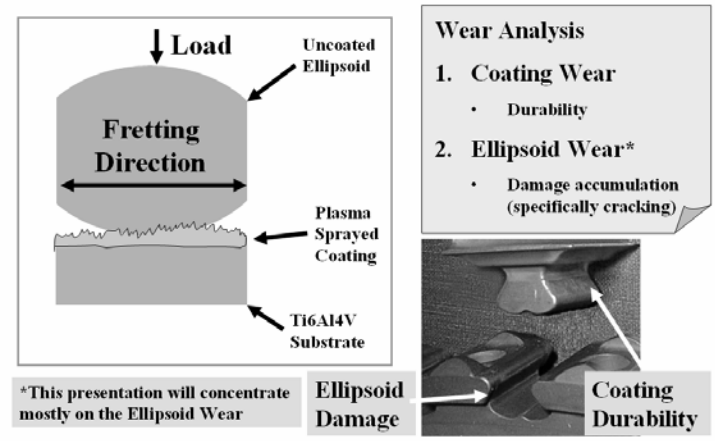

Figure 3.1. Experimental contact and its relationship to the actual engine components.

The friction measurements from the experimental fretting wear tests and the estimated coating wear are shown in Figure 3.2 and Figure 3.3. The measured coefficient of friction was determined using the applied normal load and the measured RMS friction data. The estimated coating wear was determined by multiplying the area of the formed elliptical wear track by the maximum depth measured in the wear track. The area of the elliptical wear scars were calculated using the major and minor radii from the wear geometry, as measured using the SEM. The maximum depth in the wear track was determined from a 3-D profile of the wear that was constructed using a contact stylus profilometer.

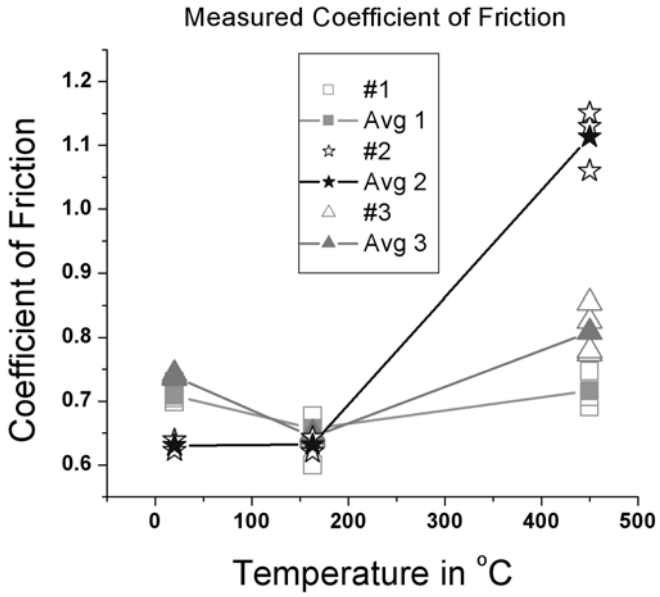

Figure 3.2. Measured coefficient of friction.

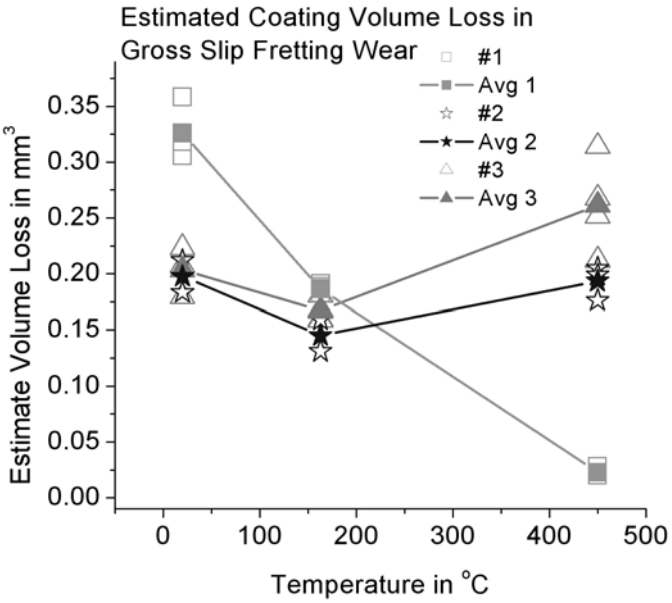

Figure 3.3. Estimated coating volume loss.

The experimental test results show that the metal/metal contact between the Al-bronze coatings and the Ti6Al4V ellipsoids exhibit high friction at all of the temperatures tested. At room temperature coating 2 had the lowest friction, while coatings 1 and 3 had the highest, refer to Figure 3.2. Coating 2 is the second of the two plasma sprayed coatings, and has the highest aluminum content of all three coatings, as determined by EDS prior to testing. However, the EDS scans that were conducted in the wear scar on the coated and ellipsoid surface, plotted in Figure 3.4 and Figure 3.5, indicate that after fretting the contact surfaces of coatings 2 and 3 (plasma and cathodic arc) have similar chemistry. It is known that coating 2 has a large amount of oxidized material through the coating thickness, in contrast to coating 3 which was applied to the titanium substrate in a vacuum. Since copper oxides can be lubricious, the increased oxide content of coating 2 could explain why it has a lower coefficient of friction than coating 3 even though the chemistry in the wear track is similar. In addition, Figure 3.6 shows that coating 3 had a lot of titanium transfer in the wear track. The worn and oxidized titanium debris would also contribute to the higher levels of friction experienced in the contact of the fretting tests on coating 3. Figure 3.4 shows that both of the plasma sprayed coatings had increased copper content in the coating wear track, with coating 1 having an increase of more than two times the levels measured on the unworn surface. Coating 1 also had a higher coefficient of friction and higher wear than coating 2. This suggests that the aluminum helps the performance of coating 2 significantly.

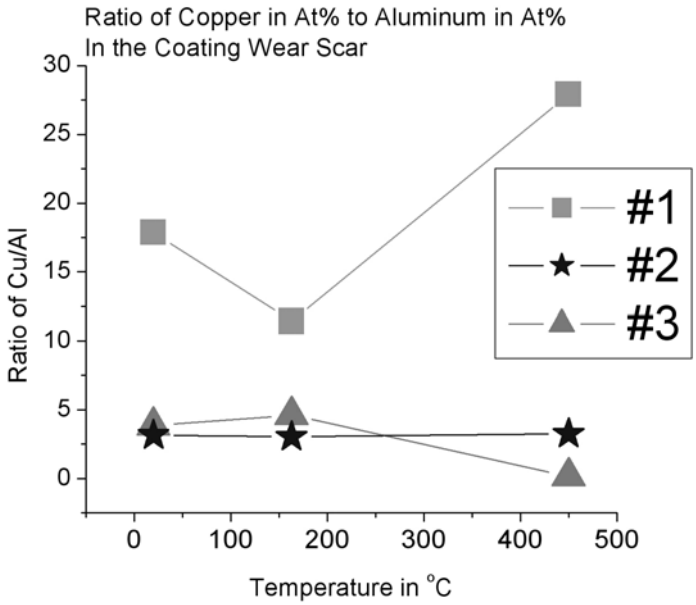

Figure 3.4. Cu/Al ratio in the coating wear scar measured with EDS.

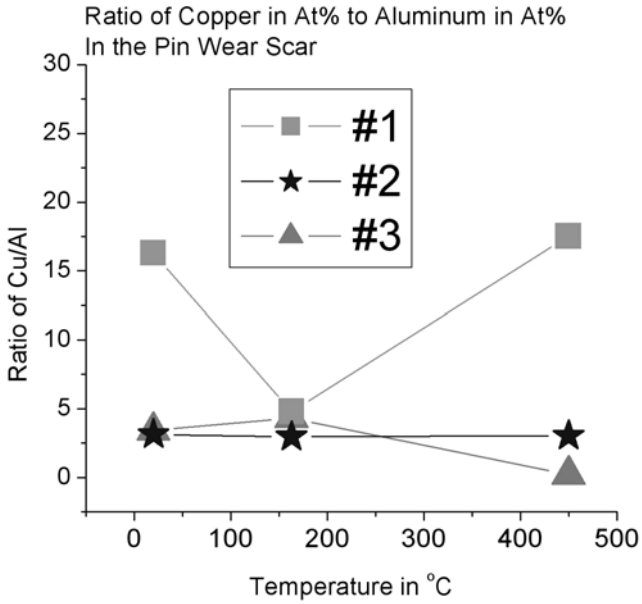

Figure 3.5. Cu/Al ratio in the ellipsoid wear scar measured with EDS.

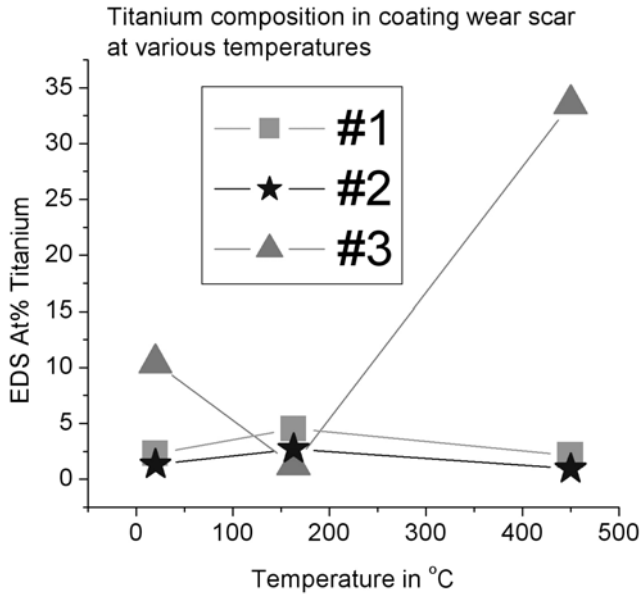

Figure 3.6. Titanium content in the coating wear scar measured with EDS.

At 163°C all of the coatings exhibited approximately the same coefficient of friction, which is the lowest for all of the temperatures tested as well. The coatings also exhibited similar amounts of wear. This phenomenon is best described by Figure 3.5, which indicates that at 163°C the transferred material to the ellipsoid surface was similar in chemistry. Therefore, the aluminum and copper content of the fretting wear tracks over time were similar and yielded similar results.

At 450°C the coatings exhibited nearly the opposite performance that they displayed at room temperature. Coating 1, which has the lowest aluminum content in both the coating and pin wear tracks, had the lowest coefficient of friction and the lowest wear. Coating 3 did not have any copper in the wear track on the coating or the ellipsoid. This is because the coating had worn completely through. The coating failure may be due to a combination of increased friction, wear rate, and the impact of increased temperature on the cohesion between the two layers in which the coating was applied. Earlier it was stated that the metallographic cross sections of the cathodic arc coating showed a clear interface between the two layers in which the coating was applied in order to get the desired 100µm thickness. Coating 2 consistently had the same chemistry in the wear track at every temperature, including 450°C. However, at 450°C the coefficient of friction for coating 2 increased dramatically. In comparison to coating 1, coating 2 has a lot more aluminum in the wear track. However, coating 1 exhibited a much better performance at this temperature than coating 2. This suggests that the aluminum becomes detrimental to the coating performance at 450°C.

3.2.2 Ellipsoid Wear and Analysis

Figure 3.1, shows that the blade/disk interface consists of a coated blade coupled with an uncoated disk. Therefore, fretting damage sustained by the disk is equally detrimental to the fatigue life of the compressor system. These coatings were designed to act as sacrificial layers to protect the uncoated Ti6Al4V counter surface as well. This section will present the microscopy

and analysis of the damage accumulated on the contact surface of the uncoated ellipsoids used in the previously described fretting wear experiments.

The fretting wear tracks on the uncoated ellipsoids were analyzed by back scatter scanning electron microscopy of cross-sections cut through the worn regions. All cross-sections were cut perpendicular to the fretting direction as depicted in Figure 3.7 by the dashed line. EDS was also conducted on the cross-sections for all chemical analysis.

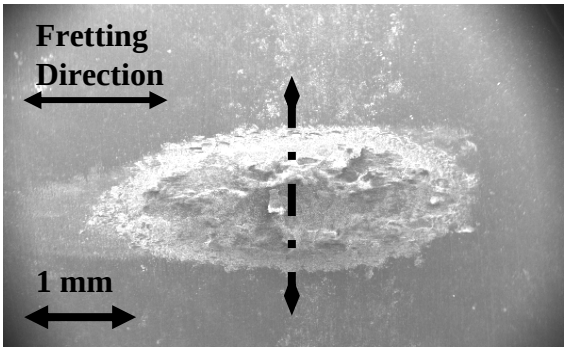

Figure 3.7. SEM image of an ellipsoid wear scar. The dashed line indicates the orientation of the cross-sections to the fretting wear scars.

The microscopy shows that the titanium surface, worn against these coatings at room temperature, experiences galling and surface plasticity which over time causes cracks and fractures of the surface, as shown in Figure 3.8. Some of these particles were on the order of 20-50μm in size. During the beginning of the fretting test these fractured particles are released into the contact and get broken up and eventually oxidized. Some of these particles have been seen imbedded in the coating surface. While this is occurring, the roughened Ti6Al4V surface and third bodies damage the coating creating Al-bronze debris in the contact. Evidence of the Al-bronze debris mixed with broken up Ti6Al4V particles can be seen pressed into the worn ellipsoid surface in Figure 3.9. As the tests progress the fine Al-bronze and Ti6Al4V debris fill in the worn craters on the ellipsoid surface, as shown in Figure 3.10. In some cases this compacted transfer layer covers over large fractured Ti6Al4V particles trapping them underneath. Evidence of this phenomenon is also shown in Figure 3.10.

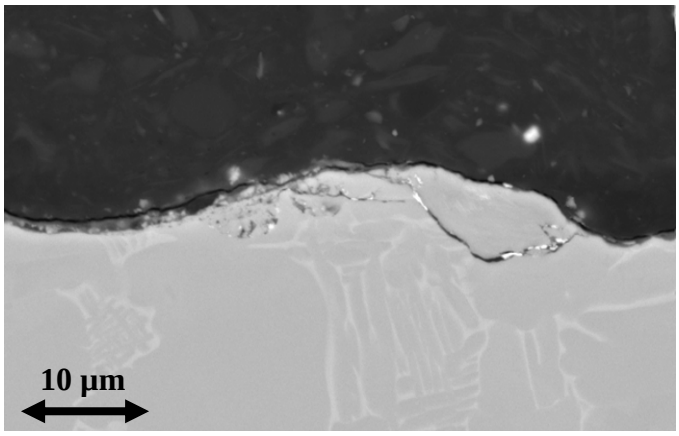

Figure 3.8. SEM image of the fractured surface of a Ti6Al4V ellipsoid worn against coating 3 at RT.

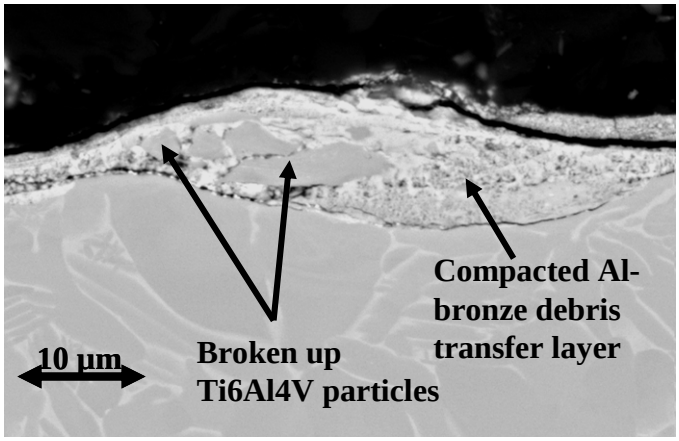

Figure 3.9. SEM image of the surface of a Ti6Al4V ellipsoid worn against coating 1 at RT.

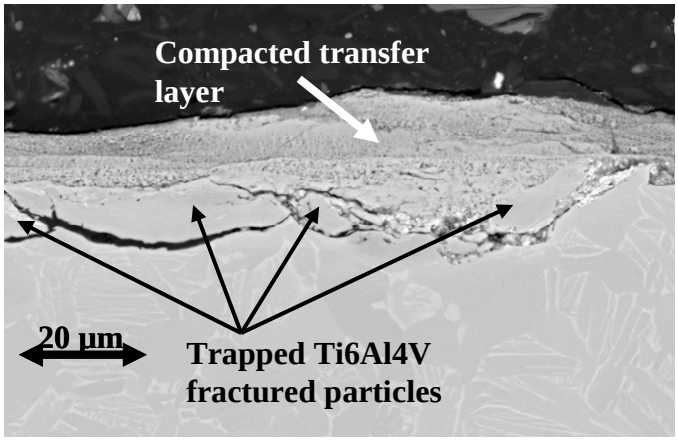

Figure 3.10. SEM image of the surface of a Ti6Al4V ellipsoid worn against coating 3 at RT.

As expected at the room temperature, the Ti6Al4V surfaces worn against coating 3 exhibited the most damage in the contact, with coating 2 causing the least damage. Both coating 1 and coating 3 had higher friction and the mating ellipsoid surfaces had the most large fracture

particles and craters evident. Coating 2 caused some initial damage, but had the thickest layer of transferred coating debris which was then covered with a transfer layer of the Al-bronze coating, shown in Figure 3.11. This transfer layer helped to reduce the friction and the damage to the ellipsoid surface.

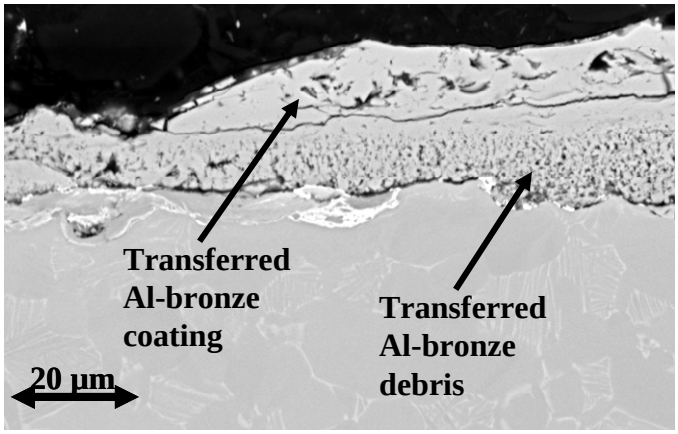

Figure 3.11. SEM image of the surface of a Ti6Al4V ellipsoid worn against coating 2 at RT.

At 163°C the surfaces of all the ellipsoids exhibited a reduction in wear, in comparison to the room temperature experiments. At this temperature all of the wear mechanisms were the same as at room temperature. However, all the ellipsoid surfaces had much less cracking, fracturing, and crater formation. The craters and particles were also much smaller and shallower. In addition, the coating transfer to the Ti6Al4V surfaces was significantly reduced, except in the surfaces worn against coating 2.

At 450°C the wear mechanisms detected on coatings 1 and 3 changed, while the mechanisms remained unchanged on coating 2. Figure 3.12 shows the typical cross-section of an ellipsoid worn against coating 2 at 450°C. This micrograph shows fractured Ti6Al4V surface particles, worn titanium rich material that has adhered to the ellipsoid surface, and transferred Al-bronze. These are all characteristics that were detected in the ellipsoid wear scars at the cooler test temperatures. However, at 450°C the damage is significantly more severe. This is most likely due to the sharp increase in friction as the ellipsoids were worn against coating 2 at this temperature. Coating 1 causes the least amount of damage to the surface of the mating ellipsoid. Figure 3.13 shows that at this temperature coating 1 causes some galling, but mostly forms a thin layer of transferred Al-bronze. From the previous section, it is known that coating 3 failed at 450°C and the coating was completely worn through in the contact region. Figure 3.14 shows the typical damage that this failure imposes on the ellipsoid contact surface. It can be clearly seen that the worn coating adheres to the uncoated ellipsoid counter surface. However, the worn Al-bronze that adhered to the ellipsoid eventually started to gall severely against the Ti6Al4V substrate that has emerged from underneath the coating. This forms a thick layer of titanium on top of the transferred coating layer, as shown in Figure 3.14.

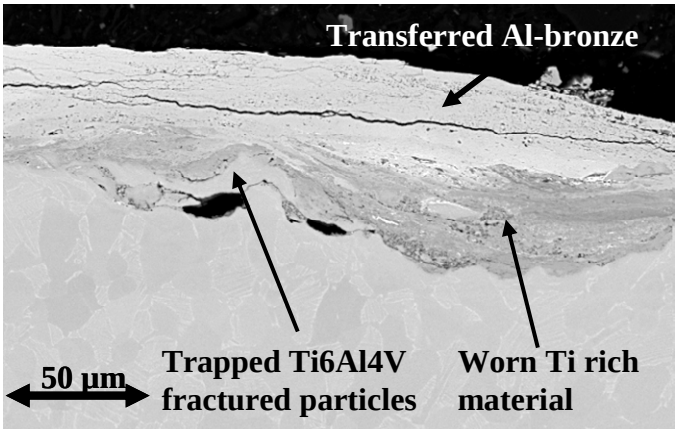

Figure 3.12. SEM image of the surface of a Ti6Al4V ellipsoid worn against coating 2 at 450°C.

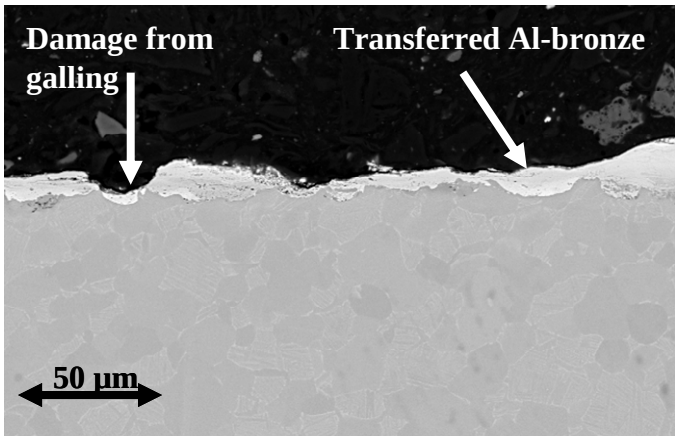

Figure 3.13. SEM image of the surface of a Ti6Al4V ellipsoid worn against coating 1 at 450°C.

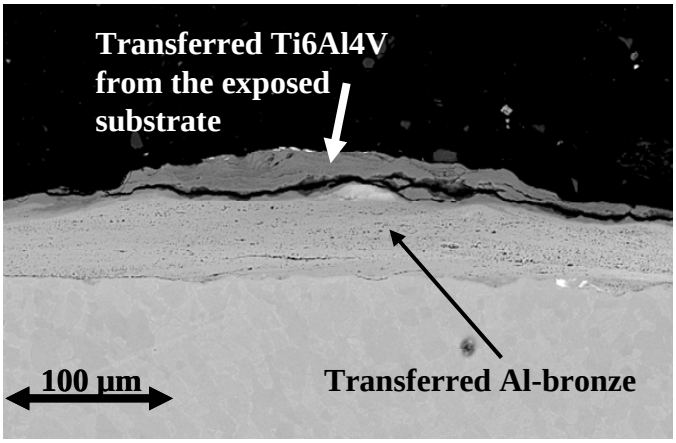

Figure 3.14. SEM image of the surface of a Ti6Al4V ellipsoid worn against coating 3 at 450°C.

3.3 Summary and Conclusions

In overview, the tests conducted in this study were designed to evaluate the performance of three different Al-bronze coatings under gross slip fretting conditions at room temperature, 163°C, and 450°C.

At room temperature the performance of the two plasma sprayed coatings suggest that the aluminum content in the coating and wear track enhances the performance of the coating. This is attributed to the good performance of coating 2 and the poor performance of coating 1, which had virtually all copper in the wear track. At this temperature it was also found that the cathodic arc coatings did not perform as well as the plasma sprayed coatings, even though there were increased levels of aluminum detected in the wear track after the test. This is believed to be attributed to the lack of available oxide within the coating, in comparison to the plasma sprayed coatings. The mating ellipsoid surfaces were all damaged significantly during the room temperature tests, and the wear scars all exhibited similar wear characteristics. All of the coatings had formed transfer layers on the ellipsoid surfaces, but the adhered material just seemed to mask the damage underneath. Each of the wear scars had medium to large craters that formed when particles fracture off of the surfaces of the ellipsoids.

The phenomenon of large particle detachment has been widely researched [1, 2, 28-36]. All of the explanations are derived from the formation of a highly plastically deformed layer near the surface that forms with a fine microstructure, and in the case of Ti6Al4V is always measured to be harder and more brittle than the bulk material. Once the accumulation of strain or stress reaches a critical level cracks form. Depending on the material, contact geometry and loading conditions, these cracks can form at the surface or just below the surface. Over time these cracks propagate relieving the built up stresses and releasing pieces of the surface into the contact.

At 163°C the friction and wear on all of the coatings was very similar. This is most likely due to the fact that all three coatings formed a transfer layer, with the same chemistry, on uncoated ellipsoid surface. In addition, all three coatings also exhibited the lowest coefficient of friction at this temperature. The decreased interfacial friction, then ultimately lead to a reduction in wear on the mating ellipsoid surface, with respect to the wear damage that occurred at room temperature. This may suggest that there is an optimal chemistry and temperature in which these coatings perform the best. In this study that was at approximately 163°C with a Cu/Al ratio of 5/1 in atomic percent in the wear track.

At 450°C the performance of the two plasma sprayed coatings suggests that more aluminum is a performance inhibitor at this temperature. Coating 1, which was almost all copper in the wear track after the fretting tests, exhibited the lowest friction, the least amount of coating wear, and the least damage to the mating Ti6Al4V ellipsoid. Coating 2, which had significantly more aluminum in the wear track, exhibited very high friction and severe damage to the mating surface. In addition, the fretting wear experiments at this temperature wore completely through coating 3. The coating failure may be due to a combination of increased friction, wear rate, and the impact of increased temperature on the cohesion between the two layers in which the coating was applied to get the desired 100μm thickness.

4. Unlubricated Gross Slip Fretting Wear of Metallic Plasma Sprayed Coatings for Ti6Al4V Surfaces

A common solution to the fretting wear/fatigue problem is to apply plasma sprayed coatings and solid lubricants to the component surfaces [4, 37, and 39]. Although the implementation of coatings and lubricants has increased component life, there is a tremendous cost associated with schedule based maintenance of these systems. Therefore, the development of new coatings, coating processes, and lubricants that are able to reduce fretting damage and withstand the hostile engine environment will provide significant reductions in maintenance costs. In order to develop these coatings, it is important to characterize the Ti6Al4V surface interactions with current coatings and compare them with potential replacement materials. In this study, an in depth wear mode analysis was conducted on the gross slip fretting wear of Ti6Al4V mated surfaces as well as Ti6Al4V worn against plasma sprayed copper-nickel-indium (CuNiIn), aluminum-bronze (Al-Br), molybdenum (Mo), and nickel (Ni). CuNiIn and Al-Br are the two most prominent thermal sprayed coatings for this application, while the Mo and Ni coatings are two wear resistant coatings that have some potential for fretting wear mitigation [6, 37, and 38]. Fretting experiments and post test analysis were used to determine the performance of these unlubricated coating systems at room temperature.

4.1 Experimental

4.1.1 Specimens

The specimens used for this investigation were Ti6Al4V, and the test geometry was an ellipsoid on a flat plate. The ellipsoid, shown in Figure 2.2, was designed to eliminate the stress concentrations that occur at the edges of cylindrical contacts. Therefore, the Hertzian contact stress profiles for the samples are smooth with a maximum stress at the center instead of near the edge of contact. In addition, the elliptical contact simplifies alignment procedures for reproducible contact areas, and the large radius in the sliding direction allows for a target maximum Hertzian contact pressure of 650 MPa with an applied normal load of 50 N. The plates were flat circular disks with a diameter of 12.7 mm on the test face and 3.2 mm thick. Average surface roughness (Ra) was 0.1μm on both the disk and ellipsoid. Prior to testing, the Ti6Al4V disks were commercially grit blasted and then plasma sprayed with CuNiIn, Al-Br, Mo, and Ni. The coatings were all in the range of approximately 75-100μm thick. The coating compositions, surface roughness, hardness, and modulus measurements are listed in Table 4.1. Metallography of coatings showed that the Al-Bronze coatings were less uniform and less dense than the other coatings, which is reflected in the measured hardness values.

Table 4.1. Substrate and coatings properties.

Materials	Composition Weight %	Roughness Ra (μm)	Nano Hardness (GPa)	Micro Hardness (HV)	Modulus (GPa)
Copper Nickel Indium	64% Cu 35% Ni 1% In	9	2.4	138	90
Aluminum Bronze	90.3 – 87.5% Cu 9-11% Al 0.7-1.5% Fe	16	1.95	-	61
Molybdenum	Commercially pure	10	5.0	291	177
Nickel	Commercially pure	7	2.1	133	82
Titanium Substrate and Counterface	90% Ti 6% Al 4% V	0.1	4.1	284	143

4.1.2 Tribological Testing and Analysis

The purpose of this study was to provide an understanding of how Ti6Al4V performed when coupled with the selected metallic plasma sprayed coatings, and subjected to gross slip fretting wear at room temperature. The room temperature tests were designed to simulate cold engine startup. Three to four repeat tests were conducted on each coating. The tests were conducted using a 200μm stroke length, 30Hz oscillation speed, and a 50N normal load for 100,000 cycles. The applied 50N normal load yields a maximum Hertzian contact stress of approximately 650MPa. In addition, shorter duration tests were conducted at 2 Hz oscillation speed, to supplement the longer tests for wear analysis.

For the duration of each test the root mean square (RMS) of the friction data and the frictional hysteresis was recorded. The fretting wear tribometer, shown in Figure 2.3, has a stage that is mounted on thin metal legs that can support the normal applied load, while acting as tangential springs in the oscillation direction. As the elliptical sample moves the friction force between the samples causes the sample stage to deflect slightly, on the order of 1 μm typically, in the direction of sliding. The stage deflection then compresses or stretches the attached piezoelectric transducer and creates a signal. The signal from the piezo is then amplified and calibrated, using a force meter, to match the amount of force applied to the stage prior to testing. The friction force is then collected using an oscilloscope data acquisition card and a computer. Once collected, the RMS of the friction force is then tabulated and plotted per test cycle in situ. In addition, a laser measuring system, shown in Figure 2.3, is focused on the face of the oscillating arm of the tribometer and is used to continuously track the displacement of the ellipsoid during each test. The real time displacement data along with real time friction data and are then collected using the same oscilloscope computer card. The real time friction and displacement are plotted to produce in situ hysteresis loops that provide real time monitoring of the fretting wear regime.

There have been a number of papers published that explain the use of hysteresis loops for the determination of fretting wear regime [15-21]. Elliptical shaped hysteresis loops have been shown to depict mixed fretting behavior and quasi-rectangular shaped hysteresis loops have been shown to depict gross slip behavior. This technique was used to ensure that each test operated in the gross slip regime throughout the entire duration of the test.

Once the fretting wear tests were completed, post test analysis was performed using scanning electron microscopy (SEM) and 3-D contact profilometery for morphology, along with energy dispersive spectroscopy (EDS) for chemical analysis. All cross-sections were cut perpendicular to the fretting wear direction using a low speed diamond saw. The coating cross-sections were mounted using an air cured epoxy mount, and the uncoated ellipses were mounted using a hard carbon filled conductive hot compression mount. The hot compression mounts were used on the ellipse cross-sections because they have a higher hardness and better edge retention, which is needed to keep the worn regions intact during the polishing process. Once mounted, all cross-sectioned samples were polished prior to microstructure and EDS analysis.

4.2 Results

4.2.1 Friction and Wear

The coefficients of friction for all the tests ranged from approximately 0.7 to 0.9. Figure 4.1 shows typical friction traces measured during the course of the fretting tests, and shows that the addition of the coatings to the interface does not significantly reduce the friction. Only the CuNiIn coating reduced the measured friction coefficient from the 0.8 exhibited by Ti6Al4V mating surfaces down to 0.7.

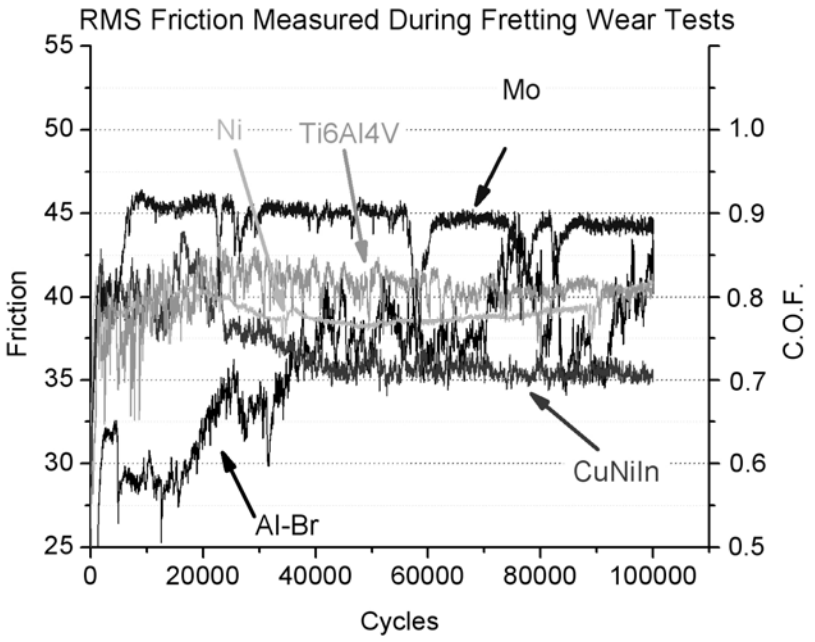

Figure 4.1. RMS friction measurements for gross slip fretting at room temperature.

In addition to measuring the friction, the coating wear was assessed by determining the maximum depth in each wear track using a 3-D contact profilometer. Figure 4.2 shows the average depths measured for each configuration tested. The Mo coating was the hardest and most wear resistant of all the coatings at room temperature, while CuNiIn exhibited the most wear. However, none of the coatings wore completely through to the substrate.

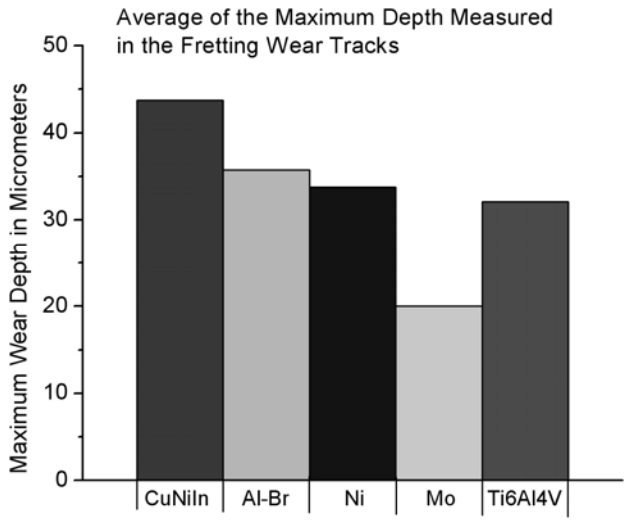

Figure 4.2. Average of the maximum wear depth measured in the coating wear tracks.

4.2.2 Wear Mode Analysis

This study consisted of fretting wear tests in which Ti6Al4V ellipsoids were worn against Ti6Al4V, CuNiIn, Al-Br, Mo, and Ni. In addition to the 30 Hz and 100,000 cycle tests at room temperature, short duration tests conducted at 2 Hz oscillation speed were conducted for further insight. Uncoated Ti6Al4V specimens were tested as a baseline to quantify how well the coatings protect the mating Ti6Al4V surfaces. Specifically, the ellipsoid wear in the uncoated case will be used as a comparison to assess the amount of damage on the ellipsoids caused by fretting against the coated surfaces. In this section the wear on the coatings as well as in the uncoated contacts will be discussed.

4.2.2.1 Uncoated Ellipsoid Wear

At room temperature the Ti6Al4V mating surfaces are damaged primarily by galling initially, and then by 3rd body wear as the large adhered particles start to break apart. After 10 cycles, with 2 Hz oscillation speed, the gross slip fretting wear at the Ti6Al4V interface of the test specimens is composed of solely adhesive wear, as shown in Figure 4.3A. The mated surfaces exhibited severe plastic deformation with large wear particles, on the order of 100 µm long and 50 µm wide, adhered to the wear track. After 100 cycles the large wear particles in the contact start to break up into smaller wear debris, as shown in Figure 4.3B. The majority of the debris gathers around the edges of the contact, with some of the debris getting trapped inside the wear track. After 1,000 cycles almost the entire wear track is filled with wear debris, as shown in Figure 4.3C. Some large wear particles can be seen near the center and the edges of the wear

track. Some of these larger particles are produced in local regions throughout the wear track where the Ti6Al4V surfaces make contact in the absence of the trapped wear debris, and some of the particles are from the adhesive wear that was predominant during the initial stages of the test. After 100,000 cycles, with 30 Hz oscillation speed, the wear track is completely filled with wear debris, as shown in Figure 4.3D. This exact wear mode has been described in detail in a fretting wear review paper by Hurricks [40], and by Blau [35] in his work with wear mechanisms in metallic interfaces. Figure 4.4A and 4.4B shows cross-sectional micrographs of a typical 100,000 cycle Ti6Al4V mating fretting wear test. The cross-sections of the ellipsoid wear tracks were cut perpendicular to the fretting direction as shown by the arrows in Figure 4.3D. In the center of the wear track, the wear scar is approximately 30 to 40 µm deep. The dark region shows a compacted powder bed of fine titanium and oxide wear debris. Using Raman Spectroscopy, Hager et al [16] determined that the accumulation of gross slip fretting wear debris in the contact of Ti6Al4V mating surfaces contains significant amounts of rutile TiO_2. Figure 4.4B shows the plastically deformed surface layers, or highly deformed layer (HDL) as defined by Rigney et al [41], near the edge of the wear scar and beneath the trapped wear debris. In these contact regions the accumulation of plastic deformation occurs until the surface material becomes too brittle to accommodate the imposed strain, as explained by Blanchard et al [3]. This eventually leads to the breakup of surface regions and the formation of large wear particles, as shown in Figure 4.4B.

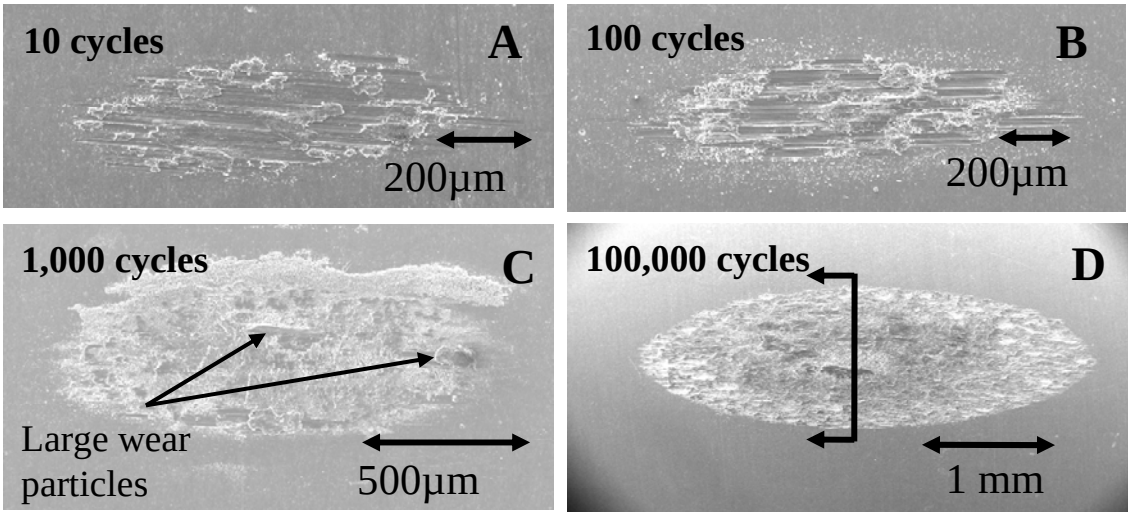

Figure 4.3. SEM micrographs of the fretting wear on the surface of the ellipsoid after being worn against a Ti6Al4V uncoated disk for A) 10 cycles at 2 Hz, B) 100 cycles at 2 Hz, C) 1,000 cycles at 2 Hz, and D) 100,000 cycles at 30 Hz.

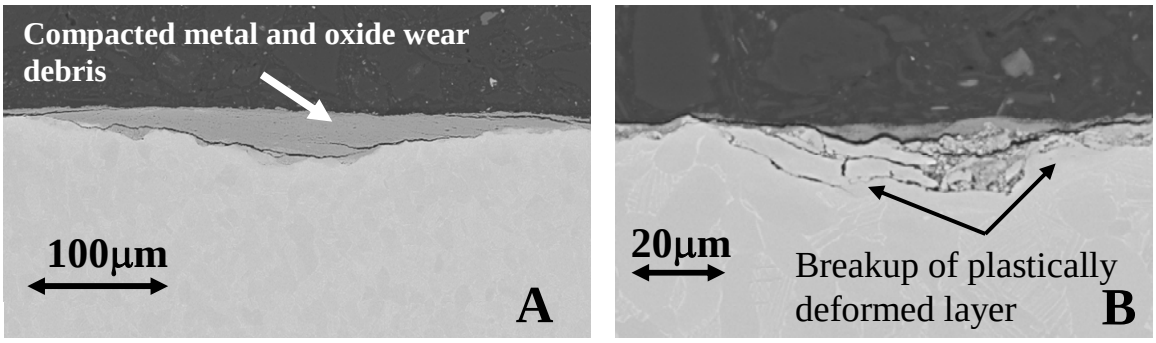

Figure 4.4. Images A and B are back scatter (BSE) SEM images showing the cross-section of a Ti6Al4V ellipsoid worn against uncoated Ti6Al4V at room temperature for 100,000 cycles, at the center and edge of the wear track respectively.

The wear mode analysis conducted on the uncoated Ti6Al4V ellipsoids, worn against the plasma sprayed CuNiIn, Al-Br, Mo, and Ni coatings, determined that the wear evolution and damage mechanisms are same as those exhibited by mated Ti6Al4V surfaces. Figure 4.5 shows SEM micrographs of the ellipsoid surface damage caused by gross slip fretting against each of the plasma sprayed coatings. After just 100 cycles, the accumulated damage is driven by adhesive wear. EDS analysis and X-ray mapping of the magnified regions showed that the large adhered particles, in all four wear tracks, are adhered metallic particles from the various coating surfaces. These large adhered particles plow large channels or make striations on the surface of the Ti6Al4V ellipsoids. In addition, the micrographs from these tests also show a significant amount of tiny wear debris trapped within the wear track. Using EDS, it was determined that these particles are a mixture of mostly oxidized Ti6Al4V and transferred coating wear debris.

Although the apparent mechanisms by which the fretting wear has damaged the surface of the Ti6Al4V ellipsoids are the same against all of the coated and uncoated surfaces, the accumulation and evolution of the wear at each interface still exhibited some distinct characteristics. All of the worn Ti6Al4V ellipsoid surfaces had adhered coating particles. However, these particles varied in size and in the amount of damage they caused. Wear against the CuNiIn coating for 100 cycles produced large adhered coating particles, on the order of 20 to 100μm in size. In addition, 100 cycles of fretting was enough to cause galling throughout most of the contact area and create large amounts of trapped oxide debris, the tiny white particles that are dispersed throughout the wear track as shown in Figure 4.5A. Fretting for 100 cycles against the Al-Br coating caused the least amount of damage to the Ti6Al4V ellipsoid, in comparison to all of the coatings tested. Figure 4.5B shows that the Al-Br coating smeared onto the Ti6Al4V surface causing galling to occur only in localized regions. The Mo coating, which was the hardest of the four coatings, caused the most severe damage to the mated Ti6Al4V surface, after 100 cycles. Adhesion between the coating and the Ti6Al4V ellipse caused severe galling and the transfer of large Mo particles. The adhered Mo particles, typically on the order of 100 μm in size, mixed with the displaced titanium at the edges of the galled regions, as shown in Figure 4.5C. Fretting against the Ni coating for 100 cycles produced a wear track on the Ti6Al4V mated ellipsoid that was similar to what was seen in the CuNiIn tests. The differences between the two are that the Ni created a wear scar with deeper galling tracks and more fine oxide debris trapped within the contact, as shown in Figure 7D.

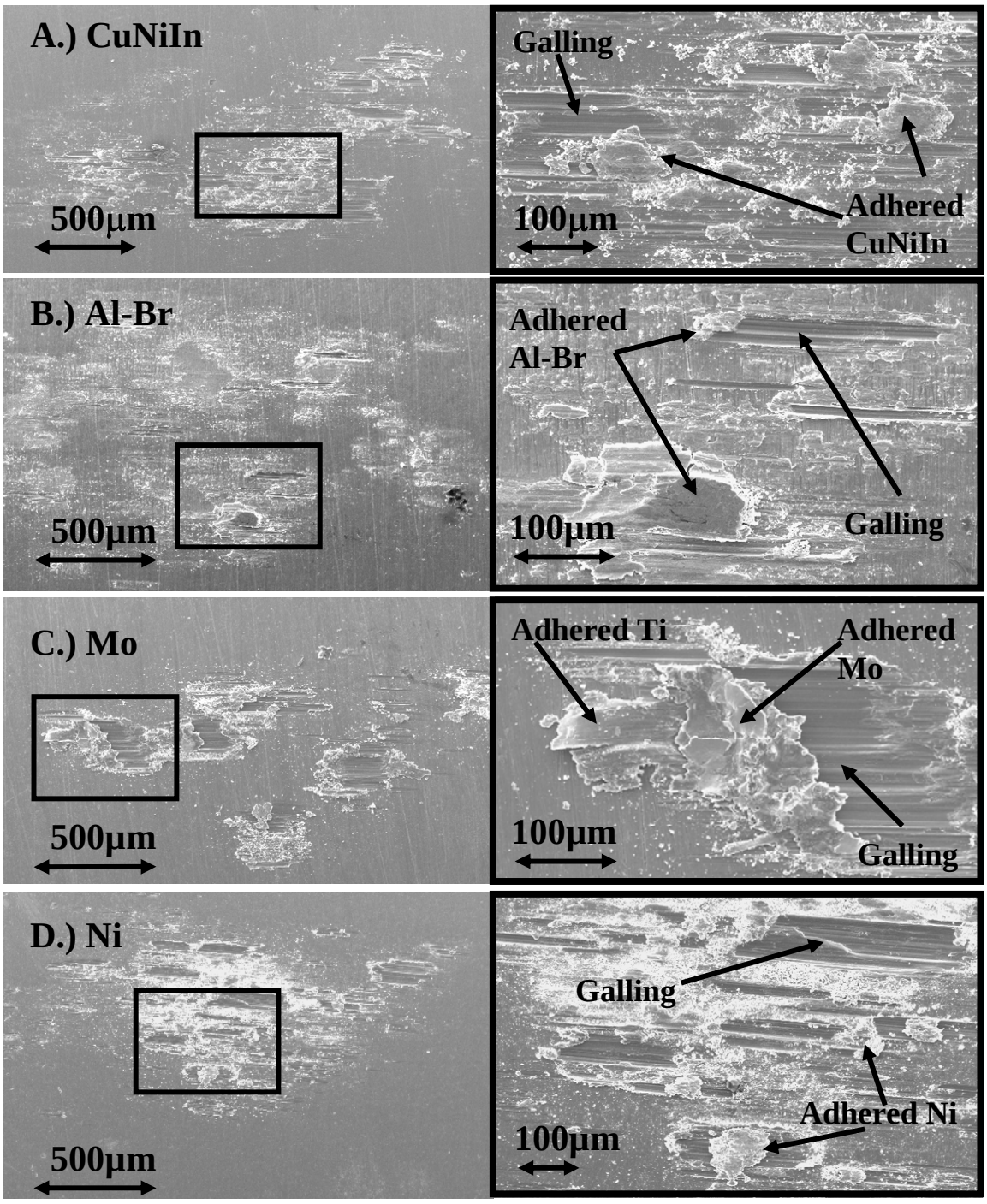

Figure 4.5. SEM micrographs of the fretting wear on the surface of the Ti6Al4V ellipsoid after being worn against the test coatings for 100 cycles at 2Hz. The images outlined in black on the right are zoomed images of what is contained in the black squares on the left.

Figure 4.6 shows micrographs of the ellipsoid wear after 1,000 and 100,000 cycle tests. In the 1,000 cycle tests conducted against Mo and Ni, Figure 4.5E and 4.5G respectively, the micrographs show that the gross slip fretting wear progression of the interfaces has lead to the break up and oxidation of the large galling products and the protruding Ti6Al4V at the edges of

the severely deformed regions that were seen in the 100 cycle tests. Therefore, the interfacial wear on the ellipsoid has transitioned from adhesive wear and galling to a 3rd body abrasive wear during the period between 100 and 1,000 cycles. In the 1,000 cycle tests conducted against CuNiIn and Al-Br, Figure 4.6A and 4.6C respectively, the wear tracks show an increased amount of fine oxide debris trapped within the wear track, and the absence of the large transfer particles that were seen in the 100 cycle tests. However, the wear scars created by CuNiIn and Al-Br exhibited large regions near the center of the contact where evidence of adhesive wear was still apparent. After 100,000 wear cycles all surfaces of the wear tracks against each of the different coatings were completely covered with a powder bed of compacted wear debris. This debris was composed of mostly oxidized Ti6Al4V and coating particles along with some larger metallic particles, typically from the coating surfaces. Micrographs of the ellipsoid wear tracks after 100,000 cycles are shown in Figure 4.6.

In addition to the wear scar surface analysis, all of the Ti6Al4V ellipsoids worn for 100,000 cycles were cross-sectioned perpendicular to the fretting direction, shown by the black arrows in Figure 4.3D, 4.6B, 4.6D, 4.6F, and 4.6H. Analysis of the back scatter (BSE) SEM micrographs of the ellipsoid cross-sections, shown in Figure 4.7, further verifies the similarities in the fretting wear mechanisms that damaged these Ti6Al4V surfaces when self mated or worn against the CuNiIn, Al-Br, Mo, or Ni plasma sprayed coatings. Fretting wear of Ti6Al4V ellipsoid surfaces mated with the CuNiIn and Al-Br coatings produced virtually identical wear to that of the mating Ti6Al4V surfaces, as seen by comparing Figures 4.7A-4.7D with Figures 4.4A and 4.4B. The only differences being that the mixture metal and oxide debris compacted into the worn ellipsoid surfaces have different chemistries, and that the ellipsoids worn against Al-Br did not have the large detached particles that were seen in the CuNiIn tests, as shown in comparing Figure 4.7B and 4.7D. The wear scars from fretting against CuNiIn and Al-Br have compacted debris composed of oxidized debris from the coating surfaces mixed with the titanium and titanium oxide debris, as confirmed with EDS analysis. The wear on the ellipsoid surfaces mated with the Mo and Ni coatings, shown in Figures 4.7E and 4.7F, also exhibit similar wear mechanisms. However, these surfaces have thinner transfer films of compacted debris and larger Ti6Al4V wear particles. Often these Ti6Al4V particles are on the order of 50μm deep and just as wide. This is typically 2 to 3 times larger than the ones seen at the CuNiIn worn Ti6Al4V interfaces.

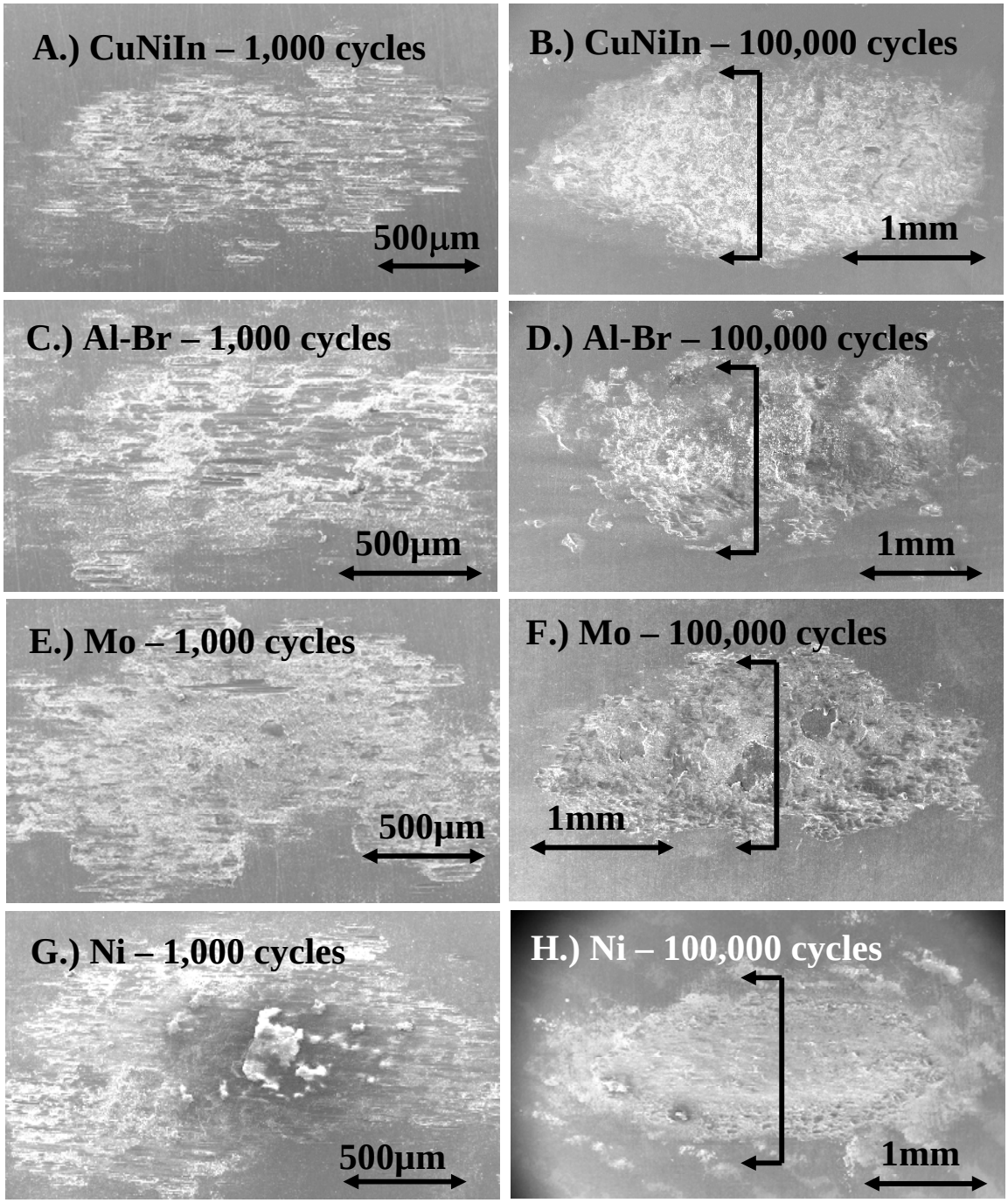

Figure 4.6. SEM micrographs of the fretting wear on the surface of the Ti6Al4V ellipsoid after being worn against the test coatings at room temperature for 1,000 and 100,000 cycles respectively.

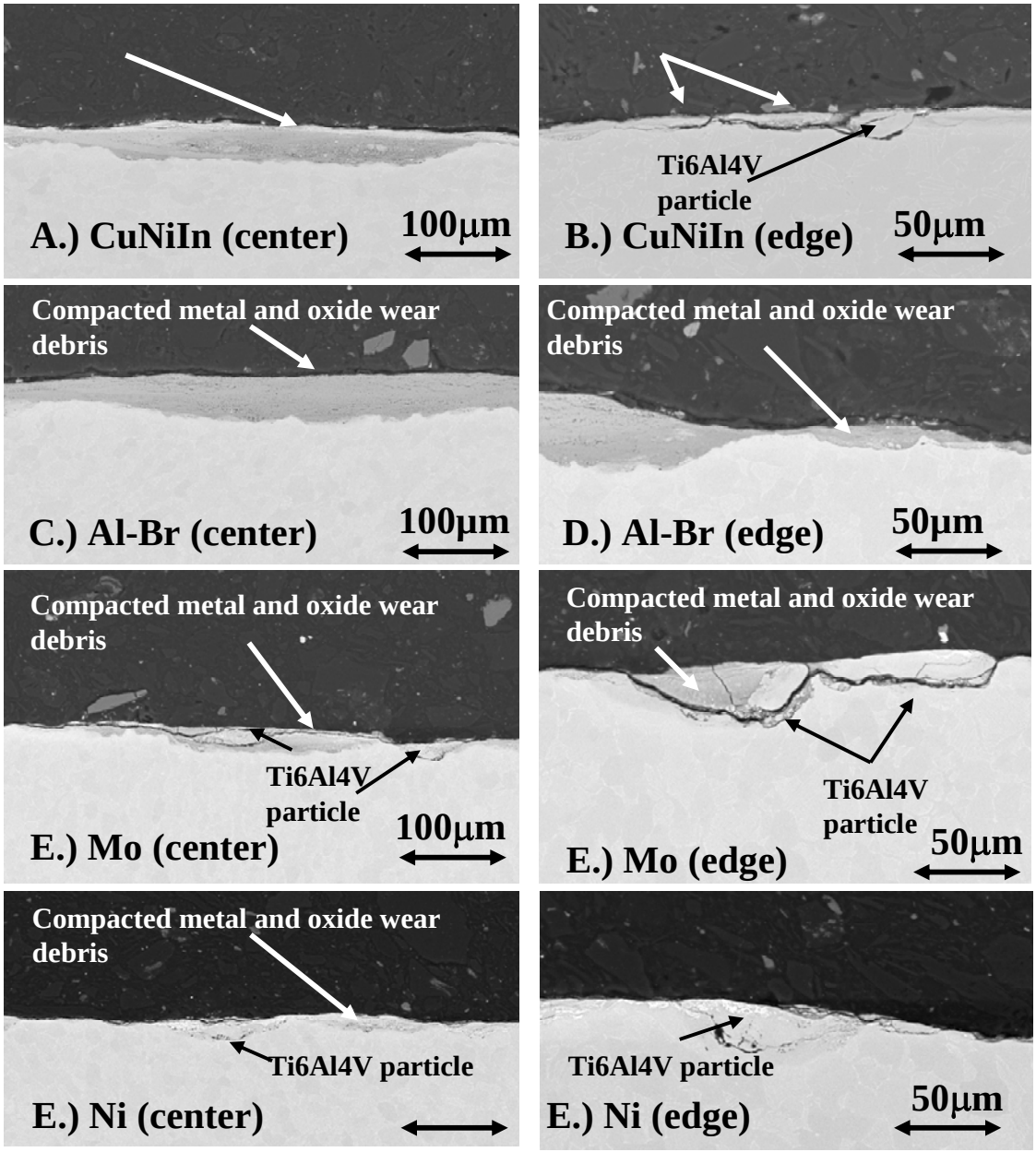

Figure 4.7. Back scatter (BSE) SEM image showing the cross-section of a Ti6Al4V ellipsoid worn against the test coatings at room temperature for 100,000 cycles. Images on the left are from the center of the wear track, and images on the right are from a region near the edge of the respective wear track.

4.2.2.2 Coating Wear

After 100 fretting wear cycles at 2 Hz, the wear on the surface of the coatings was localized to the damage of the large asperity tips of the rough as sprayed coatings. Figure 4.8 shows secondary electron and back scatter (BSE) SEM images of the wear tracks. In both sets of images it can be seen that the surface asperities of the CuNiIn, Al-Br, and the Ni coatings have been sheared and flattened, with the produced debris collected in the valleys of the coating surface. Unlike the other three coatings, the Mo coating sustained almost no surface damage

after 100 cycles. However, the surface of the Mo coating did have debris trapped in the valleys between the asperities as seen on the other coatings. The BSE images, shown in Figure 4.8, display changes in contrast with respect to changes in surface chemistry. Therefore the dark regions that are shown with arrows in Figure 4.8A, 4.8C, and 4.8D indicate Ti6Al4V particles that have adhered to the coating surface. This fact was further verified chemically using EDS. The Al-Br coating, shown in Figure 4.8B, was the only one of the tested coatings that did not have large pieces of the mated Ti6Al4V ellipsoid surface adhered to the coating wear track.

Extended fretting wear tests lead to the continued shearing of large coating asperities, as well as the breakup of the transferred Ti6Al4V particles that were seen after 100 cycles of wear. Figure 4.9 shows SEM images of the coating wear tracks after 1,000 and 100,000 cycle tests. The separate sets of tests were conducted respectively at 2 Hz and 30 Hz oscillation speeds. After 1,000 cycles, the coating asperities have been worn away completely, except on the Mo coating. The wear debris that was once trapped in the valleys between asperities is swept towards the edges of the wear track, leaving enough debris trapped within the contact to cover a large portion of the contact region. The Al-Br coating, Figure 4.9C, is the only coating with significant surface area that is uncovered by wear debris within the wear track after 1,000 cycles. After 100,000 cycles the wear tracks of coatings appeared to have reached steady state wear. With the exception of the Mo coating, the wear tracks were significantly covered with debris creating a powder bed within the contact, as shown in Figure 4.10. This indicates that the interfacial wear mechanisms are now controlled by the rheology of the wear debris trapped within the contact, as studied by Colombie et al [42], as well as by any localized metallic contact that may occur. However, the Mo coating, even after 100,000 cycles, still has valleys between the asperities that trap debris. In addition, there are some localized regions in the Mo wear tracks where EDS showed a concentration of titanium material. Figure 4.11 and Figure 4.12 show average ratios of the Ti/coating and oxygen/Ti in atomic % as measured using EDS. These measurements were made in the dark regions of the BSE SEM images, as seen in Figure 4.10. In the localized dark regions, the Mo has a Ti/Mo ratio of more than 1.5/1 and an oxygen/Ti ratio of approximately 3/1. Molybdenum will oxidize typically to MoO_3 and titanium will oxidize typically to TiO_2; therefore, there is not enough oxygen detected in these regions for the debris to be completely oxidized. This indicates that even after 100,000 cycles the Mo coating is still galling in localized regions.

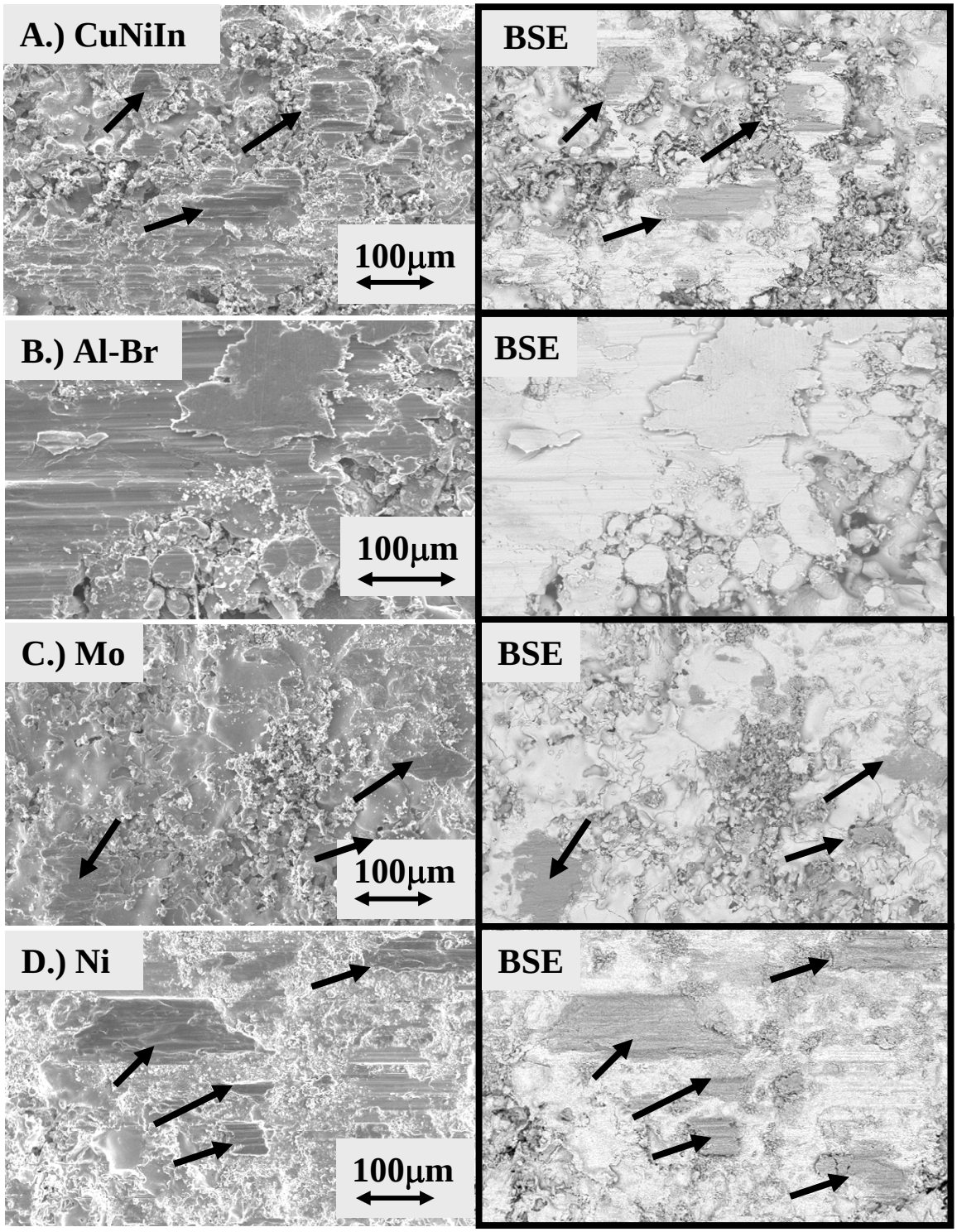

Figure 4.8. SEM micrographs of the fretting wear on the surface of the test coatings after 100 cycles at 2Hz oscillation speed. On the left are secondary electron (SE) images and on the right, outlined in black, are the exact same images in using a back scatter (BSE) detector. The black arrows in all of the images point to titanium that is adhered to the coating wear surface.

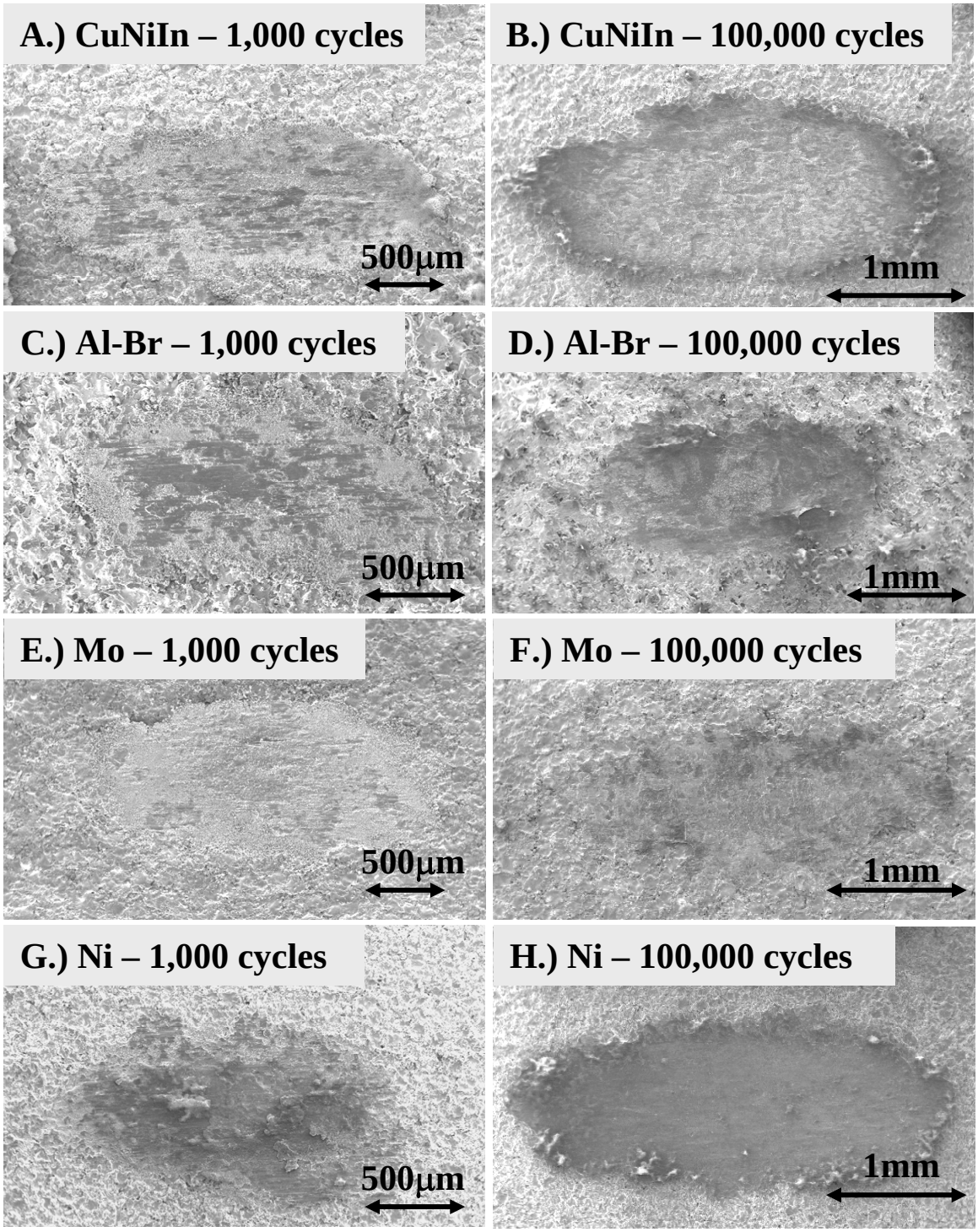

Figure 4.9. SEM micrographs of the fretting wear on the surface of the test coatings after 1,000 and 100,000 cycle tests mated with Ti6Al4V.

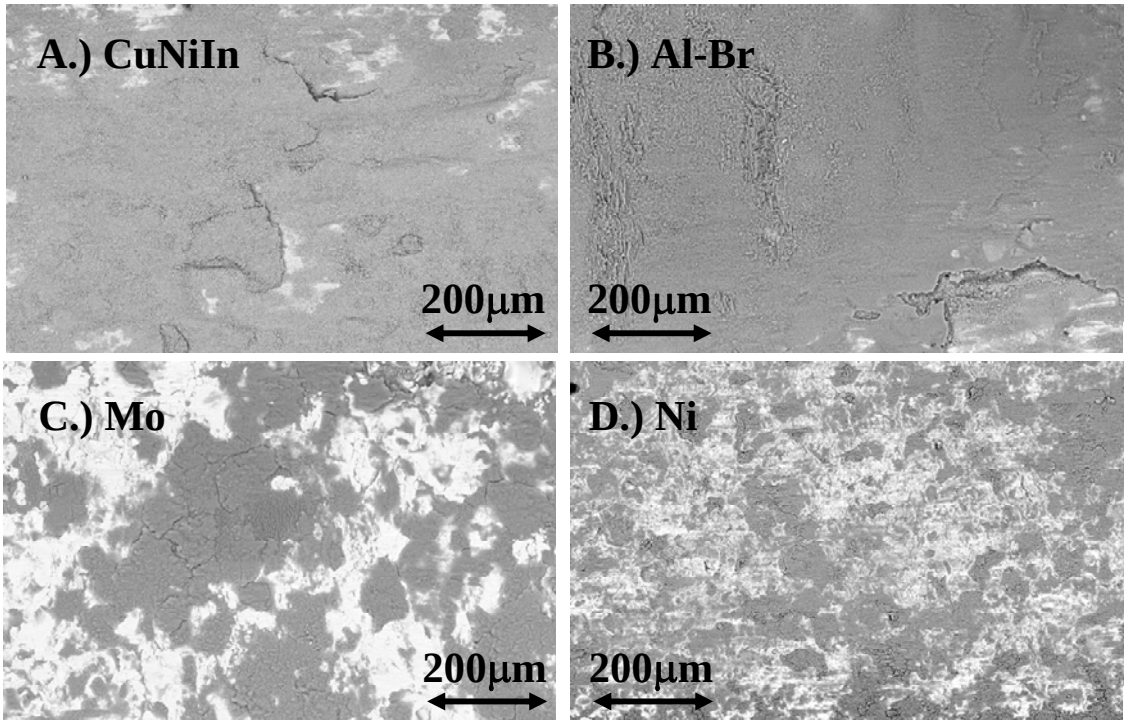

Figure 4.10. Back scatter SEM micrographs of the fretting wear on the surface of the test

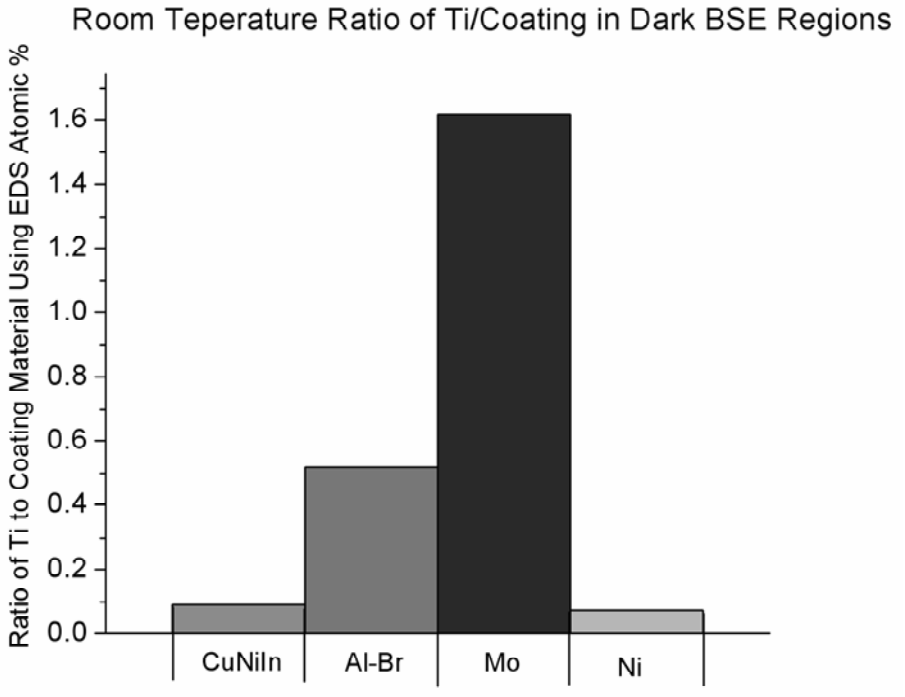

coatings after 100,000 cycle tests mated with Ti6Al4V.

Figure 4.11. Average ratio of Ti/coating in atomic % as determined from EDS scans of the dark regions shown in the BSE SEM micrographs in Figure 4.10.

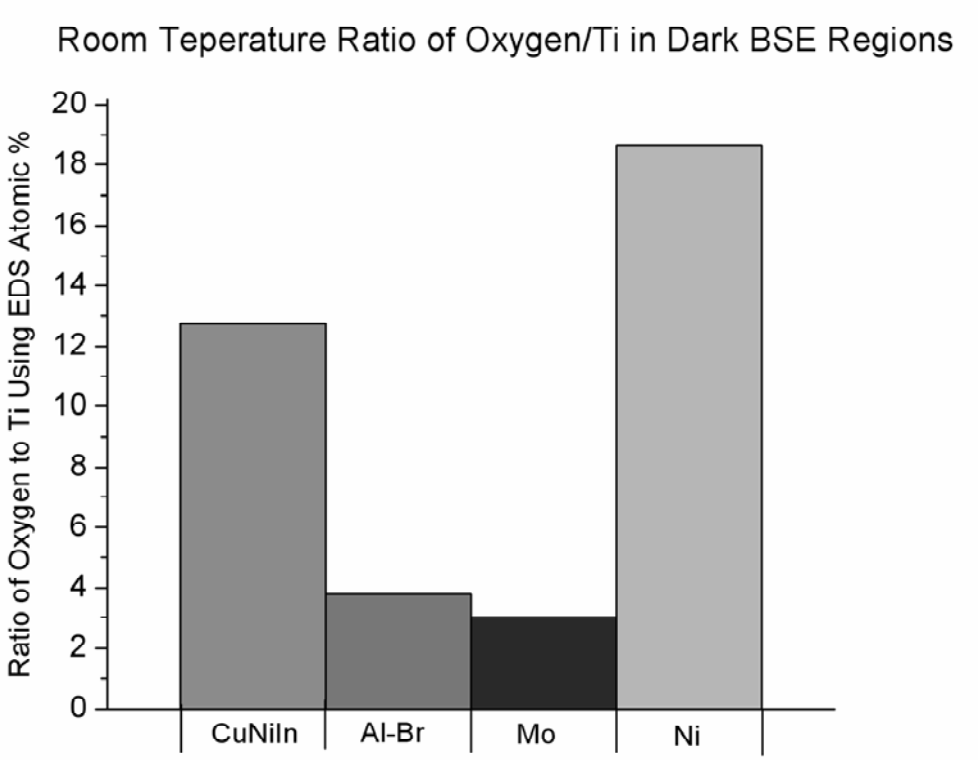

Figure 4.12. Average ratio of oxygen/Ti in atomic % as determined from EDS scans of the dark regions shown in the BSE SEM micrographs in Figure 4.10.

4.3 Summary and Discussion

In overview, this study was conducted to assess the interfacial wear mechanisms associated with gross slip fretting of Ti6Al4V in contact with four different thermal spray coatings at room temperature. These tests were conducted without lubrication and caused metallic wear in the fretting contact. All metallic engineering surfaces are covered by thin oxide layers that are typically angstroms or nanometers in thickness [40, 43]. This contaminant layer initially protects the underlying metal. However, surface species are dispersed during the first few cycles of the fretting wear process causing the intimate contact of the Ti6Al4V ellipsoid surfaces with the metallic coating surfaces. When this happens the contacting nascent metallic surfaces cause adhesive wear and ultimately galling. The galling of the Ti6Al4V ellipsoid surface coincides with the shearing of the coating surface asperities, and the simultaneous transfer of metallic material between the contacting surfaces.

All of the coatings tested were approximately half as hard as the Ti6Al4V contact surface, with the exception of the Mo coating which was slightly harder than its titanium counterpart. This would lead one to believe that material transfer at the fretting interface would consist of the softer coating surfaces transferring to the harder Ti6Al4V surface, and in fact this is what predominantly occurs. However, there are localized regions where large Ti6Al4V particles, on the order of 50 to 100μm, were adhered to the surfaces of the CuNiIn and Ni coating surfaces. Bowden et al [44] also witnessed a similar phenomenon when they observed the transfer of small fragments of mild steel to the surface of copper during sliding wear

experiments. This is an extremely devastating wear phenomenon that accelerates the ellipsoid wear, because the Ti6Al4V adhered particles form raised plateaus on the coating surface and promote further galling by creating titanium on titanium contact within the fretting interface.

Galling and material transfer, along with the shearing of coating asperities typically occurs within the first 100 gross slip fretting wear cycles. Between 100 and 1,000 cycles of wear, the highly deformed surface layer of the Ti6Al4V ellipsoid becomes too brittle to accommodate the imposed fretting displacement, as explained by Blanchard et al [3], and begins to crack and break, as shown in Figure 4.4B. In addition, the continued deformation of the transferred material plateaus causes them to breakup as well. This creates an abundance of wear debris within the contact. The wear debris represents a wear mode shift from adhesive driven wear to wear that is mostly driven by the rheology of the 3rd body debris, most likely 3rd body abrasion.

From 1,000 cycles to 100,000 cycles some of the wear debris is swept out of the wear track, and some of the wear debris remains. The trapped or active wear debris continuously gets crushed into fine particles and oxidizes. As the active wear debris builds up in the wear track, it gets compressed together and forms a powder bed that separates the contacting surfaces. If the powder bed formation is continuous, as it is in the cross sections of the ellipsoids worn against CuNiIn and Al-Br shown in Figure 4.7A and 4.7C, then the surface degradation will be concentrated at the edges of the contact and expand the wear track laterally instead of deeper. This can be seen in Figure 4.7B and 4.7D. In the case of the Mo coating, the asperities are never completely worn away and the valleys trap the wear debris preventing the formation of a powder bed. This is why there is still evidence of localized galling near the center of the wear track after 100,000 fretting wear cycles.

Ultimately, the thermal spray coatings tested did not change the associated wear mechanisms or reduce the apparent wear damage imposed on the Ti6Al4V ellipsoid surface. Although the wear may have appeared to be reduced in the first 100 cycles or so against the Al-Br coating, the eventual result after 100,000 cycles of gross slip fretting wear was the same as that seen in the Ti6Al4V mating contacts. This is because of the formation of a powder bed in all of the tested configurations. The rheology of the 3rd body debris, primarily the titanium oxide debris which is constant to all of the tests, controls the extent of the fretting wear damage to the Ti6Al4V ellipsoid after 1,000 cycles, or once enough debris has been established in the contact. In addition, the CuNiIn, Al-Br, and Ni thermal spray coatings sustained severe wear during each of the fretting wear tests. 30% to 40% of the coating thickness had been worn away after 100,000 cycles of fretting. The Mo coatings were very wear resistant and exhibited wear scars that were half the depth of the other coatings. However, the wear resistance of the Mo coatings can be more detrimental to the Ti6Al4V ellipsoid due to the localized galling that continues for at least two orders of magnitude longer than against the other coatings tested.

The wear analysis from this study supports the need for a different coating system than the current rationale. Although the actual compressor blades are coated with thermal sprayed coatings and then with solid lubricants, this study shows the dangers of what can happen if/or when the lubricants fail or are completely worn away. In gross slip fretting, these soft thermal spray coatings do not effectively protect the mating Ti6Al4V surfaces without solid lubrication.

4.4 Conclusions

This study was conducted to examine the wear mechanisms associated with the addition of four thermal sprayed coatings into a Ti6Al4V mated fretting contact, under gross slip. It was found that:

- The measured coefficient of friction in all of the tests was very high, from 0.7 to 0.9.
- All of the wear mechanisms that governed the surface damage accumulation were the same in all of the tested coating configurations.
- All of the extended tests exhibited similar amounts of Ti6Al4V ellipsoid wear against all of the coatings and in the Ti6Al4V mated tests. Therefore, all of the coatings tested were unable to adequately protect the mated ellipsoids without lubrication.

5. Gross Slip Fretting Wear of CrCN, TiAlN, Ni, and CuNiIn Coatings on Ti6Al4V Interfaces

In turbine engines, fretting wear/fatigue of Ti-alloy contacts is often mitigated by applying plasma sprayed CuNiIn coatings and solid lubricants to one of the contacting surfaces. However, literature [6 and 7] combined with the previously stated work, shows that unlubricated CuNiIn surfaces can severely damage mated Ti6Al4V components. In this study a new mitigation strategy was proposed to reduce the fretting wear damage that accumulates once the applied lubricants have been exhausted. First a plasma sprayed nickel coating was added to the test matrix along with the baseline CuNiIn. Nickel was chosen because of its potential to produce what is often called a “glaze” oxide layer at high temperature, which has been shown by Stott et al to reduce friction and wear in nickel-based alloys [45]. In addition, two thin, hard, and inert PVD coatings (TiAlN and CrCN) were applied to the uncoated counterparts and worn against the CuNiIn and Ni coatings. TiAlN (Titanium-Aluminum-Nitride) and CrCN (Chrome-Carbon-Nitride) were chosen for their high hardness, high modulus, and low surface energy. The low surface energy makes these coatings resistant to adhesive wear when coupled with the metallic plasma sprayed coatings.

5.1 Experimental

5.1.1 Specimens

The specimens used for this investigation were Ti6Al4V, and the test geometry was an ellipsoid on a flat plate. The ellipsoid, shown in Figure 2.2, was designed to eliminate the stress concentrations that occur at the edges of cylindrical contacts. Therefore, the Hertzian contact stress profiles for the samples are smooth with a maximum stress at the center instead of near the edge of contact. In addition, the elliptical contact simplifies alignment procedures for reproducible contact areas, and the large radius in the sliding direction allows for a target maximum Hertzian contact pressure of 650 MPa with an applied normal load of 50 N. The plates were flat circular disks with a diameter of 12.7 mm on the test face and 3.2 mm thick. Average surface roughness (Ra) was 0.1μm on both the disk and the ellipsoid. Prior to testing, the Ti6Al4V disks were commercially grit blasted and then plasma sprayed with 100μm thick CuNiIn, and Ni. In addition, a commercial vacuum arc deposition system was used to apply

2μm thick TiAlN and CrCN coatings to the surfaces of some of the Ti6Al4V ellipsoids. All of the coating properties are listed in Table 5.1.

Table 5.1. Substrate and coatings properties.

Materials	Composition Weight %	Roughness Ra (μm)	Nano Hardness (GPa)	Micro Hardness (HV)	Modulus (GPa)	Surface Energy (mJ/m^2)
Titanium Substrate and Counter face	90% Ti 6% Al 4% V	0.1	4.1	284	143	
Copper Nickel Indium	64% Cu 35% Ni 1% In	9	2.4	138	90	
Nickel	Commercially pure	7	2.1	133	82	
Chrome Carbon Nitride	CrCN	0.3	32*	NA	436*	35
Titanium Aluminum Nitride	TiAlN	0.3	28*	NA	330*	49

*Nano Hardness was measured on polished M50 substrates.

5.1.2 Tribological Testing and Analysis

The purpose of this study was to provide an understanding of how Ti6Al4V (uncoated and coated) performs when coupled with the selected metallic plasma sprayed coatings, and subjected to gross slip fretting wear at room temperature. Four repeat tests were conducted on each coating configuration. The tests were conducted using a 200μm stroke length, 30Hz oscillation speed, and a 50N normal load for 100,000 cycles. The applied 50N normal load yields a maximum Hertzian contact stress of approximately 650MPa. In addition, some shorter duration tests were conducted at 2 Hz oscillation speed, to supplement the longer tests for wear analysis.

For the duration of each test the root mean square (RMS) of the friction data and the frictional hysteresis were recorded. The fretting wear tribometer, shown in Figure 2.3, has a stage that is mounted on thin metal legs that can support the normal applied load, while acting as tangential springs in the oscillation direction. As the elliptical sample moves, the friction force between the samples causes the sample stage to deflect slightly, on the order of 1 μm typically, in the direction of sliding. The stage deflection then compresses or stretches the attached piezo electric transducer and creates a signal. The signal from the piezo is then amplified and calibrated, using a force meter, to match the amount of force applied to the stage prior to testing. The friction force is then collected using an oscilloscope data acquisition card and a computer. Once collected, the RMS of the friction force is then tabulated and plotted per test cycle. In

addition, a laser measuring system, shown in Figure 2.3, is focused on the face of the oscillating arm of the tribometer. The laser is used to continuously track the displacement of the ellipsoid during each test. The real time displacement and friction data are then collected using the same oscilloscope computer card. During the course of each test the displacement and friction data are plotted together to produce in situ hysteresis loops that provide real time monitoring of the fretting wear regime. This same technique was used by Hager et al in 2004 to characterize the transition between the mixed and gross slip fretting wear regimes in Ti6Al4V interfaces [16].

Once the fretting wear tests were completed, post test analyses were performed using scanning electron microscopy (SEM) and 3-D (contact and optical) profilometery for morphology, along with energy dispersive spectroscopy (EDS) and x-ray mapping for chemical analysis. All cross-sections were cut perpendicular to the fretting wear direction using a low speed diamond saw. The uncoated ellipsoid cross-sections were mounted using a hard carbon filled conductive hot compression mount. The hot compression mounts were used on the ellipse cross-sections because they have a relatively high hardness and good edge retention, which is needed to keep the worn regions intact during the polishing process. Once mounted, all cross-sectioned samples were polished prior to microstructure and EDS analysis.

5.2 Results

5.2.1 Friction and Wear

Figure 5.1 shows typical friction traces measured during the course of the fretting tests. The coefficients of friction for all the tests ranged from approximately 0.68 to 0.85. The addition of the hard coatings made the friction traces smoother over the test duration. However, the coatings made the friction slightly higher when coupled with the CuNiIn coating and slightly lower when coupled with the Ni coating. Against the Ni coating both of the hard coatings exhibited virtually equivalent steady state friction at 0.68, which is about 0.1 lower than the tests conducted without the hard coatings. Against the CuNiIn coating the hard coatings exhibited higher friction than the uncoated baseline, and the CrCN coating yielded the highest friction.

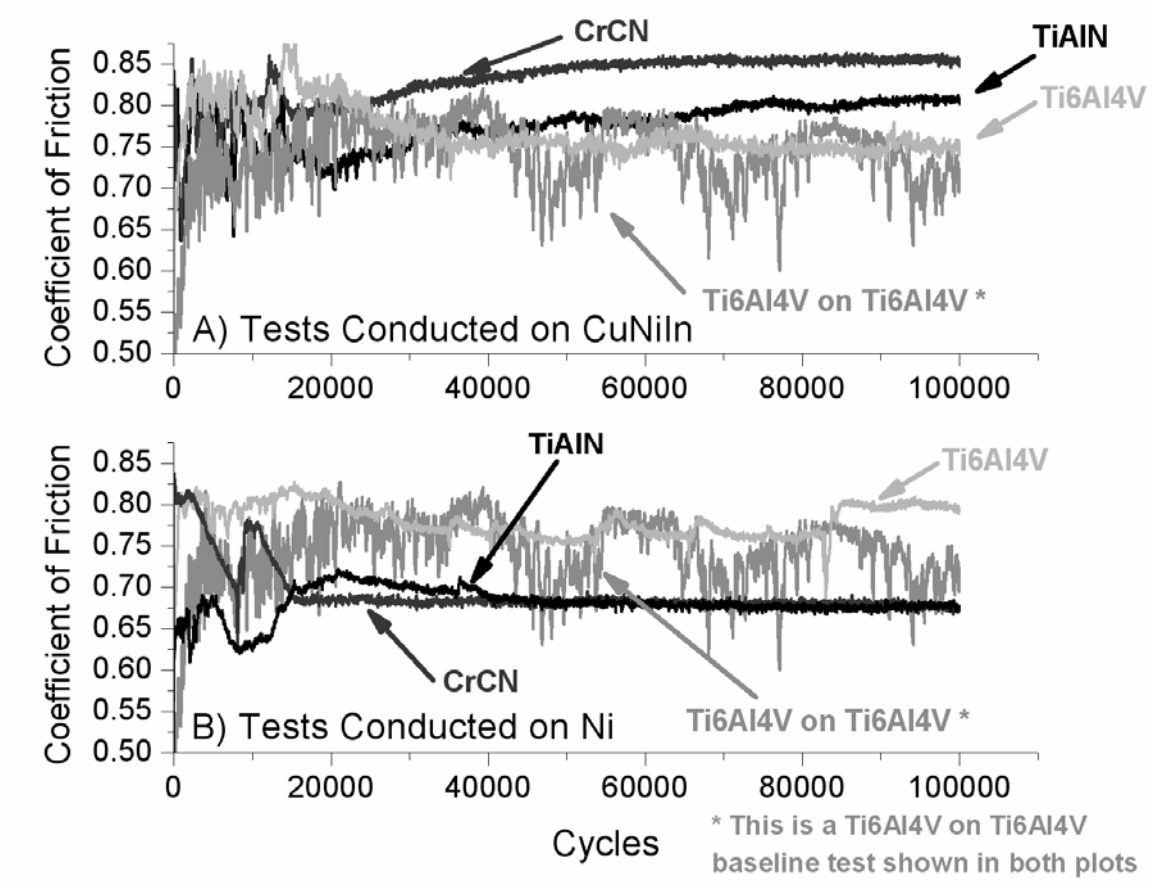

Figure 5.1. Typical friction plots for gross slip fretting tests conducted on A) the plasma sprayed CuNiIn coatings and B) the plasma sprayed nickel coatings.

In addition to measuring the friction, the plasma sprayed coating wear was assessed by determining the maximum depth in each wear track using a 3-D profilometery. Figure 5.2 shows the average of the maximum depths measured for each configuration tested. This plot shows that the Ni coatings were slightly more wear resistant than the CuNiIn coatings in every configuration. In addition, the hard coatings did not significantly affect the depth of the wear tracks created on the plasma sprayed coatings, with the exception of the TiAlN coating coupled with the plasma sprayed Ni. This shows that the implementation of the hard coatings will not adversely affect the life of the mated plasma sprayed coatings, unless TiAlN is mated with plasma sprayed Ni.

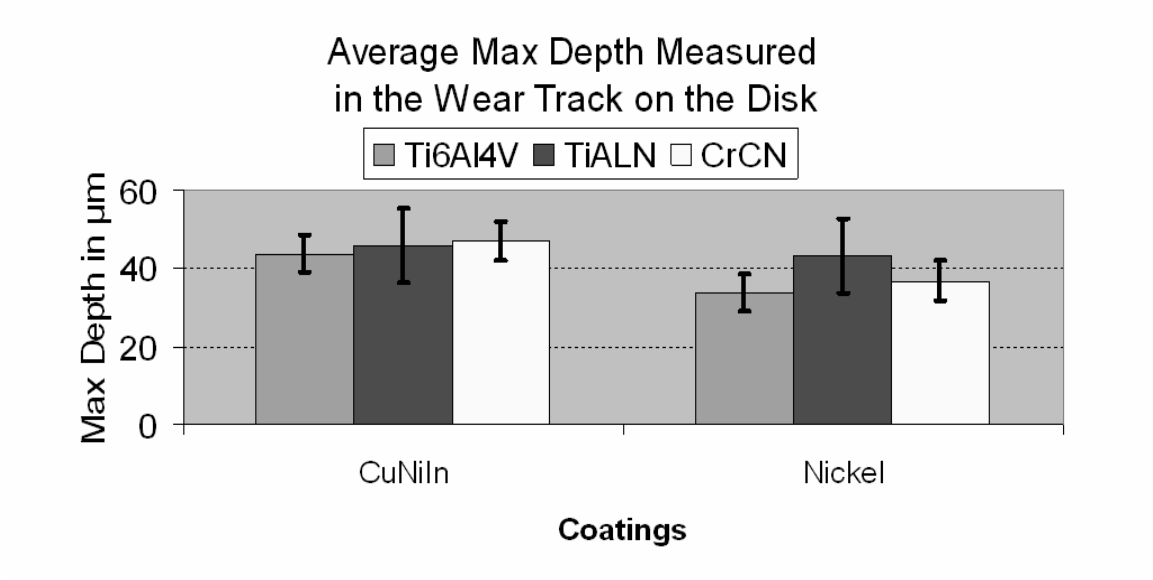

Figure 5.2. Coating wear as quantified after the 100,000 cycle tests by measuring and calculating the average maximum depth in the plasma sprayed coating fretting wear tracks.

5.2.2 Wear Mode Analysis

This study consisted of fretting wear tests in which coated and uncoated Ti6Al4V ellipsoids were worn against Ti6Al4V, CuNiIn, and Ni. Uncoated Ti6Al4V specimens were tested as a baseline to quantify how well the plasma sprayed coatings and the hard coatings protect the mated Ti6Al4V ellipsoid surfaces.

5.2.2.1 Uncoated Ellipsoid Wear

At room temperature the Ti6Al4V mating surfaces are damaged primarily by galling initially, and then by 3rd body wear as the large adhered particles started to break apart. After 10 cycles, with 2 Hz oscillation speed, the gross slip fretting wear at the Ti6Al4V interface of the test specimens is composed of solely adhesive wear, as shown in Figure 4.3A. The mated surfaces exhibited severe plastic deformation with large wear particles, on the order of 100 µm long and 50 µm wide, adhered to the wear track. After 100 cycles the large wear particles in the contact started to break up into smaller wear debris, as shown in Figure 4.3B. The majority of the debris gathered around the edges of the contact, with some of the debris getting trapped inside the wear track. After 1,000 cycles almost the entire wear track is filled with wear debris, as shown in Figure 4.3C. Some large wear particles can be seen near center and the edges of the wear track. Some of these larger particles are produced in local regions throughout the wear track where the Ti6Al4V surfaces make contact in the absence of the trapped wear debris. After 100,000 cycles, with 30 Hz oscillation speed, the wear track is completely filled with wear debris, as shown in Figure 4.3D. This exact wear mode has been described in detail in a fretting wear review paper by Hurricks [40], and by Blau [35] in his work with wear mechanisms in metallic interfaces. Figure 4.4A and 4.4B show cross-sectional micrographs of a typical 100,000 cycle Ti6Al4V mated fretting wear test. The cross-sections of the ellipsoid wear tracks were cut perpendicular to the fretting direction as shown by the arrows in Figure 4.3D. In the center of

the wear track, the wear scar is approximately 40 μm deep. The dark region is a compacted powder bed of fine titanium and oxide wear debris. Using Raman Spectroscopy, Hager et al [16] determined that the accumulation of gross slip fretting wear debris in the contact of Ti6Al4V mating surfaces contains significant amounts of rutile TiO_2. Figure 4.4B shows the plastically deformed surface layers, or highly deformed layer (HDL) as defined by Rigney et al [41], near the edge of the wear scar and beneath the trapped wear debris. In these contact regions the accumulation of plastic deformation occurs until the surface material becomes too brittle to accommodate the imposed strain, as explained by Blanchard et al [33]. This eventually leads to the breakup of surface regions and the formation of large wear particles.

The wear mode analysis conducted on the uncoated Ti6Al4V ellipsoids, worn against the plasma sprayed CuNiIn and Ni coatings, determined that the wear evolution and damage mechanisms are similar to those exhibited by mated Ti6Al4V surfaces. Figures 5.3 shows SEM micrographs of the ellipsoid surface damage caused by gross slip fretting against each of the plasma sprayed coatings after 100 cycles. The accumulated damage is driven by adhesive wear. EDS analysis and X-ray mapping of the magnified regions showed that the large adhered particles, in all four wear tracks, are adhered metallic particles from the various coating surfaces. These large adhered particles plow large channels or make striations on the surface of the Ti6Al4V ellipsoids. In addition, the micrographs from these tests also show a significant amount of tiny wear debris trapped within the wear track. Using EDS, it was determined that these particles are a mixture of mostly oxidized Ti6Al4V and transferred coating wear debris. Wear against the CuNiIn coating produced large adhered coating particles, on the order of 20 to 100μm in size. In addition, 100 cycles of fretting was enough to cause galling throughout most of the contact area and create large amounts of trapped oxide debris, the tiny white particles that are dispersed throughout the wear track as shown in Figure 5.3A. Fretting against the Ni coating produced a wear track on the Ti6Al4V mated ellipsoid that was similar to what was seen in the CuNiIn tests. The differences between the two are that the Ni created a wear scar with deeper galling tracks and more fine oxide debris, on the order of 5 to 10μm in size, trapped within the contact, as shown in Figure 5.3B.

Figures 5.4 shows micrographs of the ellipsoid wear after 1,000 and 100,000 cycle tests. In the 1,000 cycle tests conducted against Ni, Figure 5.4C, the gross slip fretting wear progression of the interfaces has lead to the break up and oxidation of the large galling products and the protruding Ti6Al4V at the edges of the severely deformed regions that were seen in the 100 cycle tests. Therefore, the interfacial wear on the ellipsoid has transitioned from adhesive wear and galling to a 3rd body abrasive wear during the period between 100 and 1,000 cycles. In the 1,000 cycle tests conducted against CuNiIn, Figure 5.4A, the wear tracks show an increased amount of fine oxide debris trapped within the wear track, and the absence of the large transfer particles that were seen in the 100 cycle tests. However, the wear scars created by CuNiIn exhibited large regions near the center of the contact where evidence of adhesive wear was still apparent. After 100,000 wear cycles all surfaces of the wear tracks against both coatings were completely covered with a powder bed of compacted wear debris, as shown in Figure 5.4B and 5.4D.

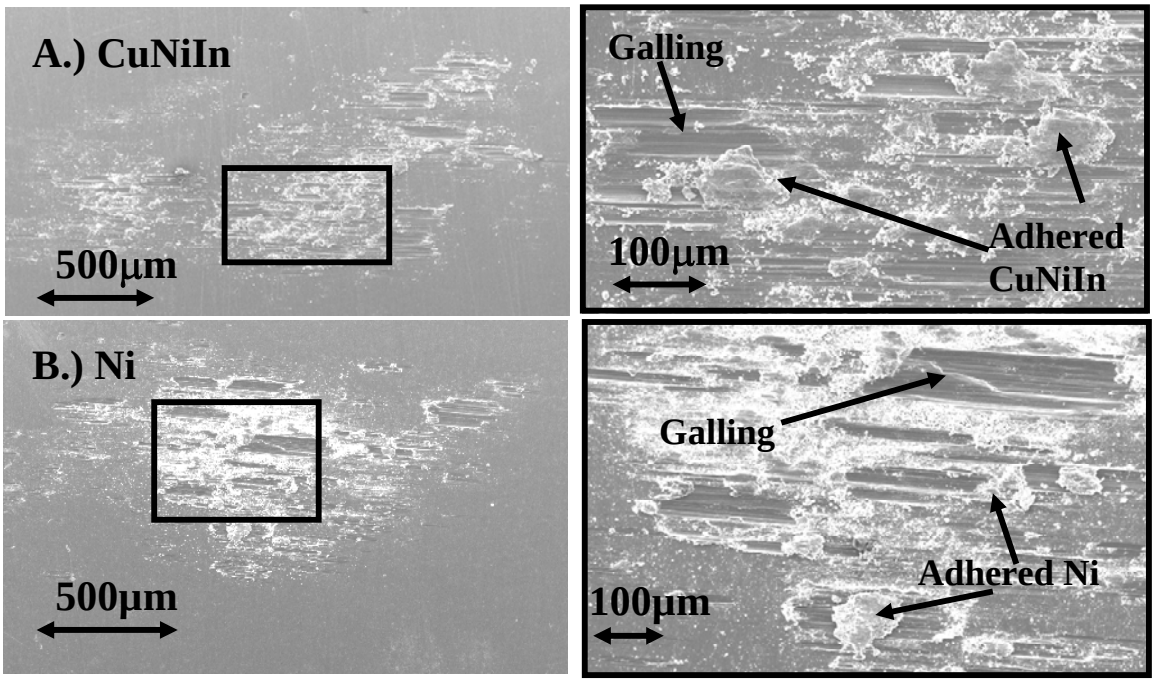

Figure 5.3. SEM micrographs of the fretting wear on the surface of the Ti6Al4V ellipsoid after being worn against the test coatings for 100 cycles at 2Hz. The images outlined in black on the right are zoomed images of what is contained in the black squares on the left.

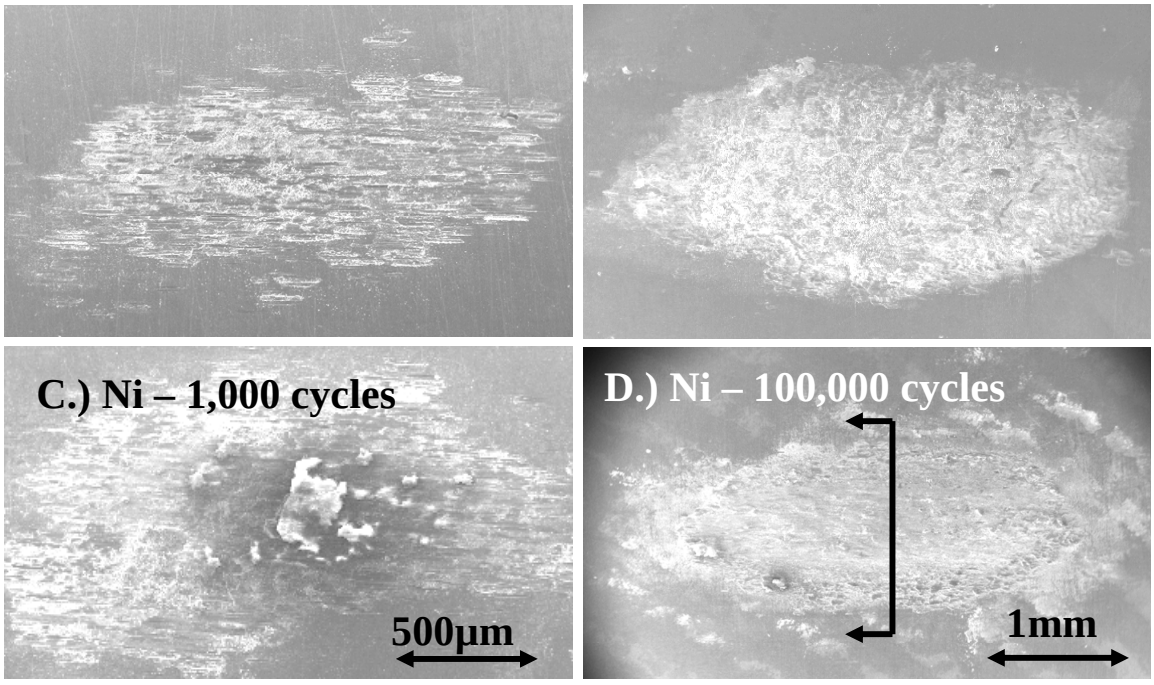

Figure 5.4. SEM micrographs of the fretting wear on the surface of the Ti6Al4V ellipsoid after being worn against the test coatings at room temperature for 1,000 and 100,000 cycles respectively.

In addition to the wear scar surface analysis, all of the Ti6Al4V ellipsoids worn for 100,000 cycles were cross-sectioned perpendicular to the fretting direction, shown by the black arrows in Figure 5.4B and 5.4D. Analysis of the back scatter (BSE) SEM micrographs of the ellipsoid cross-sections, shown in Figure 5.5, further verifies the similarities in the fretting wear mechanisms that damage these Ti6Al4V surfaces when self mated or worn against the CuNiIn or Ni plasma sprayed coatings. Fretting wear of Ti6Al4V ellipsoid surfaces mated with the CuNiIn coatings produced virtually identical wear to that of the mating Ti6Al4V surfaces, as seen by comparing Figures 5.5A and 5.5B with Figures 4.4A and 4.4B. The only differences being that the mixed metal and oxide debris compacted into the worn ellipsoid surfaces have different chemistries. The wear on the ellipsoid surfaces mated with the Ni coatings, shown in Figures 5.5C and 5.5D, also exhibit similar wear mechanisms. However, these surfaces have thinner transfer films of compacted debris and larger Ti6Al4V wear particles. Often these Ti6Al4V particles are on the order of 50μm deep and just as wide. This is typically 2 to 3 times larger than the ones seen at the CuNiIn worn Ti6Al4V interfaces.

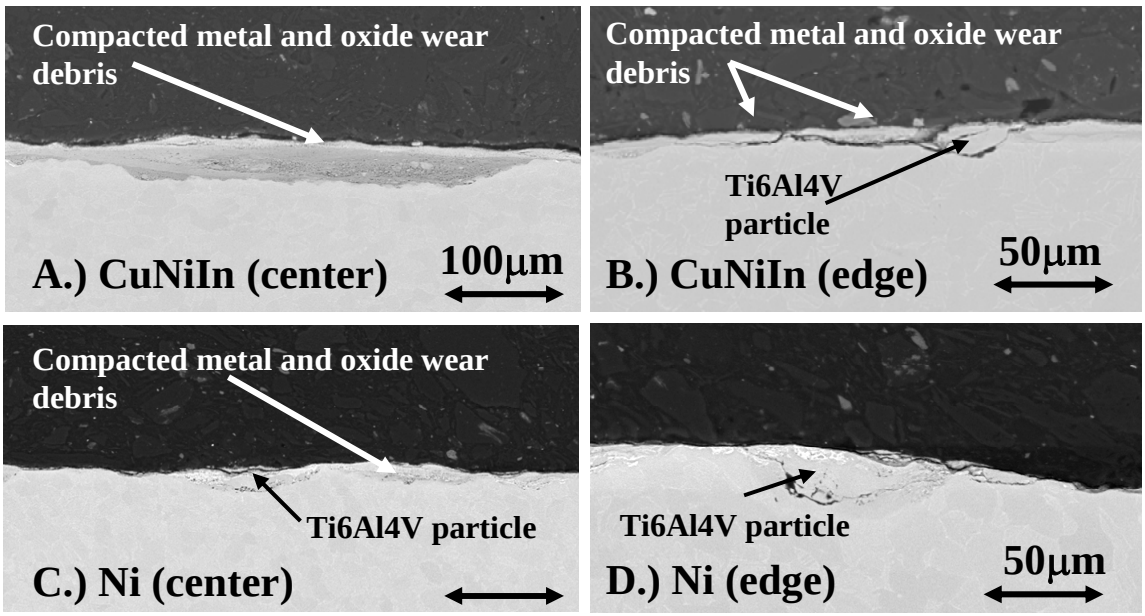

Figure 5.5. Back scatter (BSE) SEM image showing the cross-section of a Ti6Al4V ellipsoid worn against the test coatings at room temperature for 100,000 cycles. Images on the left are from the center of the wear track, and images on the right are from a region near the edge of the respective wear track.

5.2.2.2 Coated Ellipsoid Wear

The evaluation of the hard coatings began by conducting 100,000 cycle tests on both the TiAlN and CrCN coated ellipsoids against the baseline CuNiIn plasma sprayed coatings. Figure 5.6 shows that after 100,000 cycles the TiAlN coating was worn completely away. It can be seen from the cross-section in Figure 5.6C that the ellipsoids exhibited severe damage throughout the entire wear track. However, the wear track does not have any cracks or large wear particles trapped in the wear track, and there is not a thick robust powder bed formed by the wear debris, as seen in the uncoated ellipsoid tests. The CrCN coating performed significantly better. Figure 5.7C shows that the damaged region is concentrated in the center of the contact, which is the area

of highest contact stress. In fact, it can be seen in Figure 5.7B that the center of the wear track has started to gall and wear, similar to the uncoated ellipsoids had done. However, this is concentrated in the center of the contact, with evidence that the coating is still intact in some of the surrounding region of the wear track. Figure 5.7D, in conjunction with Figure 5.8, show SEM and EDS of a zoomed region just outside the galled region at the center of the wear track. In these images it can be seen that the CrCN coating has slowly worn away during the course of the test without cracking or delaminating. Therefore, the coating slowly wore out during the course of the test, with the bulk of the wear concentrated at the center of the wear track. As the substrate is exposed, the underlying Ti6Al4V began to gall and wear just as it had in the tests with the uncoated ellipsoids.

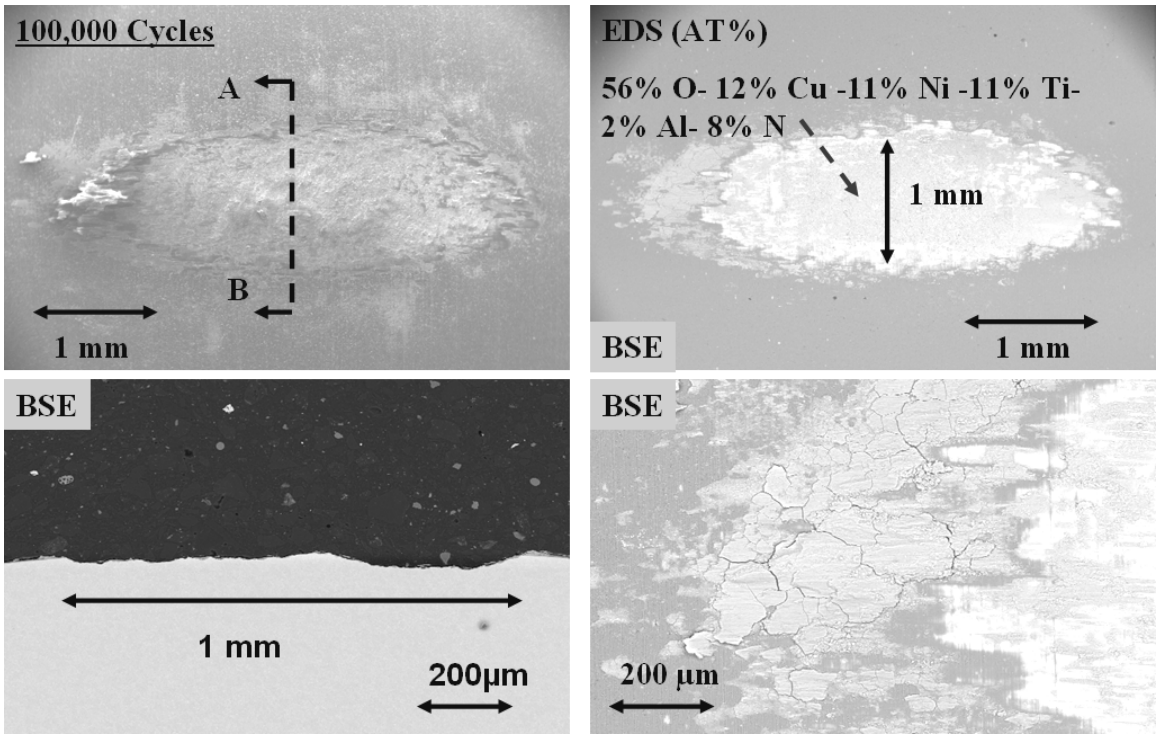

Figure 5.6. SEM images showing the wear scar from a TiAlN coated ellipsoid worn against CuNiIn for 100,000 cycles. The cross-section was cut perpendicular to the fretting wear direction as shown by the arrows in A.

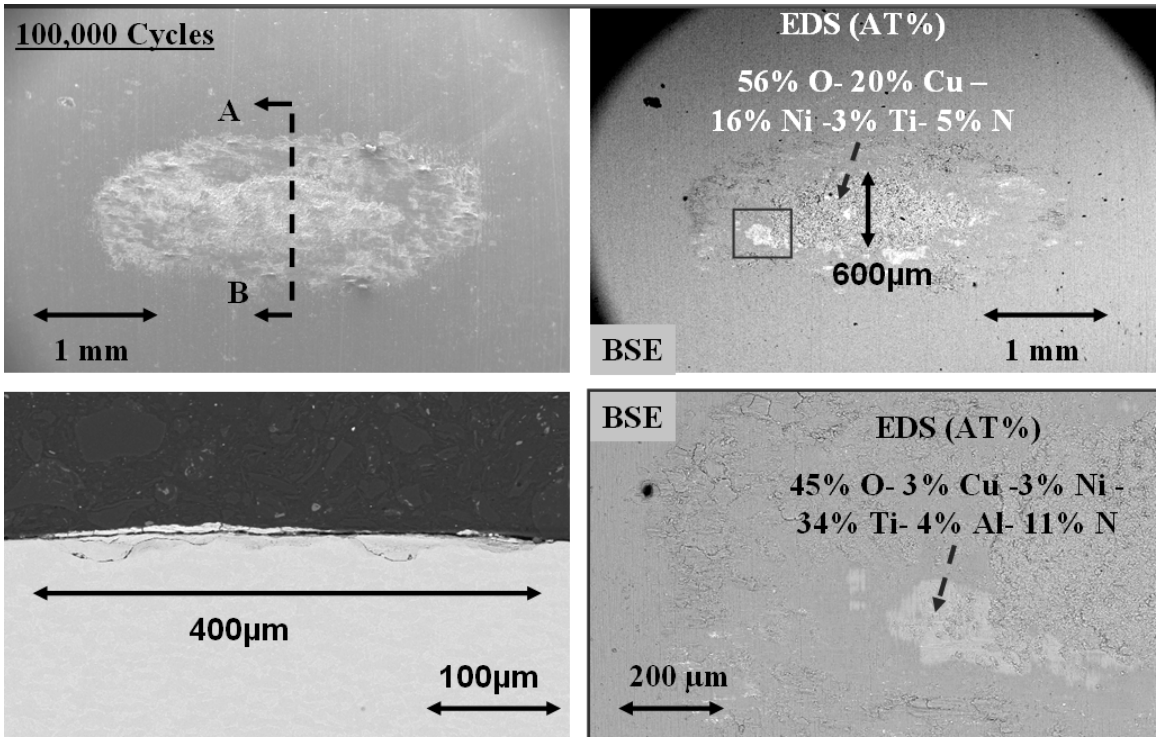

Figure 5.7. SEM images showing the wear scar from a CrCN coated ellipsoid worn against CuNiIn for 100,000 cycles. The cross-section was cut perpendicular to the fretting wear direction as shown by the arrows in A. D is a zoomed image of the boxed region in B.

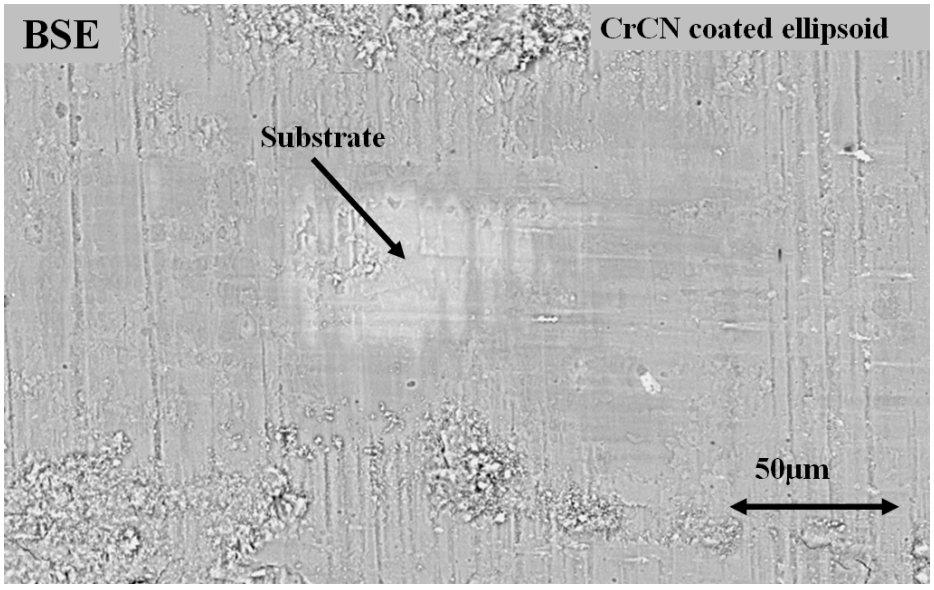

Figure 5.8. This is a BSE SEM image showing a region just outside of the galling at the center of the wear scar on a CrCN coated ellipsoid worn against CuNiIn for 100,000 cycles.

Once the CuNiIn tests were finished, 100,000 cycle tests were then conducted against the Ni plasma sprayed coatings. Both TiAlN and CrCN performed substantially better than they did when worn against the CuNiIn coatings. The TiAlN coating, shown in Figure 5.9, had a central region of the wear track that was worn. In this region the ellipsoid exhibited signs of galling and

Ni transfer. However, outside of the centrally located galling, there was evidence that the TiAlN was still intact through much of the wear track. This is shown in Figure 5.9B where the EDS results describe a high nitrogen content in the lighten regions of the wear track. The CrCN coating performed similarly. However, the centrally located wear region, as shown in Figure 5.10, was much smaller and the overall damage within the wear track was much less. Figure 5.11 is a zoomed SEM image showing the edge of the galled region at the center of the wear track in Figure 5.10B. This image, combined with EDS, shows that the CrCN is mostly intact with some localize regions where the underlying Ti6Al4V is starting to show through.

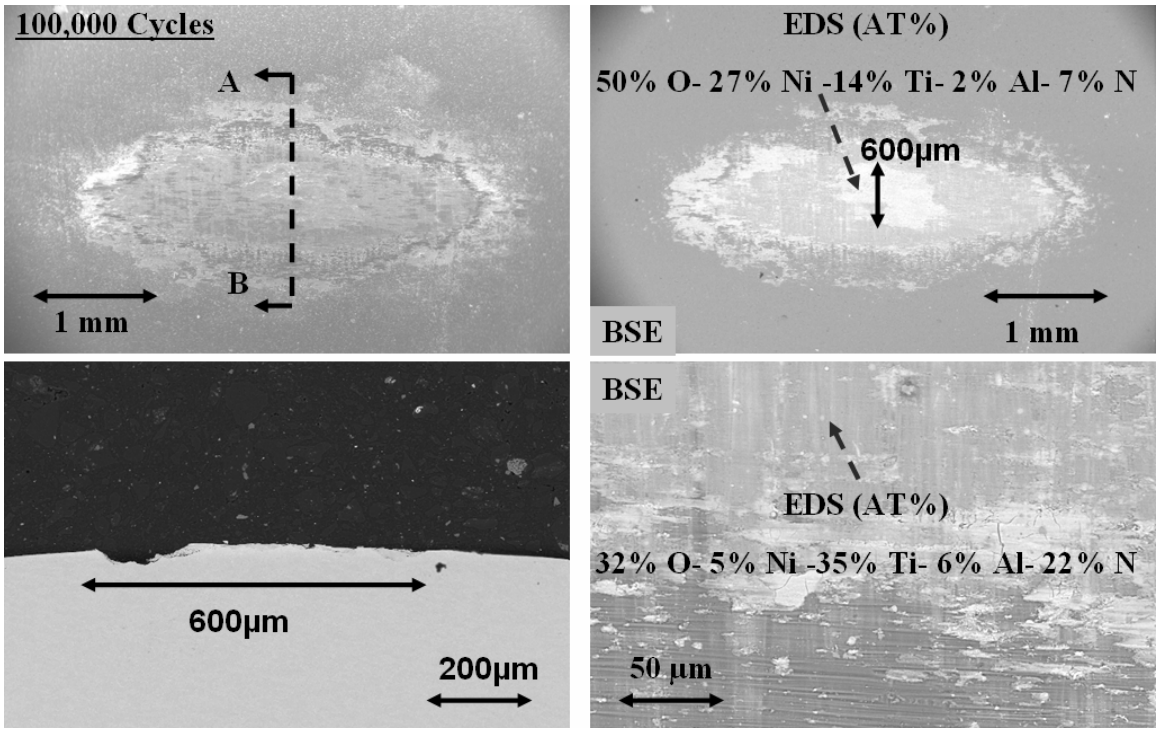

Figure 5.9. SEM images showing the wear scar from a CrCN coated ellipsoid worn against Ni for 100,000 cycles. The cross-section was cut perpendicular to the fretting wear direction as shown by the arrows in A. D is a zoomed image of the lower edge of the wear track.

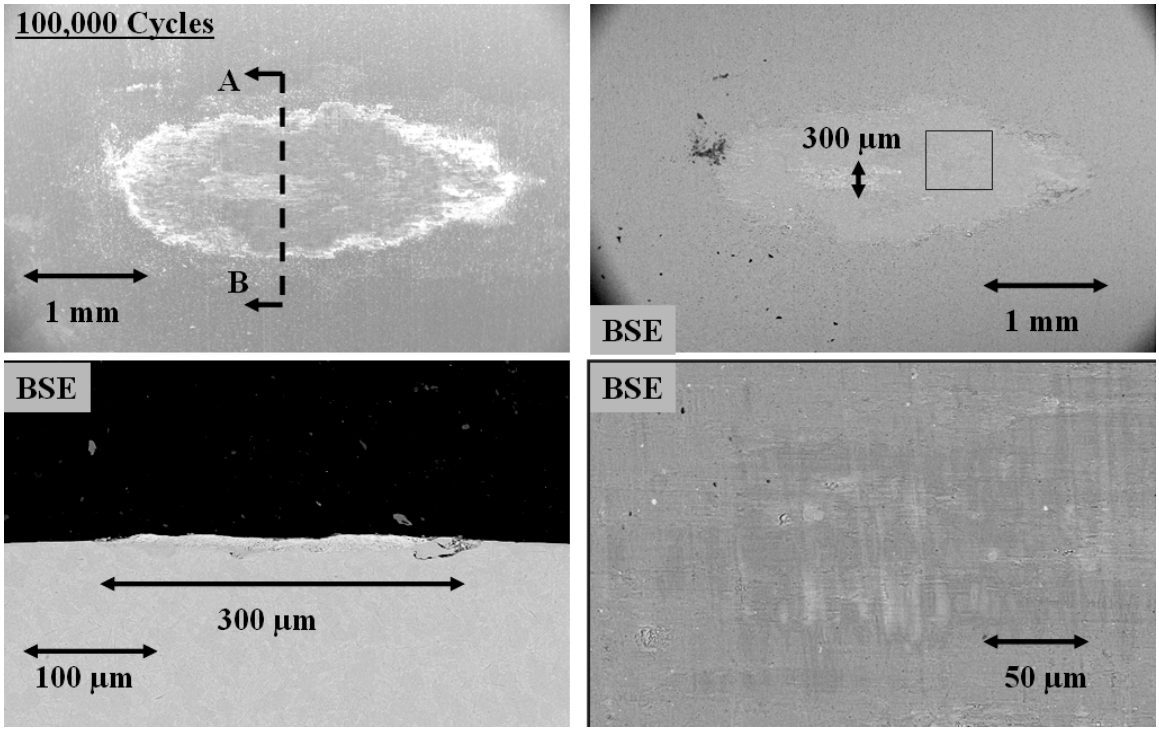

Figure 5.10. SEM images showing the wear scar from a CrCN coated ellipsoid worn against Ni for 100,000 cycles. The cross-section was cut perpendicular to the fretting wear direction as shown by the arrows in A. D is a zoomed image of the boxed region in B.

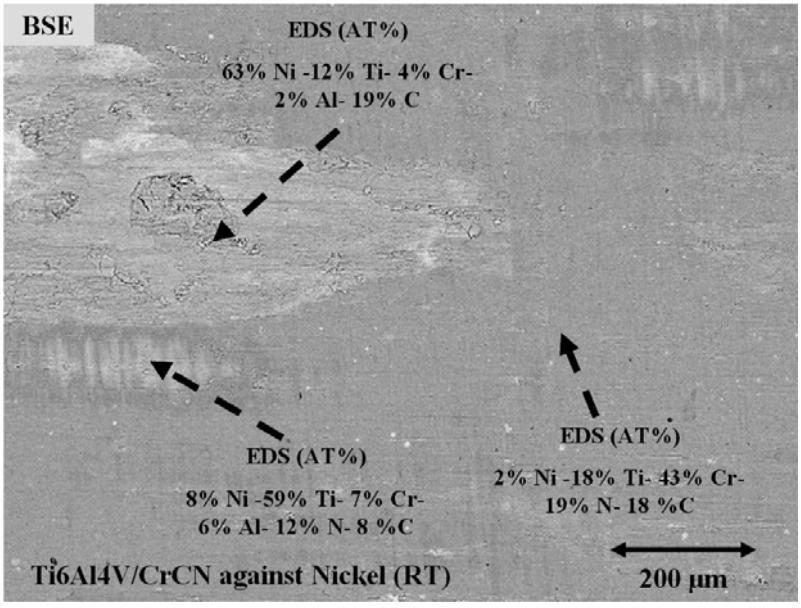

Figure 5.11. This is a zoomed BSE SEM image showing the edge of the galling region at the center of the wear scar on a CrCN coated ellipsoid worn against Ni that is shown in Figure 5.10B.

All of the 100,000 cycle tests, with the exception of the TiAlN mated with CuNiIn, showed that the hard coatings reduced the amount of wear to the Ti6Al4V ellipsoids. For more insight, shorter duration tests at 2 Hz oscillation speed were conducted using the CrCN coating mated with plasma sprayed Ni. This combination was chosen because it performed the best in the 100,000 cycle tests. Figure 5.12 shows micrographs of the fretting wear on the CrCN coated ellipsoids after tests of 10, 100, 1000, and 10,000 cycles. From these images it can be seen that the wear mechanism has been changed from what was seen in the Ti6Al4V/Ni contacts. The surfaces did not exhibit galling or severe adhesive damage. In addition, there was no evidence of 3rd body wear from trapped debris either. In fact the x-ray maps of the surface of the CrCN coated wear track after 10,000 cycles, shown in Figure 5.13, show that the hard coating is still intact and that there is a thin transfer film of Ni smeared onto the surface of the wear track.

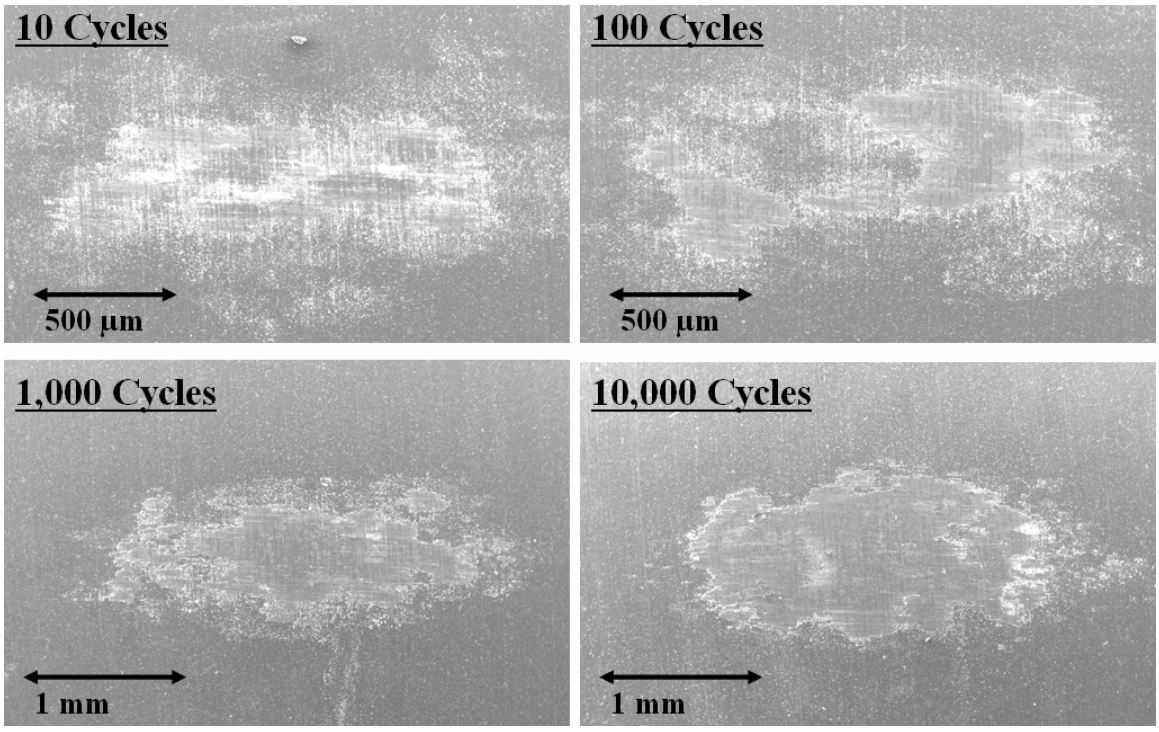

Figure 5.12. These are secondary electron SEM images of the wear track formed when CrCN coated ellipsoids were fretted against plasma sprayed Ni for 10, 100, 1000, and 10000 cycles respectively.

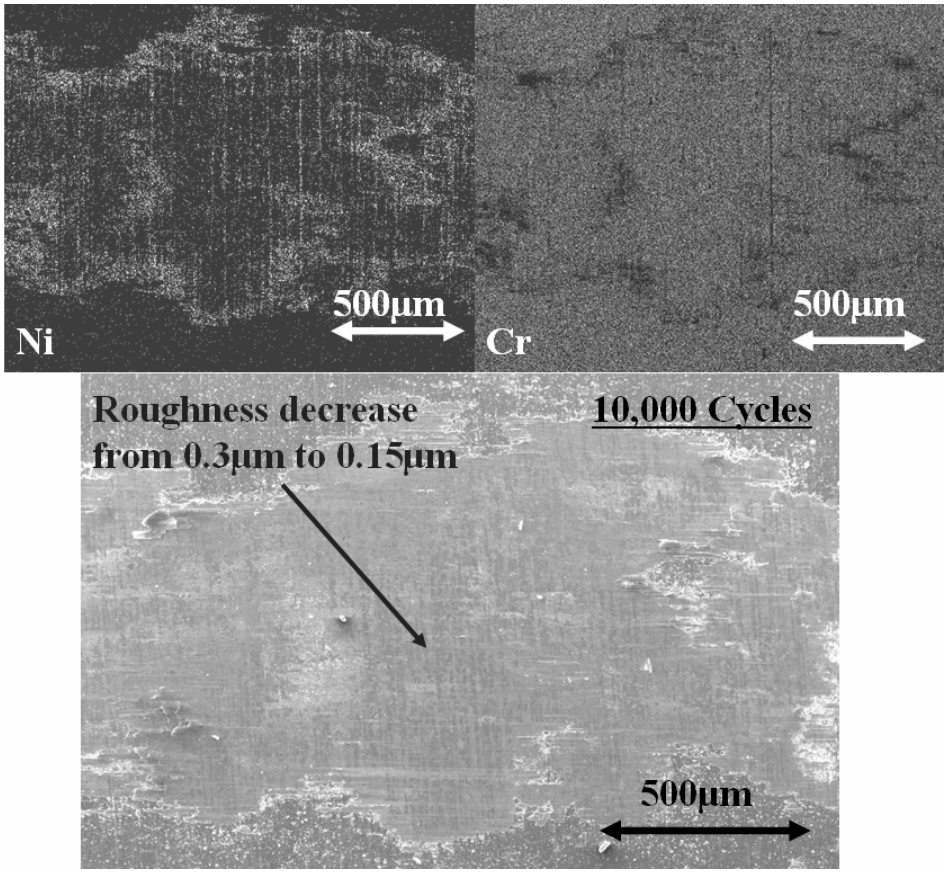

Figure 5.13. A and B are x-ray maps of the secondary electron SEM image shown in C. The light gray in the x-ray maps are for detected Ni in A and detected Cr in B.

5.3 Summary and Discussion

In overview, this study was conducted to assess the interfacial wear mechanisms associated with gross slip fretting of coated and uncoated Ti6Al4V in contacts mated with CuNiIn and Ni plasma spray coatings at room temperature. The uncoated Ti6Al4V ellipsoid tests were conducted without lubrication and caused metallic wear in the fretting contact. All metallic engineering surfaces are covered by thin oxide layers that are typically angstroms or nanometers in thickness [40 and 43]. This contaminant layer initially protects the underlying metal. However, surface species are dispersed during the first few cycles of the fretting wear process causing the intimate contact of the Ti6Al4V ellipsoid surfaces with the metallic coating surfaces. When this happens the contacting nascent metallic surfaces cause adhesive wear and ultimately galling. The galling of the Ti6Al4V ellipsoid surface coincided with the shearing of the coating surface asperities, and the simultaneous transfer metallic material between the contacting surfaces.

Both of the coatings tested were approximately half as hard as the Ti6Al4V contact surface. This would lead one to believe that material transfer at the fretting interface would consist of the softer coating surfaces transferring to the harder Ti6Al4V surface, and in fact this is what predominantly occurs. However, there are localized regions where large Ti6Al4V particles, on the order of 50 to 100µm, were adhered to the surfaces of the CuNiIn and Ni

coating surfaces. Bowden et al [44] also witnessed a similar phenomenon, when they observed the transfer of small fragments of mild steel to the surface of copper during sliding wear experiments. This is an extremely devastating wear phenomenon that accelerates the ellipsoid wear, because the Ti6Al4V adhered particles form raised plateaus on the coating surface and promote further galling by creating titanium on titanium contact within the fretting interface.

Galling and material transfer, along with the shearing of coating asperities typically occurs within the first 100 gross slip fretting wear cycles. Between 100 and 1,000 cycles of wear, the highly deformed surface layer of the Ti6Al4V ellipsoid becomes too brittle to accommodate the imposed fretting displacement, as explained by Blanchard et al [3], and begins to crack and break, as shown in Figure 4.4B. In addition, the continued deformation of the transferred material plateaus causes them to breakup as well. This creates an abundance of wear debris within the contact. The wear debris represents a wear mode shift from adhesive driven wear to wear that is mostly driven by the rheology of the 3rd body debris.

From 1,000 cycles to 100,000 cycles some of the wear debris is swept out of the wear track, and some of the wear debris remains. The trapped or active wear debris continuously gets crushed into fine particles and oxidizes. As the active wear debris builds up in the wear track, it gets compressed together and forms a powder bed that separates the contacting surfaces. If the powder bed formation is continuous, as it is in the cross sections of the ellipses worn against CuNiIn shown in Figure 5.5A, then the surface degradation will be concentrated at the edges of the contact and expand the wear track laterally instead of deeper. This can be seen in Figure 5.5B.

Ultimately, the thermal spray coatings tested did not change the associated wear mechanisms or reduce the apparent wear damage imposed on the Ti6Al4V ellipsoid surface. This may be because of the formation of a powder bed in all of the tested configurations. The rheology of the 3rd body debris, primarily the titanium oxide debris which is constant to all of the tests, controls the extent of the fretting wear damage to the Ti6Al4V ellipsoid after 1,000 cycles, or once enough debris has been established in the contact. In addition, the CuNiIn and Ni thermal spray coatings sustained severe wear during each of the fretting wear tests. 30% to 40% of the coating thickness had been worn away after 100,000 cycles of fretting.

The wear analysis from this study supports the need for a different coating system than one currently used. Although the actual compressor blades are coated with thermal sprayed coatings and then with solid lubricants, this study shows the dangers of what can happen if/or when the lubricants fail or are completely worn away. In gross slip fretting, these soft thermal spray coatings do not effectively protect the mating Ti6Al4V surfaces. Therefore, TiAlN and CrCN coatings were applied to the surface of the Ti6Al4V ellipsoid surfaces. These hard inert coatings were chosen to act as a barrier and protect the Ti6Al4V ellipsoids from the galling that occurs as the first stage in the fretting wear mode.

After 100,000 gross slip fretting cycles it was found that the hard coatings had in fact reduced the ellipsoid wear, except in the combination of TiAlN mated with CuNiIn. Because the center of the elliptical contact exhibits the highest contact stress, the coatings wore through initially at the center of the contact. This exposed the underlying titanium surface and started the fretting wear mode that was described for the uncoated ellipsoid surfaces. However, it is important to note that the hard coatings did not fail due to delamination or cracking. The gradual wear of the coatings, as shown in Figure 5.8 and 5.11, meant that the wear was concentrated near

the center of the contact and then gradually expanded. Figure 5.14 shows a plot of what is considered to be the apparent wear reduction to the Ti6Al4V ellipsoids due to the addition of the hard coatings. This plot was made by considering the area of the centrally located galled regions, with respect to the total wear area of the fretting contact. By considering the wear reduction in this way, it was found that the CrCN coating is able to reduce the wear area on the ellipsoid surface by approximately 88%. In addition to this finding, shorter duration tests were conducted on the CrCN and Ni coating pair. These tests showed that the CrCN coating was still completely intact after 10,000 fretting wear cycles. Because we have already shown that the Ni coatings caused significant damage to the Ti6Al4V ellipsoids after just 100 cycles, this is more

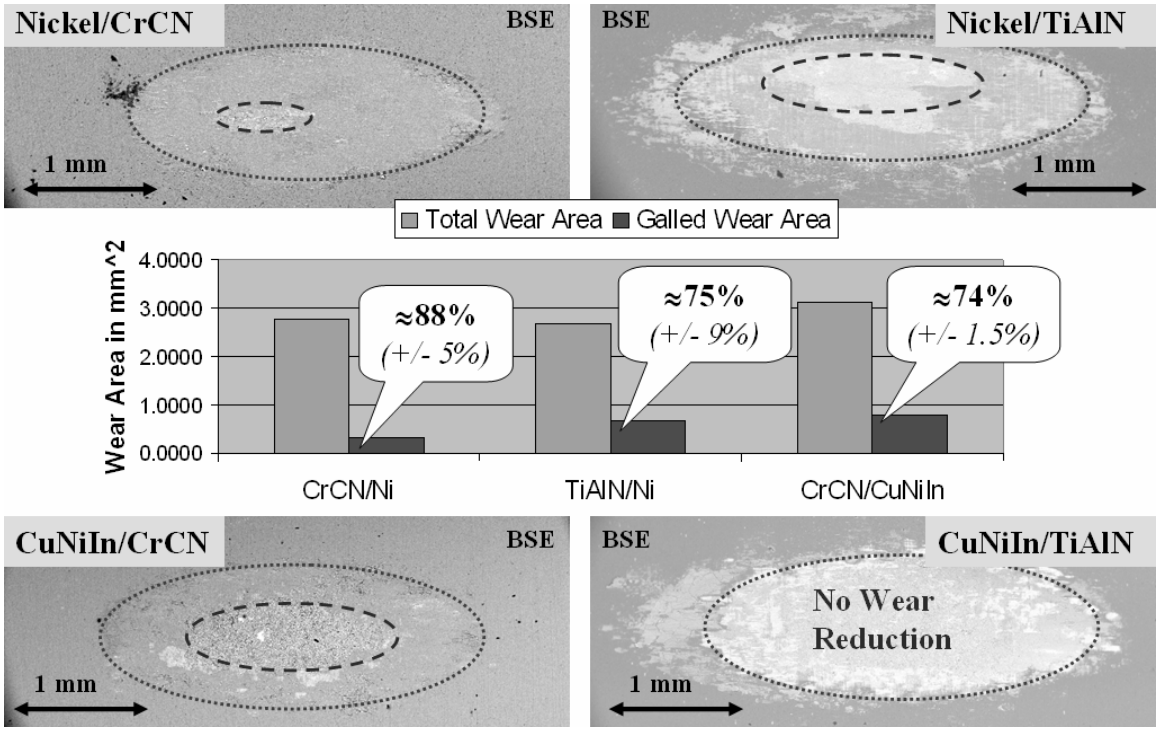

than 2 orders of magnitude improvement in wear life.

Figure 5.14. The bar chart shows the apparent reduction in wear calculated from the ratio of the galled area to the total wear area.

5.4 Conclusions

This study was conducted to examine the wear mechanisms associated with (TiAlN and CrCN) coated and uncoated Ti6Al4V mated with plasma sprayed CuNiIn and Ni coatings, and subjected to gross slip fretting. The following conclusions are drawn from this study:

- The wear mechanisms that governed the surface damage accumulation were the same in all of the uncoated ellipsoid tests, and significant damage was found on the uncoated ellipsoids after just 100 test cycles.
- The Ni coatings were slightly more wear resistant than the CuNiIn coatings, and that the addition of the hard coatings adversely affected the Ni coatings in the TiAlN/Ni mated tests.

- The addition of the hard TiAlN and CrCN coatings reduced the total wear damage in all of the tests, except for the TiAlN mated with CuNiIn tests.
- Both the TiAlN and CrCN performed better when worn against plasma sprayed Ni, than they did against the CuNiIn coatings.
- CrCN mated with the Ni coating had the best overall performance. In this configuration, the CrCN coating was shown to still be completely intact after 10,000 cycles. Uncoated Ti6Al4V ellipsoids worn against the CuNiIn and Ni coatings both showed severe damage after 100 cycles. Therefore, this shows more that 2 orders of magnitude improvement in wear life to the Ti6Al4V ellipsoids in comparison to the baseline CuNiIn and Ni configurations.

6. Research Summary and Conclusions

The four research studies conducted have provided insight into fretting wear regimes and wear mechanisms that control fretting wear of Ti6Al4V metallic contacts. By determining and defining the wear regimes, as scene with the fretting wear tribometer, test parameters can more easily be defined prior to testing. Loading conditions and stroke lengths can be chosen that will operate in the desired testing regime. In addition, the wear mode analysis of Ti6Al4V metallic contacts has shown that metallic coatings alone can not mitigate galling at the fretting wear interface. However, it has been shown that coating the Ti6Al4V surface with a hard inert coating, coupled with a soft metallic counterface, can mitigate galling for an extended number of cycles. This reduces the fretting wear without a lubricant in the contact. This could add a factor of safety to the current coating system by reducing the amount of wear on the Ti6Al4V components that come in contact with these soft metallic coatings, once the applied lubricants wear away.

7. References

[1] S. Fayeulle, P. Blanchard, L. Vincent, Fretting behavior of titanium alloys, *Tribology Transactions* 36 (1993) 267-275.

[2] E. Sauger, S. Fouvry, L. Ponsonnet, P. Kapsa, J. Martin, L. Vincent, Tribologically transformed structure in fretting, *Wear* 245 (2000) 39-52.

[3] P. Blanchard, C. Colombie, V. Pellerin, S. Fayeulle, L. Vincent, Material effects in fretting wear: Application to iron, titanium, and aluminum alloys, *Metallurgical Transactions* 22A (1991) 1535-1544.

[4] Z. R. Zhou, L. Vincent, Mixed fretting regime, *Wear* 181-183 (1995) 531-536.

[5] R. Waterhouse, Fretting fatigue, *International Materials Reviews*, 37 (1992) 77-97.

[6] H. Privett III, S. Fujishiro, Coating studies for prevention of fretting fatigue in jet engine titanium compressor blade dovetails, *Metallurgy and technology of practical titanium alloys*, (1994) 401-410.

[7] A. Freimanis, A. Segall, J. Conway Jr., E. Whittney, Elevated temperature evaluation of fretting and metal transfer between coated titanium components, *Tribology Transactions* 43 (2000) 653-658.

[8] R. D. Mindlin, Compliance of elastic bodies in contact, *J. Appl. Mech*., 16 (1949) 259-268.

[9] O. Vingsbo, On fretting maps, *Wear*126 (1988) 131-147.

[10] G. Xu, J. Liu, Z. Zhou, Prediction of the fretting fatigue resistance of various surface modification layers on 1045 steel: the role of fretting maps, T*ribology International* 34 (2001) 569-575.

[11] Z. Zhou, S. Gu, L. Vincent, An investigation of the fretting wear of two aluminum alloys, T*ribology International* 30 (1997) 1-7.

[12] I. Hutchings, Tribology: Friction and wear of engineering materials, CRC Press,

Boca Raton, 1992.

[13] H. Mohrbacher, J. Celis, J. Roos, Laboratory testing of displacement and load induced fretting, T*ribology International* 28 (1995) 269-278.

[14] J. Carton, A. Vannes, G. Zambelli, and L. Vincent, An investigation of the fretting behavior of low friction coatings on steel, T*ribology International* 29 (1996) 445-455.

[15] O. Vingsbo, J. Schon, Gross slip criteria in fretting, *Wear*162-164 (1993) 347-356.

[16] C. Hager, Jr., J. Sanders, and S. Sharma, "Characterization of Mixed and Gross Slip Fretting Wear Regimes in Ti6Al4V Interfaces at Room Temperature," *Wear*, 257 (2004) 167-180.

[17] H. Deresiewicz, R. D. Mindlin and applied mechanics, Pergamon Press Inc., New York, 1974.

[18] S. Fouvry, P. Kapsa, H. Zahouani, L. Vincent, Wear analysis in fretting of hard coatings through dissipated energy concept, *Wear* 203-204 (1997) 393-403.

[19] O. Vingsbo, S. Söderberg, in Ludema KC, *Wear of Materials 1987*, ASME (1987) 885-894.

[20] A. Ramalho, J. Celis, Fretting laboratory tests: Analysis of the mechanical response of test rigs, *Tribology Letters* 14 (2003) 187-196.

[21] S. Fouvry, P. Kapsa, L. Vincent, Analysis of sliding behavior for fretting loadings: determination of transition criteria, *Wear* 185 (1995) 35.

[22] Z. Zhou, E. Sauger, J. Liu, L. Vincent, Nucleation and early growth of tribologically transformed structure (TTS) induced by fretting, *Wear* 212 (1997) 50-58.

[23] M. Gardos, Magnéli phases of anion-deficient rutile as lubricious oxides. Part 1. Tribological behavior of single-crystal and polycrystalline rutile (Ti_nO_{2n-1}), Tribology Letters 8 (2000) 65-78.

[24] R. Boyer, G. Welsch, E. Collongs, Materials Properties Handbook: Titanium Alloys, ASM International, Materials Park, OH. 1994.

[25] R. Bowers, W. Zisman, Pressure effects on the friction coefficient of thin-film solid lubricants, *Journal of Applied Physics* 39 (1968) 5385-5395.

[26] R. Bowers, Coefficient of friction of high polymers as a function of pressure, *Journal of Applied Physics* 42 (1971) 4961-4970.

[27] I. Singer, R. Bolster, J. Wegand, S. Fayeulle, B. Stupp, Hertzian stress contribution to low friction behavior of thin MoS_2 coatings, *Applied Physics Letters* 57 (1990) 995-997.

[28] T. Lindley, Fretting fatigue in engineering alloys, *International journal of fatigue*, 19 (1997) 39-49.

[29] R. Antoniou, T. Radtke, Mechanisms of fretting-fatigue of titanium alloys, *Materials Science & Engineering*, A237 (1997) 229-240.

[30] N. Suh, The delamination theory of wear, *Wear* 25 (1973) 111-124.

[31] N. Suh, S. Jajanmir, E. Abrahamson, and A. Turner, Further investigation of the delamination theory of wear, *Journal of Lubrication Technology* October (1974) 631-637.

[32] N. Suh, S. Jajanmir, and E. Abrahamson, Microscopic observations of the wear sheet formation by delamination, *Wear* 28 (1974) 235-249.

[33] R. Waterhouse and D. Taylor, Fretting debris and the delamination theory of wear, *Wear* 29 (1974) 337-344.

[34] P. Blanchard, C. Colombie, V. Pellerin, S. Fayayeulle, L. Vincent, Material effects in fretting wear: Application to iron, titanium, and aluminum alloys, *Metallurgical Transactions* 22A (1991) 1535-1544.

[35] P. Blau, Mechanisms for transitional friction and wear behavior of sliding metals, *Wear* 72 (1981) 55-66.

[36] P. Blau, E. Doyle, Metallographic evidence for the nucleation of subsurface microcracks during unlubricated sliding of metals, *Wear* 117 (1987) 381-387.

[37] J. DeMasi-Marcin, D. Gupta, Protective coatings in the gas turbine engine, *Surface and Coatings Technology* 68-69 (1994) 1-9.

[38] S. Harris, M. Overs, and A. Gould, "The use of coatings to control fretting wear at ambient and elevated temperatures," *Wear*, 106 (1985) 35-52.

[39] A. Freimanis, A. Segall, J. Conway Jr., E. Whittney, The influence of temperature and wear mode on the deterioration of coatings used for titanium aircraft engine components, *Tribology Transactions* 45 (2002) 193-198.

[40] P. Hurricks, The mechanisms of fretting – a review, *Wear* 15 (1970) 389-409.

[41] D. Rigney, J. Hirth, Plastic deformation and sliding friction of metals, *Wear* 53 (1979) 345-370.

[42] C. Colombie, Y. Berthier, A. Floquet, L. Vincent, Fretting: Load Carrying Capacity of Wear Debris, *Transactions of the ASME* 106 (1984) 194-201.

[43] N. Tomashov, *Theory of Corrosion and Protection of Metals*, Macmillan, London, 1966.

[44] F. Bowden, A. Moore, D. Tabor, The ploughing and adhesion of sliding metals, *Journal of Applied Physics* 14 (1943) 80-91.

[46] F. Stott, D. Lin, G. Wood, The structure and mechanism of formation of the 'glaze' oxide layers produced on nickel-based alloys during wear at high temperatures, *Corrosion Science* 13 (1973) 449-469.